DEVELOPMENT AND OPTIMIZATION OF NEAR-INFRARED FUNCTIONAL LYMPHATIC IMAGING IN HEALTH AND LYMPHEDEMA

A Dissertation
Presented to
The Academic Faculty

by

Michael J. Weiler

In Partial Fulfillment
of the Requirements for the Degree
Doctor of Philosophy in Bioengineering
Department of Biomedical Engineering

Georgia Institute of Technology
August 2015

DEVELOPMENT AND OPTIMIZATION OF NEAR-INFRARED FUNCTIONAL LYMPHATIC IMAGING IN HEALTH AND LYMPHEDEMA

Reviewed by:

Dr. J. Brandon Dixon, Advisor
School of Mechanical Engineering
Georgia Institute of Technology

Dr. Edward Botchwey, Co-Advisor
School of Biomedical Engineering
Georgia Institute of Technology

Dr. Thomas Barker
School of Biomedical Engineering
Georgia Institute of Technology

Dr. Stanley Rockson
School of Medicine
Stanford University

Dr. Todd Sulchek
School of Mechanical Engineering
Georgia Institute of Technology

ACKNOWLEDGEMENTS

TABLE OF CONTENTS

LIST OF TABLES

LIST OF FIGURES

SUMMARY

The lymphatic vasculature is present in nearly all tissues of the body and serves three primary functions: (1) regulation of tissue fluid homeostasis through the transport of large proteins and excess interstitial fluid, (2) immune cell trafficking, and (3) lipid transport. When the normal function of the lymphatic system deteriorates, many complications can arise. Loss of lymphatic pump function often leads to tissue fluid accumulation, fibrosis, and lipid deposition – a disease known as lymphedema. Despite the critical roles that it performs, very little is known about the lymphatic vasculature in comparison to the blood vasculature. One of the main reasons for this knowledge gap may be the lack of in vivo imaging techniques to non-invasively visualize and obtain quantifiable information regarding lymphatic function, both in health and disease. New techniques are needed to better study lymphatic biology, elucidate the functional role of lymphatics and lymphangiogenesis in health and disease conditions, and better diagnose patients with lymphatic disease at an early stage before any resulting tissue damage is permanent.

Near-infrared (NIR) lymphatic imaging has emerged as a new technology for imaging of lymphatic architecture and quantification of vessel function. Although the technique has shown very exciting early results, the technique remains immature and several enhancements specifically for lymphatic imaging and functional quantification remain necessary. Therefore, we have characterized and optimized NIR imaging specifically for lymphatic vessels through a physical and physiological approach. Furthermore, the enhanced NIR lymphatic imaging technique was performed in the context of a novel rodent model of lymphedema to evaluate and characterize the role of lymphatic vessel function in the progression of the disease.

CHAPTER 1: INTRODUCTION AND BACKGROUND

Lymphatic Introduction

The lymphatic vasculature is present in nearly all tissues of the body and serves three primary functions: (1) regulation of tissue fluid homeostasis through the transport of large proteins and excess interstitial fluid, (2) immune cell trafficking, and (3) lipid transport(56). Approximately 10% of the fluid filtered out of capillaries is transported through the lymphatic vasculature and returned to the venous circulation in the left subclavian vein. Recently, it has been estimated that the lymphatic system transports as much as 8 liters of fluid per day from the interstitium to the blood(113).

The lymphatic system is forced to transport all this fluid without the benefit of a pumping organ such as the heart, and thus, it relies upon the driving force of interstitial fluid pressure (extrinsic pump) and the rhythmic contractions of the vessels themselves (intrinsic lymphatic pump) to propel fluid through the vasculature. The lymphatic system begins in the interstitial spaces as blind-ended initial lymphatics, which are composed of a discontinuous barrier of endothelial cells and basement membrane that facilitate the drainage and uptake of interstitial fluid, proteins, large molecules, virus particles, and bacteria(6, 204). Initial lymphatic vessels then merge to form collecting vessels, which have an inner layer of lymphatic endothelial cells and an outer layer of smooth muscle cells and are capable of contraction(33, 162). Collecting vessels are segmented into a series of individual pumping units called lymphangions, which contract to propel fluid and contain bileaflet valves to promote unidirectional flow(148, 266).

When the normal function of the lymphatic system deteriorates, many complications can arise. The lymphatic system has been implicated in several diseases including obesity(82), cancer metastasis(6), diabetes(92), and asthma(20), although the role of lymphatics in the progression of these diseases is not yet well understood. Loss of lymphatic pump function often leads to tissue fluid accumulation, fibrosis, and lipid deposition – a disease known as lymphedema(187). Post-procedure breast cancer patients are among the most at risk populations for developing such a condition due to the

lymph node and lymphatic vessel resection procedures, chemotherapy, radiation, and surgical interventions commonly associated with breast cancer treatment(189).

Lymphedema Background

Lymphedema is a severely debilitating disease and is often regarded as the most feared survivorship challenge facing patients recovering from breast cancer. While there currently is no permanent cure for lymphedema, early detection of the disease and intervention with compression garments is one of the most effective approaches for limiting its progression (220). The challenge facing clinicians is that what constitutes "early detection" is not grounded in a thorough understanding of the disease pathogenesis, but rather is defined by the limitations of the current state of the art for detection, which is routinely a tape measure. The lack of techniques and technologies for studying the lymphatic vasculature both clinically and in a research setting has long been an underlying factor in our limited understanding of lymphatic biology in both health and disease. Enhancements in lymphatic diagnostic capabilities (from genomics to proteomics to imaging) directly benefit our understanding of the disease progression, which in turn provide new targets for improving detection technologies and approaches. While current clinical approaches are aimed at capturing the symptoms of the disease (i.e. swelling) as early as possible, recent research developments suggest that methods capable of detecting underlying deficiencies of lymphatic transport could create a future where we are no longer waiting for the patient's symptom to become severe enough to be detected before we can recommend a course of treatment (Figure 1).

The modern genomic era has given us remarkable insight into the molecular mechanisms involved in lymphatic development (275) and the genetic mutations underlying many types of primary lymphedema (143). Additionally, clinical trials have provided a better understanding of the incidence of the disease for various types of surgical interventions, as well as identified a few broad risk factors that increase one's chances of developing lymphedema (165, 210, 245). Recent advances in the biology of secondary lymphedema progression as well as the development of new diagnostics for early disease detection and evaluation of lymphedema severity synergistically work

together in the race for a lymphedema cure – 1) better diagnostics are required to successfully detect and correct the underlying dysfunction at its earliest stages; 2) knowing the molecular mechanisms responsible for this dysfunction will provide new diagnostic targets and approaches for further clinical development.
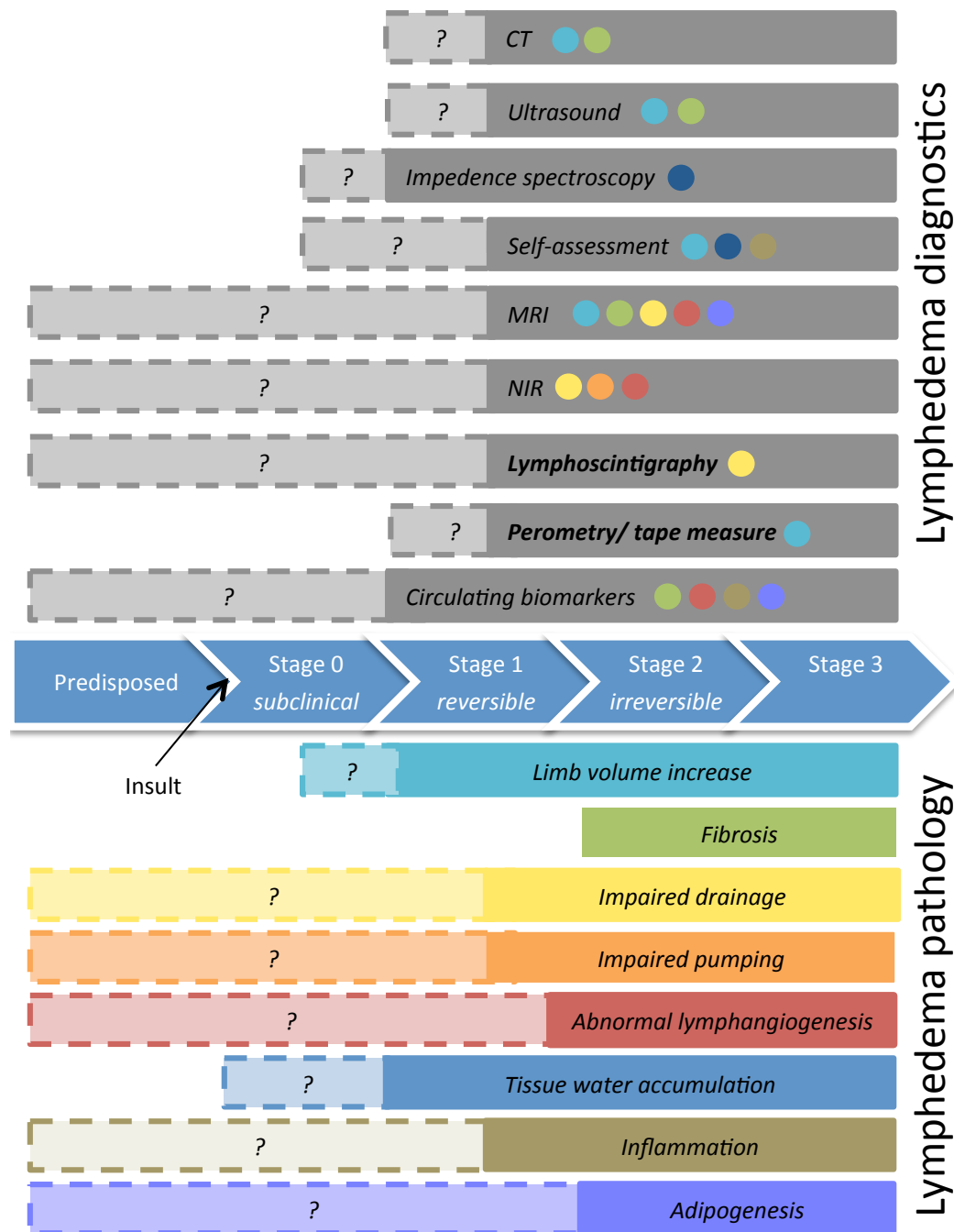
Figure 1: Relationship between lymphedema diagnostics and disease pathology. Most clinical lymphatic diagnostics have relied on detecting changes in limb volume as early as possible during the

disease progression (typically mid Stage 1). However as new diagnostics develop and our understanding of the disease process progresses, there is potential for diagnostics approached to detect various aspects of lymphedema earlier in the development of the disease and perhaps even being able to detect individuals predisposed to lymphedema. This figure summarizes the relationship between the diagnostic and the underlying pathology it is detecting (i.e. the colored circles with each diagnostic correspond to the detected pathology). Solid colors indicate strong support within the literature for the use of the diagnostic or presence of the pathology at the various stages of lymphedema. Dashed lines represent, in these authors' opinion, the potential for each pathology to show up and be detectable by a corresponding diagnostic approach earlier in the disease process.

Traditional lymphatic diagnostic techniques dating back 50 years or more (e.g. volume measurements, tissue indentation techniques, physical examination) are heavily relied upon for classifying the various clinical stages of lymphedema (Figure 2). Recent developments in lymphedema biology and diagnostic technologies suggest that the progression through these stages could be predicted earlier than classical methods permit. In the following sections I will discuss the broad categories of diagnostic techniques that are being explored both clinically and in animal models of lymphedema: 1) methods relying on patient history and routine surveillance of limb volume; 2) methods evaluating the change in the interstitium of the affected area; 3) methods involving the measurement of lymphatic fluid drainage. In each section I will discuss the underlying clinical and biological rationale that motivates the efficacy of the particular methodology as a lymphedema diagnostic, paying attention to the major recent advancements in our understanding of disease progression. This will be followed by an overview of recent developments in the methodologies themselves and how they are contributing to more mechanistic understanding of secondary lymphedema pathogenesis. I will then provide thoughts on remaining concerns and specific aims motivating my work.

Patient History and Routine Surveillance

<u>Rationale</u>

The most widely used diagnostic technique for determining lymphedema remains to carefully track changes in the patient's limb volume. Given that the transition from Stage 0 (or subclinical) lymphedema to Stage 1 is defined as the point at which a detectable change in limb volume occurs, just tracking limb volume alone will never be

able to detect subclinical lymphedema (by its very definition) or determine the extent that a person is predisposed. However, recent data has identified several risk factors associated with lymphedema, which could identify patient subsets that can be flagged for more frequent and attentive monitoring. Obesity has been linked with lymphedema risk, development and severity in numerous clinical trials and animal studies (4, 11, 45, 86, 115, 130, 133, 137, 165, 168, 184, 194, 195, 199, 213, 280). While accumulation of adipose tissue is known to be a hallmark of the edematous limb and is seen in nearly all animal models of lymphedema (11, 45, 194, 195, 280), preoperative body-mass-index (BMI) is one of the few predisposing factors for lymphedema that has continuously been demonstrated in clinical trials (4, 86, 130, 133, 137, 165, 184). Utilizing this information coupled with other risk factors that can be easily measured such as elevated blood pressure (133) and the number of lymph nodes removed (29, 165, 168) could provide a powerful tool for identifying those patients most at risk. It is unclear why these risk factors have not gained wide spread clinical use as a means for aggressively monitoring lymphedema onset is subsets of high-risk patients. It is likely that the burdensome and tedious nature of current diagnostic approaches, along with the prevalence of the belief that there is no therapeutic option for these patients anyway, have all contributed to the lack of widespread adoption. As genetic screening becomes cheaper and more routinely available, this could provide an additional avenue for risk assessment as several different studies have identified possible combinations of genetic risk factors that could predispose a person to developing secondary lymphedema (63, 64, 99, 112, 137, 154).

Diagnosis

One of the most common ways to diagnose and track the progression of lymphedema is through limb volume (LV) measurements, especially in unilateral cases in which the unaffected limb can serve as a control (8, 28, 245). Serial measurement of limb circumference with a tape measure has therefore become the most common LV assessment methodology. This method can be rather time-intensive, requires significant training, and is potentially susceptible to extensive inter-operator variability, but the technique is also comparably inexpensive and has been shown to be reproducible if anatomical landmarks are used to help standardize the procedure (28). Perometry is a 3D

LV scanning technique that alleviates some of the operational challenges of the tape measure and water displacement because it is quick and easy to use, mostly automated, and alleviates hygienic concerns. However, it is quite expensive, especially for smaller clinics with lower operating budgets, which has prevented widespread adoption (8, 217, 245). It is also unclear exactly how perometry compares to tape measure assessments; a study by Armer and colleagues found that the tape measure tended to diagnose lymphedema at a higher rate than with perometry (91).
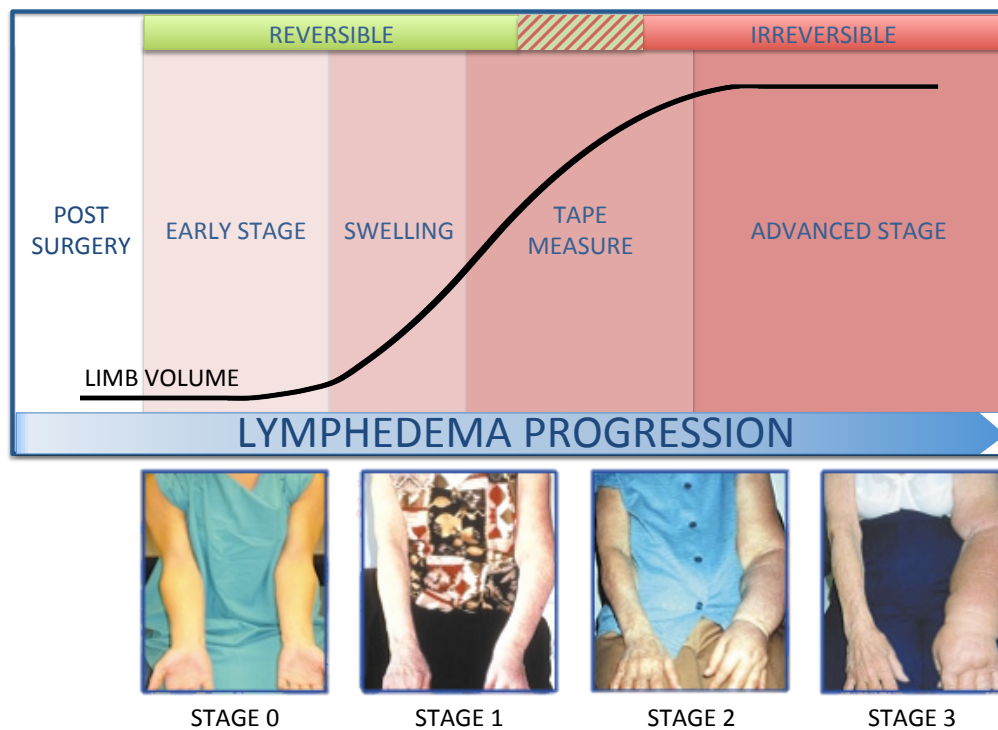
Figure 2: Stages of lymphedema progression. Stage 0 or subclinical lymphedema marks the period after the initial insult in which lymphatic fluid transport has begun to deteriorate, but clinical manifestations are not yet apparent. The beginning of the swelling cascade marks the shit to Stage I. At this point the limb becomes swollen, may feel heavy, and exhibits pitting edema. Limb volume diagnosis of lymphedema is often performed during the latter part of Stage I, and the disease is generally still reversible at this stage. The shift to Stage II lymphedema is characterized by advanced swelling and the beginning of fibrosis and adipose deposition. The limb begins to feel hard and exhibits non-pitting edema. Limb volume measurements are still performed on Stage II patients, but the disease quickly becomes irreversible as more tissue remodeling occurs. Stage III lymphedema, although rarely seen in breast cancer survivors, is the most advanced stage of swelling and is also called lymphostatic elephantiasis. – Images courtesy of Dr. Charles McGarvey and Guenter Klose.

Given that the rate of lymphedema incidence increases for at least up to 2 years after surgery (168), and early detection is crucial for the best therapeutic outcome, perometry is not an ideal solution as ultimately one needs a diagnostic tool or approach that can be placed in the hands of a patient. This is probably one of the reasons that preemptive surveillance, both in a clinical setting and by the individual patient at home has been one of the more effective approaches (28). Clinical lymphedema surveillance should ideally be performed in regular intervals following a risk-inducing procedure: pre and post-operatively, quarterly for the first year, semi-annually for years 1-3, and annually thereafter (8, 245). However, patients are instructed to constantly monitor the state of their affected extremities for pain, skin changes, increases in size, and feelings of "heaviness" or fatigue (176). Clinical surveillance includes a physical examination of affected limb(s) for signs of soft pitting edema (initial stages of lymphedema) and a focused patient history regarding age, cancer history and associated treatments, family and/or personal history of lymphedema, BMI, post-procedure weight gain, and post-op trauma or infection(s) (10, 28). Patients are also routinely given self-assessment questionnaires, such as the Lymphedema Breast Cancer Questionnaire (LBCQ) or the Gynecologic Cancer Lymphedema Questionnaire (GCLQ), which have been validated as reliable lymphedema diagnostic aids (9, 36, 245).

While, as discussed in the following sections, there have been significant advances in the sophistication of various techniques to measure and quantify lymphedema development at various stages of the disease, the approaches that appear to have the most widespread impact on lymphedema diagnosis to date involve the development of better educational pamphlets and relying on the patient to self-diagnose. This situation is certainly reflective of the value of better patient education, but it also provides insight into the significant gap that remains between cutting-edge lymphatic technologies and the ability to improve patient prognosis for those faced with a life of lymphedema risk.

Measurement of Interstitial Changes

<u>Rationale</u>

The ultimate pathology of the disease clinically presents itself through the gross remodeling of the interstitium and the skin. Thus, it is not surprising that many of the recent discoveries of the biological mechanisms underlying disease development occur largely in the interstitium (22). Lymph formation itself is driven by the balance of Starling forces, and therefore, changes in the oncotic and hydrostatic pressure in the interstitium will alter the demand placed on the lymphatics (113). This fluid must first traverse the interstitium as interstitial flow where it drains into the initial lymphatics. Interestingly both interstitial flow (30, 78, 85, 135, 229, 253) and pressure (170) are important cues for initiating and directing lymphangiogenesis. As the physical properties of the interstitium change during the course of the disease, these changes will in turn alter the hydraulic conductivity of the tissue and thus, both the clearance of fluid and the lymphangiogenic response (194, 231). In fact it is the mechanical changes of the tissue itself (i.e. tissue fibrosis) that is a hallmark of disease severity and its progression to irreversible, Stage II lymphedema (13-15, 115, 282).

While these mechanical changes are significant manifestations of the disease, they are not merely the result of the physical loss of lymphatic transport and interstitial protein accumulation (126). Recent data from numerous animal and human studies of lymphedema have made it abundantly clear that inflammation is a key, if not the most important, factor in driving lymphedema progression, (7, 15, 16, 115, 136, 199, 237, 279) particularly as it relates to the changes that occur in the interstitium. Of course inflammation is also helpful in the lymphangiogenic healing response after surgery and if balanced could be beneficial to lymphedema resolution (41, 66, 101). The molecular mechanisms that regulate the switch from a beneficial inflammatory response to chronic, unresolved inflammation in lymphedema (and other lymphatic-implicated disease) is an active and important area of research. Given that inflammatory cytokines have also been demonstrated to affect collecting lymphatic pump function (37, 38, 114, 283), it is likely that the consequences of inflammatory driven lymphedema progression not only alter the interstitium, but severely compromise pump function and drainage by the collectors, providing a positive feedback loop that when triggered, leads to the drastic pathologies observed in Stage II and III patients.

Diagnosis

8

Just as detectable volume changes in the limb have classically been the defining factor used to draw the diagnostic line between Stage 0 and Stage I lymphedema, permanent changes in the tissue itself define the transition from Stage I and Stage II. Therefore, assessment of tissue composition is another method used to diagnose and track the progression of lymphedema. Where these methods differ, lies in their sensitivity to detect tissue changes before permanent remodeling has set in. Again, just like in volume measurements, the methods are focused on detecting the symptoms of the disease as early as possible, rather than the underlying cause.

Bioimpedance

Perhaps the most common composition assessment is bioelectrical impedance spectroscopy, which measures extracellular fluid content by passing a small electrical current through the tissue. It has been reported that bioimpedance measurements can detect subtle changes in tissue properties indicative of lymphedema onset months before detection is possible with a tape measure, presumably by measuring the early-stages of inflammation and fluid stagnation (262). Variations of the technique have been reported in the literature for more than 2 decades, but recent research in this area has been focused towards enhancing the diagnostic capabilities of the technique, especially for breast cancer survivors. It has been demonstrated that using frequencies below 30kHz is optimal for the assessment of extracellular fluid volume, and such frequencies should be implemented in impedance spectroscopy devices moving forward (75). Several studies by Ward and colleagues have established impedance ratio ranges for lymphedema diagnosis (260-262), while Kilbreath et al. demonstrated that comparing the postoperative change in extracellular fluid volume of the ipsilateral extremity to a preoperative baseline may provide a more effective diagnosis of edema than comparison to reported thresholds (100). Newman and colleagues demonstrated that bioimpedance spectroscopy has sufficient sensitivity to assess not only extracellular fluid volume, but also lean mass and fat mass between affected and unaffected extremities of Stage II unilateral breast cancer-related lymphedema patients, which could provide additional diagnostically-relevant metrics to monitor the progression of later-stage lymphedema (153). Most recently, and arguably most excitingly, Ridner et al. recently developed and reported the first self-

measurement protocol for bioimpedance testing, which may pave the way for a home-use diagnostic in the future (183).

Tissue Composition

Tissue composition can also be assessed through various imaging techniques as well, although they have seen relatively limited clinical implementation to date. Dual energy X-ray absorptiometry has been shown to be equally sensitive as bioelectrical impedance spectroscopy for detecting extracellular fluid and lean and fat mass (153). Ultrasound has been used to measure and track changes in soft tissue thickness (109), with Lee et al. able to detect reductions in soft tissue thickness in breast cancer-related lymphedema patients after 2 weeks of complex decongenstive physiotherapy. MRI has also recently been shown useful to assess circumferential and volumetric measurements as well as track morphological changes in breast cancer-related lymphedema patients (70).

Tonometry

Tissue texture measurements may also be useful in the diagnosis and tracking of lymphedema because it is well known that as lymphedema progresses, the tissue becomes resistant to compression. Moseley et al. used tonometry, a measure of tissue compressibility, to quantify differences between normal and lymphedematous breast tissue (146). Similarly, Adriaenssens et al. used elastography, a measure of tissue elasticity, to also show a difference between healthy and affected breast tissue (3). However, Suehiro and colleagues were unable to detect differences between normal and Stage II lymphedematous legs (222), which suggests these techniques, in their current state of development, may only be useful in very advanced stages of lymphedema after significant fibrosis and adipose deposition has occurred.

Measurement of Lymphatic Drainage

Rationale

Given that lymphedema presumably develops due to the inability of the remaining intact lymphatic vasculature to return fluid from the interstitium back to the circulation at

the same rate at which lymph is formed, detecting this deficiency would be one of the most promising ways to transition from diagnostic approaches that rely on detecting symptoms of the disease, to those that can detect its underlying cause. Given that lymphedema can present itself several years after surgery, it is possible that the remodeled lymphatic vasculature after surgery is predisposed to failure. This phenomenon was recently demonstrated in a rat foreleg model of lymphedema, in which the lymphatic system was allowed to regenerate for 73 days after an axillary lymph node dissection (ALND) surgery (136). At this time point the animals exhibited no external signs of swelling. However, upon challenge with an inflammatory stimulus, ALND animals showed significant signs of swelling and skin remodeling compared to controls, suggesting that the remodeled lymphatics possessed an underlying deficiency in their transport capabilities that was only detectable when challenged.

Others have provided evidence in vitro, in animal models, or in human lymphedema patients that ineffective lymphangiogenesis could be a driving factor in secondary lymphedema (19, 25, 29, 41, 78, 115, 135, 138, 180, 195, 247, 278). It is less clear, however, whether the abnormal lymphangiogenesis, usually described by enhanced proliferation of initial lymphatic capillaries (25, 41, 135, 195, 278), the presence of tortuous lymphatic vessels (29, 180, 247), and hyperplastic lymphatic vessels (195), is an underlying cause in the development of the lymphedema, or merely a remodeling response to the highly inflammatory environment of later stage lymphedema. The latter is supported by the fact that these vessel phenotypes are usually noticed in situations where lymphedema has already developed (135), and inflammation itself is known to significantly upregulate lymphangiogenesis (101).

While there are numerous theoretical possibilities in which lymphatic transport might fail, only limited experimental data exists demonstrating correlation (much less causation) between failure of the lymphatic pump and lymphedema development. Collecting vessels have been demonstrated to remodel and become stenotic, with the severity of the stenosis correlating with lymphedema stage (Figure 3) (139). In a clinical study, Stanton and colleagues demonstrated that breast cancer related lymphedema developed in the arms of individuals with higher peripheral lymph flows, suggesting the higher filtration rates are a risk factor for lymphedema, perhaps by placing demands on

the lymphatics that exceed their capacity (218). Alternatively, upon radiation in a rabbit model it has been shown that the lymph node remodels and increases its resistance to flow, possibly impeding transport of lymph from the downstream afferent vessel (19). Lastly, under modest mechanical loading, the valves of isolated lymphatic vessel chains have been demonstrated to "lock" resulting in an inability to pump flow against an adverse pressure gradient (49). Given that the behavior of lymphatic valves are highly sensitive to pressure (50) and mutations affecting the proper formation of lymphatic valves is one of the most common causes of primary lymphedema (132, 143, 167), it is possible that certain patients could have undetectable valve defects in their lymphatics that fail when faced with the elevated fluid demand placed on them during the earliest stages of lymphedema. Lymphatic pumping is highly sensitive to the mechanical loading placed upon the vessel (48, 71, 104, 156, 202, 203) and since lymphedema is usually a battle against gravity, understanding both how the mechanical environment changes during the disease and the consequence of these changes to pump function is an important area of future research.

Diagnosis

The recent evidence regarding the role of lymphatic pump failure in the etiology of lymphedema, has provided renewed promise that a diagnostic approach capable of capturing this failure (or propensity to fail) in the earliest stages would be a significant advancement in patient care. Numerous imaging approaches have been investigated, each with a variety of advantages and disadvantages in terms of cost, accessibility, and ability to capture the various underlying lymphatic defects postulated above. Unfortunately, to date, most of these techniques have been unable to capture subclinical defects. Yet all of them are not-surprisingly, quite adept at demonstrating lymphatic dysfunction in Stage 2 and 3 lymphedema patients, which provides hope that continued advances can provide a subclinical diagnosis. The current state of lymphatic imaging, both clinically and in research settings, will be discussed in the next section.
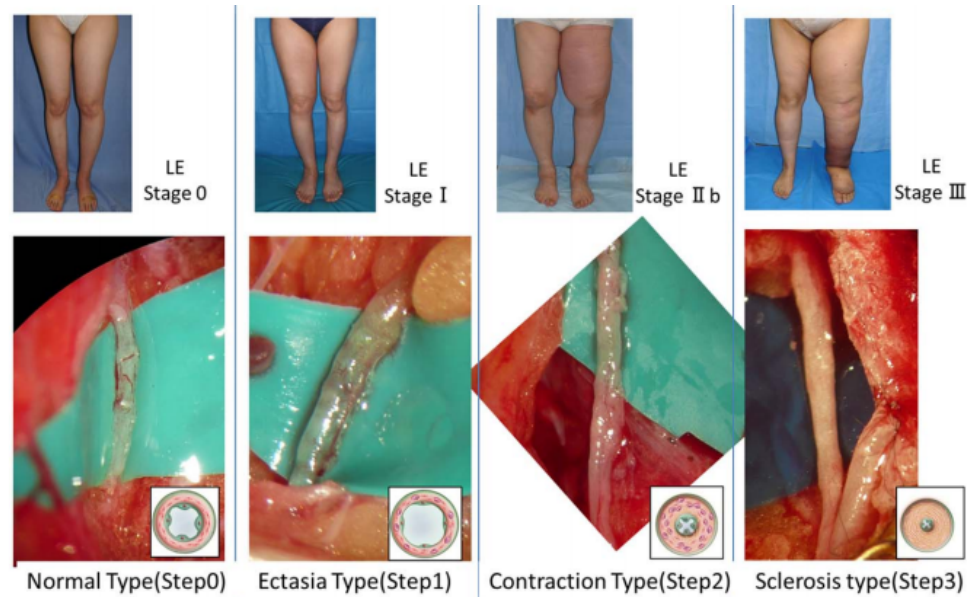
Figure 3: Staging of lymphedema and the macroscopic anatomical findings in the collecting lymphatic vessels associated with the stages. In the normal type, microvascular networks were found to nourish the largely developed walls of the collecting lymphatic vessels. The microvascular networks were gradually lost with the progression of the disease stages. In addition, the lymphatic vessel lumen was found to be dilated in the ectasis type, which was associated with an increase in endolymphatic pressure. Because increases in smooth muscle cells and collagen fibers are the major causes of the cloudiness and thickening of the lymphatic vessel wall, they were found to be prominent in the contraction type and the sclerosis type. LE: lymphedema. – Reproduced from the work of Mihara et al. 2012 (139).

Current State of Lymphatic Imaging

Here, we summarize imaging techniques currently used clinically to study lymphatics in vivo and discuss their advantages and limitations as they relate to lymphatic imaging. A quick survey of the literature shows that the primary application of lymphatic imaging has been the detection of lymph nodes, rather than lymphatic vessels. This is due in part because the clinical interest in lymph node targeting as it relates to cancer far outweighs the clinical interest in lymphatic diseases. However, another reason for this disparity is that the most successful techniques used clinically for mapping nodes do not meet the spatial or temporal resolution criterion for imaging lymphatic vessel function. Thus the title of "lymphatic" imaging in a majority of the literature (including what is discussed here) is not really focused on imaging lymphatics, but rather lymph nodes. However, most of the techniques that target lymph nodes work because there is a

functional network of vessels that drains the contrast agent to the node; thus these approaches can also indirectly be a useful tool for assessing lymphatic function and are worth mentioning.

Lymphatic Imaging Considerations

When evaluating the various imaging modalities it is important to consider the requirements the approach must meet for the designated lymphatic function or architecture that is being investigated. In general these can be divided into four categories: 1) spatial resolution requirements; 2) temporal resolution requirement; 3) contrast requirements; and 4) penetration depth requirements. The specification of these parameters depends on the context of the lymphatic physiology/anatomy under investigation. In humans, lymphatic vessels range anywhere for 20 um in diameter for the smaller capillaries to up to 5 mm for the thoracic duct and up to a few centimeters for lymph nodes(68). The collecting lymphatics, which provide a majority of the pumping activity for promoting lymph flow, range from 100-600 um. The temporal resolution needed depends on the importance of imaging this dynamic pumping function. Contractions of collecting lymphatics range from 10-50 contractions per minute, so frame rates of up to several frames per second are often needed to capture these dynamics(54). Nearly all tissues are supported by a lymphatic vasculature and thus these vessels reside at various depths. There are both lymphatic capillaries and collectors in the dermal layer just a few millimeters below the skin as well as vessels deep in the thoracic cavity.

Most lymphatic imaging techniques rely upon the injection of a particular contrast agent into the interstitium (or directly into a vessel itself) and the subsequent drainage of this contract agent by the lymphatic vessels. When the contrast agent is of the appropriate size, or binds to something of the appropriate size, (usually 3 nm – 100 nm) it is exclusively taken up into the lymphatic vessels, provided they are functioning. While essentially all lymphatic imaging techniques require contrast agents, the ideal injection should be a very small volume to minimize the effects of this added volume on interstitial fluid pressure, particularly if one is trying to capture a measurement of baseline lymphatic function. This is less important when imaging solely for architectural reasons or for sentinel lymph node mapping. Additionally, the contrast agent itself should have

14

minimal biological effects on lymphatic function and should be rapidly cleared from the circulation.

Lymphoscintigraphy

One of the long-time gold standards of lymphatic imaging is lymphoscintigraphy, the most common nuclear imaging method for lymphatics(284). Lymphoscintigraphy usually serves two main purposes with regard to lymphatic imaging: sentinel lymph node (SLN) mapping for post-cancer lymph node resection surgery(60, 257) and lymphatic vessel visualization for the assessment of lymphedema progression and treatment efficacy(270). The technique typically relies upon an intradermal or subcutaneous injection of Tc-99m sulfur colloid (11.1-111 MBq)(272), Tc-99m-labeled human serum albumin(185, 196), or Tc-99m-labeled dextran(166) given between 30-120 minutes before the imaging event. The scintigram takes a relatively long period of time to acquire, between 20 minutes and 2 hours depending on the imaging conditions(212).

Lymphoscintigraphy can be used in the diagnosis of lymphedema by examining differences in radioactivity between affected and unaffected regions, calculating clearance rates of radionuclide injections, and by observing dermal backflow of radionuclides in lymphatic vessels. Szuba and colleagues demonstrated the ability of lymphoscintigraphy to quantitatively estimate the radioactivity ratio between the axilla of a healthy arm and an affected arm as well as identify dermal backflow patterns in lymphedema patients(234, 236). A numerical index was also developed specifically for postmastectomy lymphedema patients in order to assess lymphedema progression based upon observations of dermal backflow and visualization of proximal lymph nodes. There was a correlation between the lymphoscintigraphic lymphedema numerical index and elevated limb volume as well as a correlation between the ratio of radioactivity and the post-treatment percentile change in edema. Taken together, these results indicate that lymphoscintigraphy can be used clinically to diagnose and assess lymphedema and that the technique has been used with moderate success in breast cancer-related lymphedema (BRCRL) patients. In addition to diagnosing lymphedema, lymphoscintigraphy has been used to evaluate new strategies for the treatment of lymphatic diseases such as autologous lymphatic transplant(269), VEGF-C treatment(235), surgical lymphatic-venous

anastomoses(31), the efficacy of manual lymphatic drainage(94), and the management of chylous ascites(35) to name a few.

The most prevalent use of lymphatic imaging using lymphoscintigraphy is for SLN mapping. The sentinel lymph node is theoretically the nearest downstream lymph node from a primary tumor, and as such, collects metastatic cancer cells. Contrast agents can thus be introduced in or near the primary tumor to be taken up by the local lymphatic vessels and transported to the SLN to assess the metastatic state of the tumor(76, 106, 145). A preoperative lymphoscintigraphy study in breast cancer patients has shown the technique to have an 87% success rate in identifying SLNs as hot spots(46). Recently, a new "dual mapping" procedure was performed in 60 breast cancer patients using dye injections in combination with isotopes capable of identifying SLNs in 59 patients (98.3%) with a false-negative rate of only 1.7%(151). In an effort to reduce or prevent the need for lymphatic vessel resection and BCRL, Thompson et al.(243) has developed an axillary reverse mapping (ARM) technique to identify and distinguish lymphatic vessels that drain the arm instead of the breast, but a long-term study is needed to verify the technique limits the risk of BCRL without compromising nodal staining accuracy. Modi and colleagues developed a novel technique to equip lymphoscintigraphy with more quantitative capabilities(142). After attaching a sphygmomanometer to the arm of BCRL patients and inflating to a pressure to cutoff lymphatic flow (as determined by lymphoscintigraphy), they were then able to gradually reduce this pressure until lymph flow was restored giving an estimation of lymphatic pumping. This study showed that this pumping pressure was reduced in women with BCRL providing some of the strongest evidence that the disease is strongly associated with the inability of these collecting vessels to adequately pump.

To summarize, lymphoscintigraphy is a 2D imaging technique to visualize the lymphatic vasculature and SLNs. While clinical SLN mapping is becoming more common, evaluation of lymphatic function and the state of lymphedema remains mostly qualitative with only minimal quantitative capabilities based upon clearance rates. The major limitations of lymphoscintigraphy are poor temporal resolution resulting from long gamma camera integration times and poor spatial resolution that limits the identification of exact SLN locations. While the technique is useful in identifying lymphatic

dysfunction as the general underlying cause in cases of limb swelling or chylous ascites, the resolution limitation make it difficult to assess the exact location or functional cause of the lymphatic failure.

Positron Emission Tomography

In an effort to address the drawbacks of lymphoscintigraphy, a hybrid SPECT/CT imaging modality has been implemented in lymphatic imaging to offer higher spatial resolution (~2mm) than traditional lymphoscintigraphy(251, 252, 254, 255). The technique combines positron emission tomography (PET) and X-ray CT to detect diseased lymph nodes(52, 160, 205), a process that uses the traditional intravenous injection of positron-emitting radiopharmaceuticals to specifically target molecules of interest and provides the added benefit of structural information from the X-ray CT(88). While the technique has shown promise for detecting nodes not found by traditional lymphoscintigraphy(256), it comes with a very high cost, and thus is not widely used for routine SLN mapping(159). Also, while the 2 mm resolution limit is an improvement for mapping nodes, it is still well below the requirements needed to image the primary unit actually responsible for lymphatic flow: the lymphatic collectors.

Magnetic Resonance Imaging

MR lymphangiography is the second traditional gold-standard in lymphatic imaging. The technique involves the injection (interstitial or intravenous) of various contrast agents including iron oxide particles, gadolinium-labeled diethylene-triaminepentaacetic acid (Gd-DTPA), Gd dendrimers or liposomes, and nanoparticles(21, 43, 83, 141, 216, 264) and analyzes the alignment, behavior, and interaction of protons when a magnetic field is applied. MR as it relates to lymphatic imaging is most commonly used for visualization of lymphatic vessels and cancer staging of lymph nodes with the advantage of better spatial resolution than nuclear techniques. The technique's feasibility was established a decade ago and has been used with a variety of contrast techniques including injections of gadoterate meglumine, an extracellular paramagnetic agent(193), nonionic water-soluble paramagnetic contrast agents gadodiamide and gadoteridol(118-120), and gadobenate dimeglumin(116) all injected into the dorsum of

the foot. Recently, Ruddell et al. developed a dynamic contrast-enhanced MR imaging (DCE-MRI) technique to assess lymphatic dysfunction by measuring and dynamically mapping changes in lymph flow and drainage in mice models(191). The technique begins with an intravenous injection of a contrast agent and then acquires serial MR images. Wash-in and wash-out curves can then be generated using specified regions of interest. In the study, they were able to show that tumor growth increased lymphatic flow through draining lymph nodes over a three week period.

Others have taken a different approach by exploring unenhanced MR lymphatic imaging(121, 122, 127). Matsushima and colleagues showed in their studies that using heavily T2-weighted imaging in combination with respiratory triggering can allow for the distinction between lymphatic flow and venous flow such that they can visualize lumbar lymphatics, cisterna chili, and the thoracic duct noninvasively without contrast agents. One concern is that lymphatic flow may be distorted by other fluid flow aside from venous circulation (especially slow fluid flows), but the possibility of imaging the lymphatic vasculature without the addition of contrast agents would be very valuable since the addition of most contrast agents probably alters true lymphatic function to a certain degree.

A new technique known as lymphotrophic nanoparticle-enhanced MRI (LN-MRI) may offer a solution to achieve more accurate lymph node staging(44, 103) by using a novel set of MR contrast agents possessing unique biochemical and physical properties(87, 192, 193). MR lymphatic imaging with ultrasmall superparamagnetic iron oxide (USPIO) particles may provide adequate contrast necessary to resolve salient features of normal and cancer-positive lymph nodes(21, 23, 24, 147, 182, 212, 271, 284). Harisinghani et al. used highly lymphotropic superparamagnetic nanoparticles to detect lymph node metastases with significantly improved sensitivity compared to traditional MR lymphatic imaging(80). Likewise, Ross et al. used an intravenous injection of fermoxtran, a lymph node specific contrast agent, to detect prostate cancer lymph metastases with excellent sensitivity(190). Recently, Kimura et al. also used USPIO lymphography and differences in T2*-weighted and T1-weighted enhancement patterns to identify normal and diseased lymph nodes(102).

It is important that many of the USPIO techniques for lymph node mapping do not directly rely on lymphatics for targeting the node, but rather take advantage of the leaky vasculature present in tumors to achieve extravasation from the blood. Thus, techniques that are promising for identifying lymph nodes do not necessarily translate for imaging the lymphatic vasculature. Another challenge with these nanoparticle approaches is that there is often a trade-off between ease of uptake from the interstitium into the lymphatics and their subsequent retention in the lymph node(95).

MRI offers excellent spatial resolution, which has a lot of potential for imaging the structure and morphology of the lymphatic vasculature and lymph nodes. Perhaps the most exciting direction of MR lymphatic imaging is the potential to fully develop an unenhanced MR lymphangiography technique to visualize the lymphatic system without contrast agents. Such a breakthrough would revolutionize lymphatic imaging and greatly improve diagnostic capabilities for detecting lymphatic diseases.

Computer Tomography

X-ray computer tomography (CT) is commonly used to assess differences in tissue density between soft tissue and electron-dense bone, and contrast agents are often incorporated to help discern healthy and diseased tissue(277). CT is commonly used as a diagnostic method for the screening and identification of tumors before surgery is performed for many cancers including breast cancer(159). One particular subset of CT imaging, computed tomographic lymphography (CT-LG) has been used to visualize lymphatic drainage pathways and to discern enlarged or metastatic lymph nodes(284). The current technique utilizes a class of small organic iodinated molecules that are highly water soluble (examples include iopamidol, ioxaglate, ioversol, and iohexol) to provide additional contrast for CT SLN imaging. Suga et al. employed iopamidol in CT-LG for the visualization of breast lymph vessels and the mapping of SLN locations in healthy dogs and healthy human volunteers and were able to observe the direct path of lymphatic vessels from the injection site to the SLN, detect a localization of the contrast agent in the SLN, and visualize distant nodes(223, 224, 226). Others have built upon this technology and had similar successes using CT-LG for SLN mapping(225, 238, 274).

Despite the success of water soluble organic iodinated contrast agents in SLN detection, the molecules offer a very short imaging duration because they drain rapidly to the blood vasculature and are cleared through the renal system(284). Additionally, the technique is limited by difficulty of injecting the necessary millimolar concentrations of contrast agents in the dermal space. In an attempt to mitigate this drawback, several new CT contrast agents are under development(212). Rabin et al. has synthesized a polymer-coated bismuth sulfide nanoparticle as a novel CT contrast agent with a longer hemovascular half-life, but concerns remain regarding the long-term toxicity of this nanoparticle(174). Although to date CT-LG cannot detect occult metastases, the technology has a lot of potential as a strong alternative to lymphoscintigraphy for the visualization and identification of SLNs for biopsies. The detailed anatomy of the lymphatic vasculature that CT-LG can provide may help to minimize several of the shortcomings of lymphoscintigraphy as well as increase the accuracy and sensitivity of SLN biopsy. However, the major limitation of CT-LG as compared to other imaging modalities is the inability to image dynamic lymph flow or lymphatic contractions, which is due to a lack of spatial resolution. Radiation concerns associated with CT may also limit its clinical usefulness.

It should also be noted that another x-ray-based technique similar to angiography requires the cannulation of lymphatic vessels and direct injection of contrast agents (e.g. Lipiodol, an iodinated poppy seed oil) directly into the cannulated vessels. Originally termed lymphangiography (or lymphography), it has been used postoperatively in patients with lymphatic fistulas, lymphocele, and chylothorax as a means of detecting lymphatic leakage(105). While the term lymphangiography is now broadly used for a variety of techniques that involve the uptake of a contrast agent into a lymphatic vessel for subsequent imaging, traditional lymphographies have largely been abandoned due to the increase in availability of other techniques, the technical expertise required for vessel cannulation, and complications that have been shown to arise from the procedure(214, 244, 258).

Ultrasound

Ultrasound is the primary imaging modality used to study and diagnose secondary lymphedema resulting from filariasis, a disease common to tropical regions around the world in which parasitic nematodes enter a human host via mosquito vectors and come to reside in the lymphatic vasculature. The biggest advantages for ultrasound imaging of lymphatics are the relatively low cost and availability of equipment, the achievable penetration depth, and the lack of ionizing radiation. Ultrasound has been employed to visualize dilated lymphatic vessels in filarial patients[59, 157], and Doppler ultrasound has been used to successfully measure nematode motion in lymphatic vessels[227] and evaluate the efficacy of treatment strategies on filarial infection[58, 158, 242]. Doppler ultrasound is not regularly used in lymphatic imaging, however, because the lower number of scattering objects (e.g. cells) present in lymph flow severely limits measurements of lymph drainage patterns, while the abundance of red blood cells in the blood vasculature has allowed it to be widely used for measuring blood flow. Additionally, ultrasound poses some spatial resolution limits when compared to other techniques that make it difficult to image the smaller vessels. High frequency ultrasound has been able to achieve spatial resolution down to 20 μm, however a tradeoff exists between spatial resolution and penetration depth with these high frequency systems being limited to depths under 5 mm.

Despite the limited applications in lymph flow measurements, ultrasound has been used to assess the malignant state of lymph nodes based upon geometric features[21]. Since ultrasound images do not necessarily require contrast agents, the technique may serve a very unique role in mapping SLNs characterized by afferent lymph vessel blockage that would otherwise prevent contrast agents from reaching the node and produce a false-negative result. Contrast-enhanced ultrasound imaging (CEUS)[79] is much more widely used in preclinical and clinical imaging of lymphatics than ultrasound alone because the technique has the advantages of high signal-to-noise ratio, contrast sensitivity, spatial resolution[193, 284]. The most widely used contrast agents for CEUS are submicron-sized microbubbles, which are often made with lipids, polyethylene glycol polymers, or denatured albumin[51, 259]. Microbubble contrast agents have been employed in CEUS imaging to visualize lymph nodes, lymphatic vessels, and other areas of interest in the microcirculation[43, 77, 105, 155, 206, 207,

273). Like all contrasts agent approaches, the probes can rely on the drainage of the lymphatics to be delivered from the primary tumor to the node, or they can be functionalized with specific ligands for targeting the nodes and thus can be administered via the blood(84).

Optical Imaging Techniques

Optical fluorescent imaging may provide the best combination of spatial and temporal resolution for specifically visualizing lymphatic vessels and propulsive lymphatic flow out of any of the imaging modalities previously mentioned, and the technique has the added bonus of not exposing patients to ionizing radiation(21). The basic principle is to exploit the natural function of the lymphatic system by giving an intradermal or subcutaneous injection of a fluorescent tracer and visualizing the uptake and transport of the fluorophore by the lymphatic vessels (Figure 1). Fluorescent imaging allows the use of camera integration times as low as 100ms(107), which enables excellent temporal resolution for the dynamic visualization of lymphatic uptake and transport characteristics. While dynamic pulsatile lymph flow has been recorded via intravital microscopy techniques in mesenteric and isolated lymphatic vessels(53-55), there is no other imaging modality capable of obtaining such high resolution lymphatic imaging non-invasively in vivo.

Optical fluorescent imaging of lymphatics was first reported in the form of fluorescence microlymphangiography using the fluorophore fluorescein, which is maximally excited and emits fluorescence at visible wavelengths, thus limiting its usage to imaging very superficial lymphatic vessels(65, 134). McGreevy et al. also used a visible contrast agent, Cy5, to detect lymph nodes in swine(129). The limited penetration depth of visible light, however, prevented the visualization of any deeper lymphatic vessels, such as collecting vessels. Quantum dots have also been employed for sentinel lymph node mapping(215), but most quantum dots are excited in the visible range, which limits the ability to image deeper collecting lymphatic vessels despite the mild improvement in tissue penetration depth over visible fluorescent dyes(212). Additionally, there remain serious concerns about the long-term toxicity of quantum dots due to their heavy metal content.

Emerging Technique: Near-Infrared Functional Lymphatic Imaging

More recently, near-infrared (NIR) fluorescence lymphatic imaging using fluorescent dyes has gained traction. NIR imaging technologies may provide the ideal solution to functional lymphatic imaging for the purposes of disease assessment and management as they reside in the optimal range where light absorption and scattering are low in biological tissue and there is minimal autofluorescence, thus affording deeper penetration depths and excellent contrast and spatial resolution, all of which are vital for measuring lymphatic contractile properties(177). NIR imaging with an FDA-approved fluorescent dye, indocyanine green (ICG), has been reported as an optical diagnostic dating back to the 1950's as it was originally used to assess cardiac output and hepatic function(39). Based upon its fluorescent properties, the indications for ICG use expanded over the next 50 years to include microcirculation of skin flaps, visualization of retinal and choroidal vasculatures, pharmacokinetic analysis, object localization in tissue, tissue welding, fluorescence probing of enzymes and proteins, and tumor screening(169, 200). ICG-based NIR imaging has emerged as a novel method for lymphatic vasculature and sentinel lymph node mapping and quantitative assessment of lymphatic function in animals and in humans; a technique in which ICG is injected intradermally, excited with a laser diode, and imaged with an NIR-sensitive detector as it is taken up by the lymphatic system(89, 163, 197, 208).

ICG-based NIR imaging specifically designed for lymphatics was first reported in two separate studies by Sharma et al.(212) and Unno et al.(247) in 2007. The study by Sharma and colleagues showed, for the first time non-invasively, dynamic propulsive lymph flow in anesthetized swine. The rhythmic contractions of sequential lymphangions and the series of one-way valves force the fluid to flow in discrete "packets" along the lymphatic vessels. The packets were recorded as traveling between 0.1-1 cm/s, which was orders of magnitude above the μm/s lymph velocities previously reported by fluorescence lymphangiographies in animal preparations(27, 105, 228, 232) as the previous studies were only able to image the initial capillaries and not the contractile collecting lymphatics. The study by Unno and coworkers used NIR lymphatic imaging to identify four characteristics of lymphatic flow associated with lymphedema including dermal backflow, extended fluorescence in the injection site, dilated lymph

channels, and fluorescence diffusion otherwise known as leaky vessels. Sevick-Muraca et al. also showed lymphatic vessel visualization in breast cancer patients using microdose administration of ICG(209), which was significant because smaller fluorophore injections will limit the effects of the procedure itself on baseline lymphatic function.

One of the major advantages of NIR lymphatic imaging over other imaging modalities is the emergence of new quantitative measures of lymphatic pump function. Such quantifiable metrics will be enormously valuable in objectively defining lymphatic health and assessing the progression of lymphatic disease. Rasmussen et al. established discrete regions of interest (ROIs) along lymphatic vessels and recorded spikes in intensity corresponding to packets traveling through the various ROIs. If the distance between ROIs is known, metrics such as average packet velocity and packet frequency can be calculated as representative metrics of lymphatic pump function(178-180). Unno et al. adapted a previously described technique(142) to measure lymphatic pumping pressure to NIR imaging(248). ICG was injected into the dorsum of the foot of human volunteers and real-time fluorescence images of lymphatic transport were recorded while a custom sphygmomanometer was used to increase the pressure around the legs until lymphatic flow was observed to have stopped. The pressure was then slowly released until lymphatic flow was restored, which was defined as the lymphatic pumping pressure, P_{pump}. Using NIR imaging of ICG transport through dermal lymphatic vessels during this procedure gives a very accurate measure of the exact time and corresponding applied pressure at which lymphatic flow is stopped. Healthy patients were reported to have a P_{pump} of 29.3 mmHg while lymphedema patients had a significantly lower P_{pump} of 13.2 mmHg, indicating reduced lymph transport capabilities in lymphedema patients. More recently this technique was also applied to assess the decline in P_{pump} associated with aging(250), although currently the technique does not take into account changes in tissue compliance and how this might affect the transmission of the externally applied pressure to the lymphatic vessel.

NIR lymphatic imaging has the potential to revolutionize the study of lymphatic transport phenomena, especially in the context of lymphatic disorders, with the development of new imaging techniques and quantification metrics. However, the

technique is still in its infancy and several advancements need to be made to maximize the effectiveness of lymphatic transport functional assessment. This leads to three specific aims that will form the basis of this work. First, we will characterize and optimize NIR imaging specifically for imaging the dynamics of dermal collecting vessels. Secondly we will characterize the physiology of multiple lymphatic collectors draining a single tissue space and explore the effects of various flourophores in time course imaging. Finally, we will create a new model of lymphedema specifically designed to use NIR imaging to quantify changes in lymphatic collecting vessel function associated with the disease. Cumulatively, these aims will provide necessary advances in our understanding of the physics (aim 1) and the physiology (aim 2) of NIR lymphatic imaging, which will enable a novel and impactful assessment of the relationship between lymphedema and lymphatic pump function (aim 3).

Specific Aims

Specific Aim 1

There has been very little experimentation or discussion on the effects of the interstitial environment or the various quantifiable parameters historically used with this technique, such as the effects of vessel depth and scattering on the ability to resolve differences in vessel diameter or the effects of protein binding on ICG fluorescence. Quantifying these and other effects will allow for potential optimization of component selection and configuration, will establish performance metrics of imaging functionality, and will provide more detail in regards to the limitations of the technique as a non-invasive tool for quantifying lymphatic function.

Therefore, we will characterize and optimize NIR imaging for the visualization and quantification of lymphatic pump function specifically focusing on excitation/emission wavelengths, tissue penetration depths, and hardware optimization. Furthermore, we will validate the performance of the NIR imaging system to detect functional changes in lymphatic transport by intentionally modulating lymphatic contractility in vivo using nitric oxide (NO) and performing in vivo NIR imaging to detect the resulting changes in lymphatic function.

Aim 1 Hypotheses

H1.1: ICG fluorescence in lymphatic collectors is dependent upon protein concentration and optimizing the ICG solution will lead to an increased SNR in the vessels.

H1.2: Dermal application of nitric oxide ointment will reduce lymphatic function in a manner that can be quantified with NIR lymphatic imaging. Specifically, dermal nitric oxide ointment will:

> H1.2.1: increase transport time
>
> H1.2.2: decrease packet frequency
>
> H1.2.3: decrease packet velocity.

Specific Aim 2

The field is still learning to understand and interpret the wealth of data NIR functional lymphatic imaging can uniquely provide compared to other modalities. In particular, recent work has suggested that functional differences exist between various collecting vessels in a rodent hind limb (171), but no studies have specifically examined the differential transport abilities of multiple collecting vessels draining a single tissue space. Such an analysis is a necessary advancement of NIR functional lymphatic imaging, which has historically focused on quantification of only a single vessel, to better understand the physiology of draining lymphatic networks at the tissue level.

Therefore, we will simultaneously characterize the functional transport capabilities of the two collecting vessels in the rat tail model using NIR lymphatic imaging. The rat tail provides the simplest model of lymphatic network drainage for NIR imaging purposes due to the simple geometry and the consistent position of the two collecting vessels. Using the rodent tail also allows comparisons to many previous studies as it has been one of the most widely used models in lymphatic research, providing insight into basic lymphatic physiology and lymph flow (111, 268), lymphangiogenesis (30, 42, 78, 276), and lymphedema pathology (195, 237, 279). The results of this characterization will establish a framework by which future lymphatic research can be performed using NIR imaging in the tail model and will enhance our understanding of differential vessel function.

Additional controversy also remains regarding the most appropriate fluorophore for NIR lymphatic imaging. Several studies are beginning to explore novel probes with higher quantum yields specifically for NIR lymphatic imaging(47, 96, 124, 172), but the most commonly used probe to date has been indocyanine green (ICG). Despite the low quantum yield of the molecule, ICG remains the hallmark of NIR lymphatic imaging because it is FDA approved for use in humans and represents the most likely probe for the development of a point-of-care diagnostic. However, the literature is mixed regarding the effects of ICG on lymphatic function.

It has been shown in isolated lymphatic vessels that ICG inhibits vessel contraction in a dose-dependent manner and continues to alter function even beyond complete washout from the vessel (73). Given that near-infrared fluorophores have been shown to accumulate in the intracellular space (69), and ICG, in particular, has been shown to exhibit extremely cumulative cellular uptake (1, 62), we hypothesize that ICG is retained in the tissue space and contributes to a decrease in lymphatic function for an extended period of time following initial injection. A follow-up study using NIR imaging was unable to detect changes in lymphatic function after ICG injections of various concentrations (5), but the study only examined this phenomenon at one time point.

Therefore, we will first examine the retention of ICG in the tissue space of the rat tail and measure lymphatic function with NIR imaging beyond the duration of retention to analyze the time course changes in lymphatic function following initial ICG injection. For comparison purposes, we will also perform this analysis with a competing NIR fluorophore, the LI-COR IRDye 800CW PEG. The results will contribute to a further characterization of the rat tail model for NIR lymphatic imaging and will inform future studies involving multiple, repeat injections of NIR probes in this model.

<u>Aim 2 Hyopotheses</u>

H2.1: When multiple collecting vessels drain the same tissue space, they will have heterogeneous transport capacities, and may exhibit a differential response to stimuli.
H2.2: Lymphatic transport as measured through NIR imaging will vary as a function of time after initial injection due to the transient alteration in interstitial fluid pressure resulting from the bolus injection.

H2.3: ICG has a time-delayed effect on lymphatic function such that it will decrease lymphatic transport capacity in the context of time-course experiments with repeat fluorophore injections. Specifically:

H2.3.1: ICG remains present in the tissue space for an extended period of time following a bolus injection for NIR lymphatic imaging.

H2.3.2: ICG will cause a reduction in lymphatic function in a time-delayed manner such that repeat measurements at later time-points will exhibit significant reductions in NIR lymphatic measurements. This time-course of reduced lymphatic function may correlate with the retention of ICG in the tissue space.

H2.3.3: ICG will demonstrate evidence of inflammation that will correlate with retention of the dye in the tissue space.

Specific Aim 3

It remains unclear how the response of the lymphatic system during the post-trauma period correlates with the onset and progression of lymphedema, which has severely limited our ability to understand the disease mechanism and cascade. Since lymphatic flow is driven primarily through the contractility of collecting lymphatic vessels, the ability to quantify lymphatic pump function through the imaging of functional lymphatic transport in the context of early lymphedema onset would greatly enhance our understanding of the disease progression. We hypothesize that lymphedema is associated with a progressive loss of lymphatic function, which can be visualized and subsequently quantified with NIR imaging, thus affording novel insights into the disease cascade. The latency period commonly associated with lymphedema, in particular, motivates a hypothesis of remodeling-induced lymphatic failure, which has begun to gather support in the literature(136). Importantly, however, all of the animal models reported in the literature to date have severed all of the collecting vessels draining the tissue space of interest, and the analysis has focused exclusively on morphological changes occurring in the dermal layer and functional changes occurring in the initial lymphatics. No study to date has investigated the changes in collecting vessel function associated with lymphedema, and no model currently exists that allows preservation of collecting vessel trunks.

Therefore, we will develop a new rodent tail model of lymphedema allowing for selective preservation of certain lymphatic collectors in order to track changes in the collecting vessel transport metrics over time using NIR lymphatic imaging. We will take baseline NIR functional measurements before surgery, immediately after surgery, and in regular follow-up intervals to record changes in collecting vessel transport function over the course of the disease cascade. The goal is to develop a model that exhibits similar pathological progression as the classic rodent tail model of lymphedema while preserving a single intact collecting vessel trunk. Doing so will provide the first opportunity to study the link between lymphedema progression and lymphatic transport as well as help to generate new insights into the potential mechanisms of lymphatic failure during disease progression.

<u>Aim 3 Hypotheses</u>

H3.1: Ligating the mouse tail such that one lymphatic collector remains intact will create a pathological model of lymphedema while simultaneously allowing NIR functional metrics to be obtained from the intact vessel. The tails may exhibit slightly less swelling than the standard full ligation tail model.

H3.2: Ligating the dominant vessel will produce significantly increased swelling as compared to ligation of the dominant vessel.

H3.3: Swelling will correlate with reductions in lymphatic function as quantified through NIR lymphatic imaging.

H3.4: The disease cascade will contribute to remodeling of the intact collecting vessel such that the pumping capacity is reduced.

CHAPTER 2: SENSITIVITY ANALYSIS OF NEAR-INFRARED FUNCTIONAL LYMPHATIC IMAGING

Near-infrared (NIR) imaging of lymphatic drainage of injected indocyanine green (ICG) has emerged as a new technology for clinical imaging of lymphatic architecture and quantification of vessel function, yet the imaging capabilities of this approach have yet to be quantitatively characterized. Therefore, we sought to quantify its capabilities as a diagnostic tool for lymphatic disease. Imaging was performed in a tissue phantom for sensitivity analysis and in hairless rats for in vivo testing. To demonstrate the efficacy of this imaging approach to quantifying immediate functional changes in lymphatics, we investigated the effects of a topically applied nitric oxide (NO) donor glyceryl trinitrate ointment (GTNO). Premixing ICG with albumin induces greater fluorescence intensity, with the ideal concentration being: 150 μg/mL ICG and 60 g/L albumin. ICG fluorescence can be detected at a concentration of 150 μg/mL as deep as 6 mm with our system, but spatial resolution deteriorates below 3mm, skewing measurements of vessel geometry. NO treatment slows lymphatic transport, which was reflected in increased transport time, reduced packet frequency, reduced packet velocity, and reduced effective contraction length. NIR imaging may be an alternative to invasive procedures measuring lymphatic function in vivo in real time.

Introduction

The lymphatic system plays a critical role in regulating tissue fluid balance by draining the interstitial space and preserving protein concentrations to maintain oncotic pressure(57). If the natural function of the lymphatic system is disrupted, several pathologies can develop, most notably lymphedema, which often results in irreversible tissue damage presumably through the disruption of lymphatic transport, thus leading to subsequent interstitial fluid stagnation and lipid accumulation in the affected tissues(175). However, our current understanding of the lymphatic vasculature pales in comparison with the blood vasculature, a phenomena that can partly be attributed to lack of in

vivo imaging techniques suitable for visualizing lymphatic vessels. In the case of lymphedema, in particular, a major limitation in the development of new treatments has been the lack of in vivo imaging diagnostics capable of quantifying differences in the dynamic pump function of lymphatic vessels in real-time(181).

Recently, the lymphatic system has garnered increased interest as its roles in tumor metastasis(97), dermal drug delivery(81), chronic inflammation(93), and lipid transport(56) are beginning to be appreciated. With the new understanding of the role of lymphatic vessels in disease processes and therapies there is now a greater need for major advances in the diagnostic imaging tools available to adequately visualize and quantify lymphatic pump function. Since lymphatic flow is driven primarily through the contractility of collecting lymphatic vessels(148, 266), the ability to quantify lymphatic pump function through the imaging of functional lymphatic contractions and fluid flow would greatly improve the understanding of lymphatic contractile physiology and enhance the diagnosis of disease states. However, the two traditional gold standards of clinical lymphatic imaging, lymphoscintigraphy and magnetic resonance imaging (MRI), while very effective for systemic lymphatic mapping, are inadequate for the assessment of lymphatic function because draining vessels are below the spatial resolution of MRI and lymphoscintigraphy lacks the real-time temporal resolution needed to image the dynamics of lymphatic contractile function(21, 141, 173, 212).

Near-infrared (NIR) imaging technologies may provide the ideal solution to functional lymphatic imaging as both a research tool and a disease diagnostic because NIR light resides in the optimal wavelength range where light absorption and scattering are low in biological tissue and there is minimal autofluorescence, thus affording deeper penetration depths and excellent contrast and spatial resolution, all of which are vital for measuring lymphatic contractile properties(177). NIR imaging with an FDA-approved fluorescent dye, indocyanine green (ICG), has recently emerged as a novel method for quantitative assessment of lymphatic function in animals and humans (107, 108, 178, 180, 249); a technique in which ICG is injected intradermally, excited with a laser diode, and imaged with an NIR-sensitive detector as it is taken up by the lymphatic system(211, 247).

NIR lymphatic imaging, although in its infancy, has shown great promise to enhance the understanding of functional lymphatic transport characteristics both in health and disease as the technology has the potential to develop into an early-stage diagnostic of lymphatic dysfunction(2, 209, 247, 248). Such a device would be strongly suited to enhance the diagnosis and treatment of lymphatic disorders through the visualization and quantification of changes in functional lymphatic transport before clinical manifestations are present and tissue damage is irreversible. Current NIR lymphatic imaging technology has been quite successful at demonstrating differences in lymphatic function and architecture in patients who have already been diagnosed with lymphedema(128, 180, 247), differences in lymphatic function in response to manual lymphatic drainage(241) and pneumatic pressure devices(2), as well as a decline in lymphatic pumping pressure in response to aging(250). However, it is currently unclear how effective this approach will be at predicting lymphedema disease risk or providing early detection, as most of its successes to date have involved showing differences in lymphatic function after significant deterioration has already occurred. Additionally, there has been very little experimentation or discussion on the effects of the interstitial environment on the various quantifiable parameters historically used with this technique, such as the effects of vessel depth and scattering on the ability to resolve differences in vessel diameter or the effects of protein binding ICG fluorescence. Quantifying these and other effects will allow for potential optimization of component selection and configuration, will establish performance metrics of imaging functionality, and will provide more detail in regards to the limitations of the technique as a non-invasive tool for quantifying lymphatic function.

The purpose of this study, therefore, is to investigate these issues for characterizing and optimizing NIR imaging for the visualization and quantification of lymphatic pump function. Furthermore, the current state of the art for studying lymphatic contractile dynamics and their biophysical and molecular regulation in vivo requires invasive, terminal procedures(32, 53, 55, 114), but NIR lymphatic imaging may have the potential to generate similar data regarding lymphatic function in a completely noninvasive manner. Therefore, we will validate the performance of the NIR imaging system to detect functional changes in lymphatic transport by intentionally modulating lymphatic contractility in vivo using nitric oxide (NO) and performing in vivo NIR

32

imaging to detect the resulting changes in lymphatic function. We expect NIR imaging to be able to detect functional changes in lymphatic transport after differential applications of NO, which may establish a novel research tool for studying the regulatory effects of NO on lymphatic pump function in vivo in real time.

Hypotheses

H1.1: ICG fluorescence in lymphatic collectors is dependent upon protein concentration and optimizing the ICG solution will lead to an increased SNR in the vessels.

H1.2: Dermal application of nitric oxide ointment will reduce lymphatic function in a manner that can be quantified with NIR lymphatic imaging. Specifically, dermal nitric oxide ointment will:

       H1.2.1: increase transport time

       H1.2.2: decrease packet frequency

       H1.2.3: decrease packet velocity.

Materials and Methods

Near-Infrared Functional Lymphatic Imaging System Set-Up

The NIR lymphatic imaging device, which is depicted in Figure 4, was developed using a 150mW 808nm laser diode (Thorlabs part no. M9-808-0150) powered by accompanying diode driver and temperature control boxes to provide excitation light. A 20° beam diffuser (Thorlabs part no. ED1-C20) was mounted in front of the diode to achieve a uniform excitation field of approximately $75cm^2$ with less than 1.9 mW/cm^2. Fluorescence emission centered at 840 nm was captured using a PIXIS 1024B back-illuminated CCD camera (Princeton Instruments) with an attached Infinity K2/SC video microscope lens (Edmund Optics) and a bandpass filter (CW:840 nm, FWHM:15 nm, Omega Optical). NIR images were recorded via a custom LabView (National Instruments) image acquisition code.
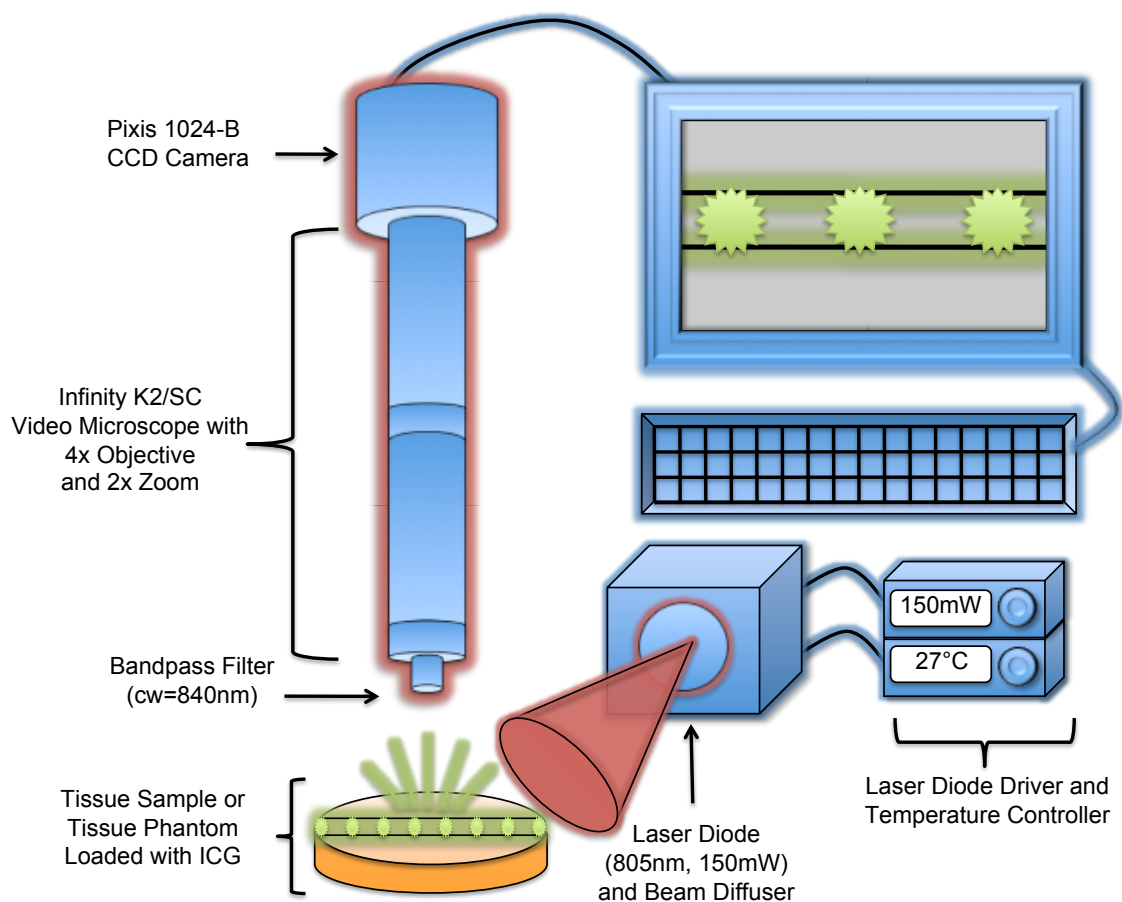
Figure 4: NIR lymphatic imaging system schematic. Excitation light is provided by 150mW 808nm laser diode powered by accompanying diode driver and temperature control boxes. Emission light centered at 840nm is captured by a CCD Camera with an Infinity K2/SC video microscope lens and a bandpass filter (CW:840 nm, FWHM:15 nm).

ICG Solution Preparation

To determine the optimal excitation and emission wavelength of ICG for use in NIR lymphatic imaging we created an albumin-physiological salt solution (APSS) (in mM: 145.00 NaCl, 4.7 KCl, 2.0 $CaCl_2$, $1.17MgSO_4$, $1.2NaH_2PO_4$, 5.0 dextrose, 2.0 sodium pyruvate, 0.02 EDTA, 3.0 MOPS, and 10g/L bovine serum albumin)(72) designed to mimic interstitial fluid and added a commonly used concentration of 250 μg/mL of ICG (Across Organics)(209) to simulate an injection of ICG into the interstitial space. For comparison purposes, the same concentration of ICG was also dissolved in 0.9% saline water. Peak excitation of both solutions was recorded using a

spectrophotometer (Hitachi U-2900) and peak emission at the previously recorded peak excitation was recorded using a fluorometer (Shimazu RF-1501).

The optimal ICG solution for maximizing fluorescence yield within the dermal layer was determined by dissolving various concentrations of ICG ranging from 0.01 μg/mL to 1000 μg/mL in 0.9% saline and in APSS solutions with albumin concentrations ranging from 0 g/L to 100 g/L. The various solutions were flowed through the tissue phantom at a depth of 2mm to simulate flow through a dermal lymphatic vessel. The vessel was imaged using the NIR system, and fluorescence intensity was recorded for each sample to determine the optimal ICG and albumin concentrations. In order to quantify the enhancement of premixing ICG with albumin, follow-up testing was performed to compare the signal to noise ratio (SNR) of the optimal ICG/albumin solution (150 μg/mL ICG + 60 g/L albumin) and ICG alone (150 μg/mL ICG) both at the injection site and 10 cm downstream in the collecting vessel, where SNR was calculated as $SNR = 20 \times \log\left(\dfrac{Fluorescence}{Background}\right)$. Functional lymphatic testing (detailed below) was also performed to verify that premixing ICG with albumin does not alter lymphatic function, as measured by transport time, packet frequency, and packet velocity.

Tissue Phantom Preparation

In order to characterize the parameters of NIR lymphatic imaging in the dermis, a tissue phantom was created with the same optical properties as the dermal layer. Mock lymphatic vessels of known diameters were created in the tissue phantom at known depths, thus affording complete control over the phantom and allowing idealized characterization of NIR imaging capabilities regarding spatial resolution and signal penetration depth. As can be seen in Figure 5, the tissue phantom was molded in a standard petri dish using a mixture of 97.52% silicone elastomer base (Sylgard 184, Dow Corning), 2.22% Aluminum Oxide (Sigma Aldrich), and 0.26% cosmetic powder (Max Factor Crème Puff Deep Beige 42) according to previously published methods(123). Channels were created in the tissue phantom molds by suspending standard copper electrical wire of known diameters at known depths in the mold prior to curing and removing the wires after curing. The tissue phantom was also connected to a syringe

pump (PHD 2000, Harvard Apparatus) to flow various ICG solutions through the mock vessels for imaging, a schematic of which is depicted in Figure 5-D.
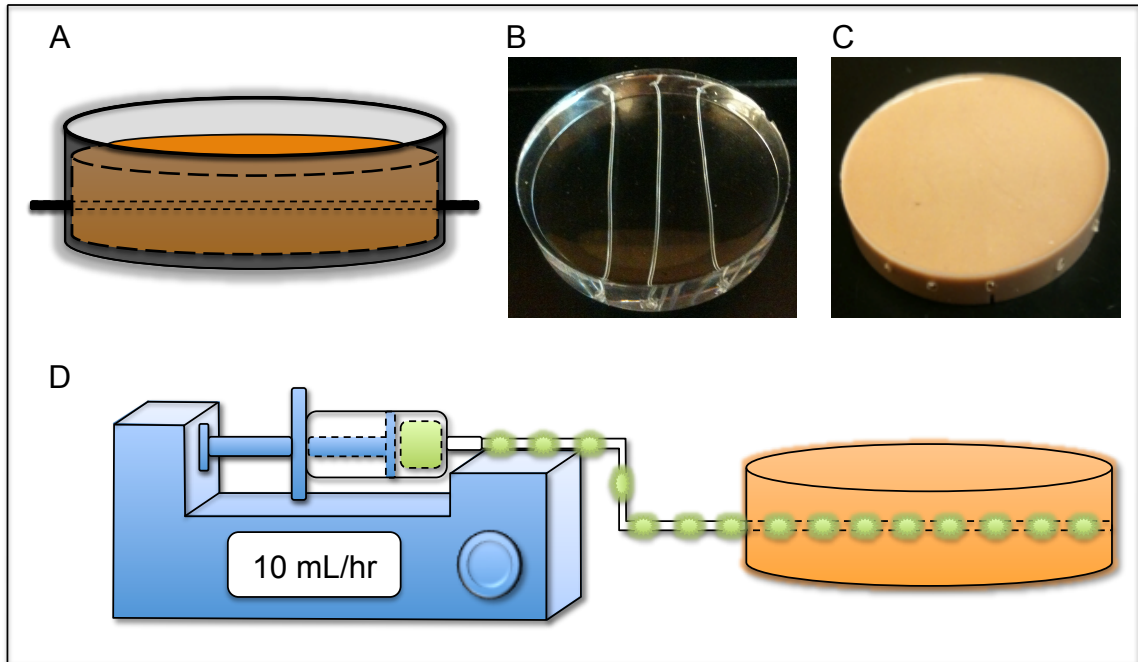
Figure 5: Tissue phantom schematic and operation. (A) Tissue phantoms were molded in standard petri dishes using a mixture of 97.52% silicone elastomer base, 2.22% Aluminum Oxide, and 0.26% cosmetic powder. Channels were created in the tissue phantom molds by suspending standard electrical wire of known dimensions at known depths. (B) Image of the resulting channels after the molds are cured and the wires are removed. This is an example image created using 100% silicone to allow visualization of the channels. (C) Image of the final tissue phantom construct in which the channel outlets can be seen protruding from the side of the phantom. (D) The tissue phantom was connected to tubing containing preloaded "packets" of ICG to test the spatial and temporal resolution of the NIR imaging system. The flow rate through the tissue phantom was precisely controlled with a syringe pump and the ICG packets were imaged as they passed through the phantom.

Sensitivity Analysis of NIR System

Mock vessels of 1mm diameter were created in a phantom at depths ranging from 1mm to 10mm in 1mm increments, the optimal ICG solution (150 μg/mL ICG, 60 g/L albumin) was loaded into each of the mock vessels, and fluorescence intensity was recorded at each depth in order to characterize the change in signal sensitivity of the NIR system as a function of depth. Vessel diameter calculations were performed at all depths

to characterize the scattering effect on apparent vessel diameter. Fluorescence intensity measurements were recorded for 4 conditions to quantify excitation light leakage: (1) CCD shutter closed (background), (2) excitation light source on without ICG in the phantom, (3) low concentration of ICG (1 μg/mL + 60 g/L albumin), and (4) ideal concentration of ICG (150 μg/mL + 60 g/L albumin).

ICG typically flows through lymphatic vessels in the form of discrete "packets"(107, 211), presumably due to valve closure that is known to occur during periods of short flow reversal, when a favorable pressure gradient exists to close the valve(50, 54). To mimic the pulsatile packet flow of ICG in lymphatic vessels, mock ICG packets were created by preloading a length of tubing with drops of ICG solution separated by olive oil (to prevent mixing of the ICG packets through diffusion). A syringe pump was then used to flow the packets of ICG through the tissue phantom at known velocities to test the accuracy of a custom lymph velocity quantification algorithm we developed. The algorithm, a similar version of which was first reported by Sharma et al. in 2007(211), utilizes line intensity profiles placed sequentially along a lymphatic vessel in the direction of flow at known distances from each other (Figure 6-A). The line intensity profiles record spikes when packets pass over that particular area (Figure 6-B), and by measuring the time between spikes in the three sequential line profiles, average velocity of packets can be calculated.
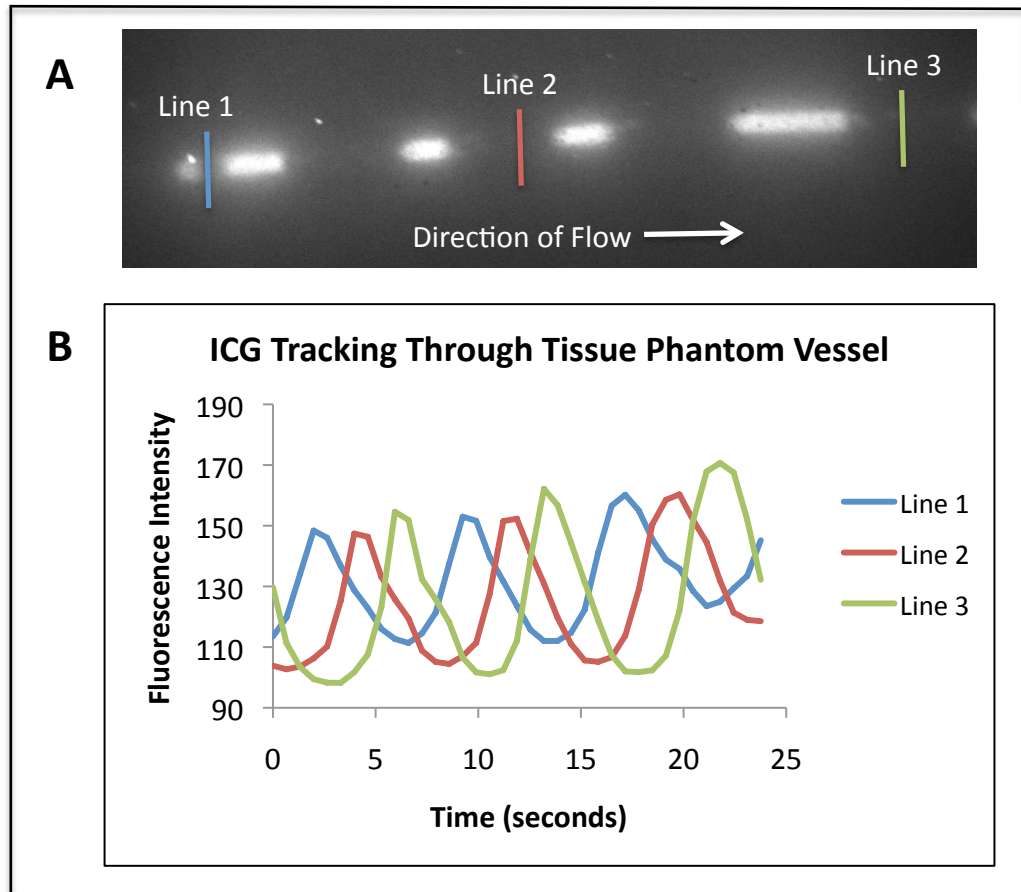
Figure 6: Quantification of ICG packet travel through tissue phantom. "Packets" of ICG were created by separating small amounts of ICG with olive oil (to prevent mixing of separate packets) in a segment of tubing connected to the tissue phantom. A syringe pump was used to precisely control the flow rate of the fluid through the tubing/tissue phantom construct. A custom code was used to process the data by calculating intensity values over three line profiles placed sequentially along the channel. (A) Example image of ICG packets flowing through the tissue phantom at a depth of 1 mm. The three lines depicted show the placement of the three line integrals used in the processing algorithm to detect fluorescence intensity. (B) Example of the fluorescence intensity plots at the three line intensity profiles over time. Peaks in fluorescence intensity correspond to packets traveling over the lines. Fluid velocity can be calculated using the known dimensions of the channel and the time intervals between packets reaching sequential line profiles.

In Vivo Imaging

Lymphatic function was quantified in vivo in the tail of six-week-old female hairless rats (Charles River Laboratories, Wilmington, MA) that were divided into a treatment group and a control group (n=3). The treatment group received a topical

application of a glyceryl trinitrate ointment (GTNO) (0.2% wt/wt, Rectogesic, Care Pharmaceuticals, commercially available), which is an ointment with an NO donor group that has previously been reported to slow lymphatic transport time(198). The control group did not receive any topical treatment. Both groups were anesthetized with an intramuscular injection of Fentanyl (0.12 mg/kg), Droperidol (6 mg/kg), and Diazepam (2.5 mg/kg given 10 minutes after Fentanyl/Droperidol). The treatment and control groups were then both given 10 μL intradermal injections of ICG (150 μg/mL ICG, 60 g/L albumin) in the tip of the tail (given 1 minute after the GTNO application for the treatment group).

The NIR lymphatic imaging system was positioned such that the excitation source and the field of view of the CCD emission detector were centered on the rats' tail 10cm downstream (towards the base of the tail) from the injection site at the tip of tail. The animals were imaged continuously from the time of injection until 20 minutes post-injection with a camera exposure time of 0.05 seconds. To evaluate lymphatic function in each of the rat subjects, three parameters were measured: the time necessary for the bolus injection of ICG to travel the 10 cm distance from injection site to emission recording site (transport time), the average velocity of the packets traveling through the field of view of the recording site, and the average frequency of packets passing through the field of view. The transport time was calculated as the time between ICG injection and the arrival of fluorescence in the field of view 10 cm downstream from the injection site. The arrival of fluorescence was defined as a 20% increase in fluorescence intensity in the collecting vessel. A plot of fluorescence intensity over time during fluorescence arrival can be seen in Figure 7.
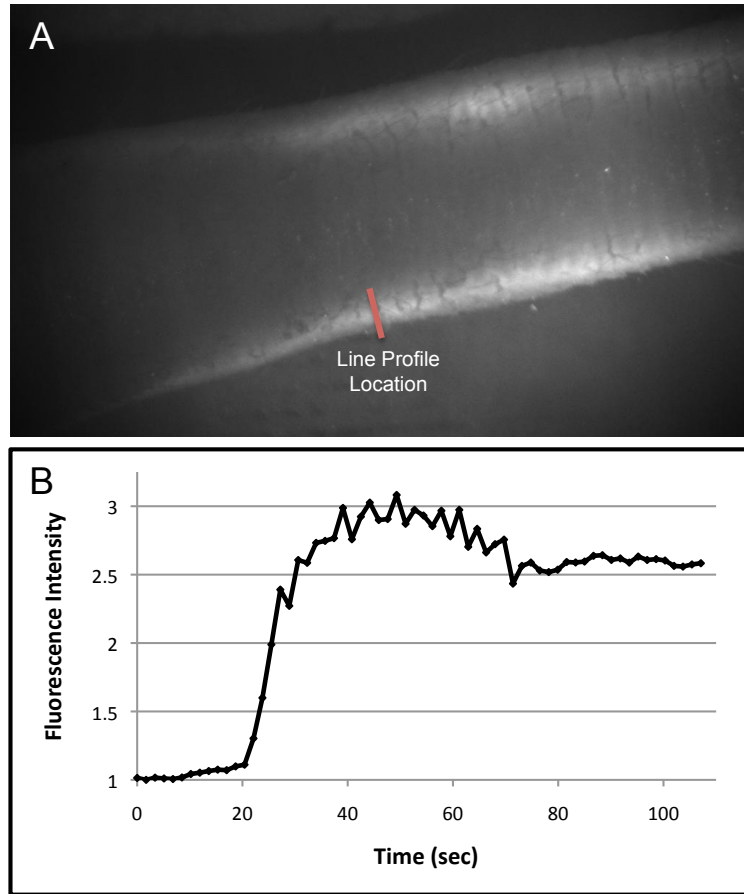
Figure 7: Fluorescence intensity over time during fluorescence arrival. (A) Image showing location of line profile for fluorescence arrival example. (B) Example plot of intensity versus time during arrival of fluorescence.

Packet frequency and velocity were measured using plots of fluorescence intensity over time generated from two regions of interest (ROIs) in a collecting vessel. ROIs were placed approximately 3-6 mm apart in regions of the vessel exhibiting large fluctuations in fluorescence intensity over time, where packet movement could easily be visualized and quantified. Packet frequency and velocity measurements began 10 frames after the arrival of fluorescence (to allow fluorescence values to stabilize) and measured for a duration of 10 packets. Of the two vessels in the tail, measurements were taken only on the vessel first producing fluorescence. Average packet frequency was calculated as 10 packets divided by the time necessary for 10 packets to occur (in minutes). Average packet velocity was calculated as the distance between the two ROIs divided by the average time necessary for packets to travel between the two ROIs (as indicated by peaks in the intensity plots). Figure 8 shows control and GTNO treatment

examples of ROI selection and intensity versus time plots of the 10 packets used for frequency and velocity measurement.
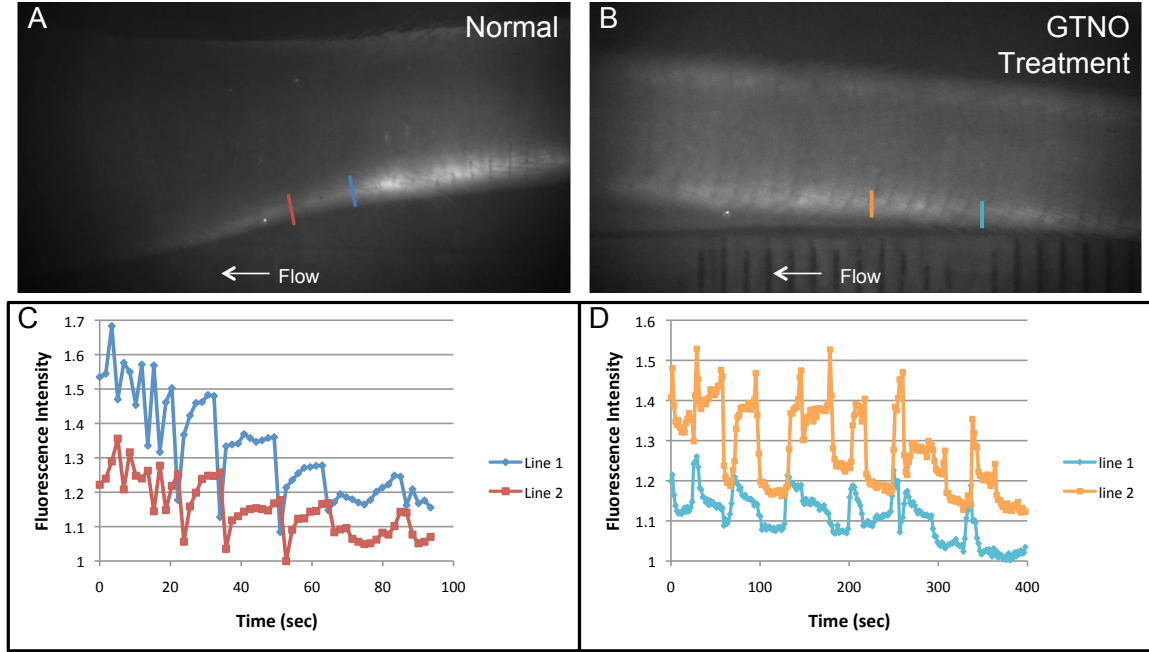
Figure 8: Example intensity plots over time for normal and GTNO treatment conditions. (A) Image showing location of line profiles for normal condition example. (B) Image showing location of line profiles for GTNO treatment condition example. (C) Example plot of intensity versus time for normal condition. (D) Example plot of intensity versus time for GTNO treatment condition.

To calculate the average delay time between contractions we wrote a Matlab script that analyzes a given video sequence to find the region of highest fluctuation within the vessel. The fluorescence in this region was then quantified as a function of time and that signal was processed by the code to calculate the average number of frames for each interval in which there was no fluorescence fluctuation. This value was multiplied by the time interval between frames and reported as the average delay time, t_d, for that vessel.

The data for each of the three functional imaging parameters was averaged for the treatment and control group, subsequently checked for normality using the Anderson-Darling test, and analyzed for statistical significance using a 2-sample t-test.

Quantifying Lymphatic Function Parameters

We sought to define a term describing the average length a packet of fluid would travel between contraction events (referred to as the effective contraction length, L^*) as a metric of lymphatic function that could be calculated from parameters obtained with our

41

system. Briefly, the time, t, it would take for the bolus injection to travel 10 cm along the tail is governed by the following equation: $t = \dfrac{1}{f}\dfrac{10\ \text{cm}}{L^*}$, where f is the average frequency of contraction events. Knowing the rate of contraction events and the average time it takes for the moving front to reach a fixed distance allows us to estimate the average length each contraction event transports the fluid.

Each contraction event is composed of a delay time and a contraction time in which the vessel is actively moving the fluid along the contraction length L^*: $\dfrac{1}{f} = t_{L^*} + t_d$. From this equation we can estimate t_{L^*} given that we calculate the other two parameters from the image analysis. We also sought to develop a method for describing the systolic pumping power of the vessel from parameters measured by our system. During a contraction event the fluid packet accelerates to a maximum velocity and then decelerates back to rest, having traveled a distance L^* over the entire cycle. If we assume that these two events are split evenly over this cycle, then the distance traveled by the packet during the systolic phase is $L^*/2$. To estimate the acceleration of the fluid packet during the systolic phase we divide the average maximum packet velocity (which is measured as described above), V_p, by the duration of systole, which we estimate as $t_{L^*}/2$. From these approximations the systolic pumping power can be estimated as $P_s = \left[m\dfrac{V_p}{t_{L^*}/2}\dfrac{L^*}{2}\right]\dfrac{1}{t_{L^*}/2}$,

where m is the mass of the fluid packet. While we do not know m, we can report the parameter $\left[\dfrac{V_p}{t_{L^*}}L^*\right]\dfrac{1}{t_{L^*}/2}$ as the average systolic pumping power per unit mass.

Characterization of Packets in Isolated Vessels and In-Vivo

Two experimental setups were used to help characterize packets, as they appear in collecting vessels in-vivo. In the first setup, mesenteric collecting vessels were excised from Sprague Dawley rats (Charles River Laboratories, Wilmington, MA) and were cannulated and pressurized in a living system chamber according to previously published methods(72). A solution containing the commercially available fluorophore LI-COR IRDYE 800CW PEG (LI-COR Biosciences, Nebraska, USA) diluted to 10% of the

42

manufacturer's recommended concentration for lymphatic imaging was flowed through the vessel. Images were taken in brightfield to record vessel contraction and in NIR to observe transport of the dye through the vessels. The purpose was to assess the relationship between the appearance of packets and contractions of the vessel.

The second experimental setup to characterize packets utilized in-vivo NIR imaging with the skin removed. In-vivo NIR imaging was performed as detailed above with the exception that the imaging was performed in the forelimb and the injection was given in the footpad. Once fluorescence arrived in the collecting vessels downstream from the injection site, images were taken with the skin on and with the skin off to determine the effect of skin on the appearance of packets.

Results

ICG Spectrum and Fluorescence

The excitation peaks for ICG dissolved in saline and APSS were approximately 785 nm and 805 nm respectively while the emission peaks of ICG in saline and APSS were approximately 815nm and 840nm respectively (Figure 9).
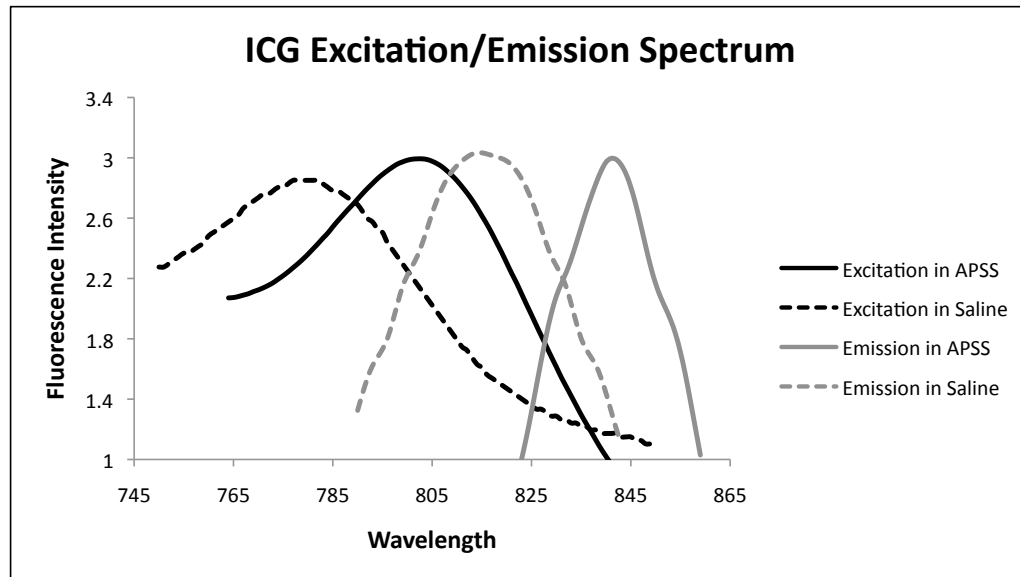
Figure 9: ICG dissolved in albumin salt solution (APSS) exhibits a shift in the excitation/emission spectrum. Excitation and emission curves were generated for ICG (250 μg/mL) dissolved in 0.9% saline (dotted lines) and APSS (solid lines). A shift of approximately 20 nm was observed in the excitation spectrum of ICG dissolved in APSS versus saline, with peak fluorescence occurring at 805

nm and 785 nm respectively. A shift of approximately 25 nm was observed in the emission spectrum of ICG dissolved in APSS versus saline, with peak fluorescence occurring at 840 nm and 815 nm respectively. These spectra guided the design of excitation and emission detection wavelengths of the NIR imaging system.

ICG fluorescence was highly dependant on albumin concentration and the intensity reached a maximum at an albumin concentration of 60 g/L (902.8 μM) (Figure 10-A), and the maximum fluorescence yield at this albumin concentration was produced at an ICG concentration of 150 μg/mL (193.5μM) (Figure 10-B). Thus the solution producing maximal fluorescence was 150 μg/mL ICG and 60 g/L albumin. When injected into a rat tail, premixing 150 μg/mL ICG with 60 g/L albumin produced a greater SNR as compared to 150 μg/mL ICG alone with more than a four-fold increase in SNR observed in the collecting vessels (Figure 10-C) ($p<0.05$). Additional functional lymphatic testing was performed in response to ICG and ICG/albumin injections, and no significant differences were observed in transport time, packet frequency, or packet velocity (Figure 11).
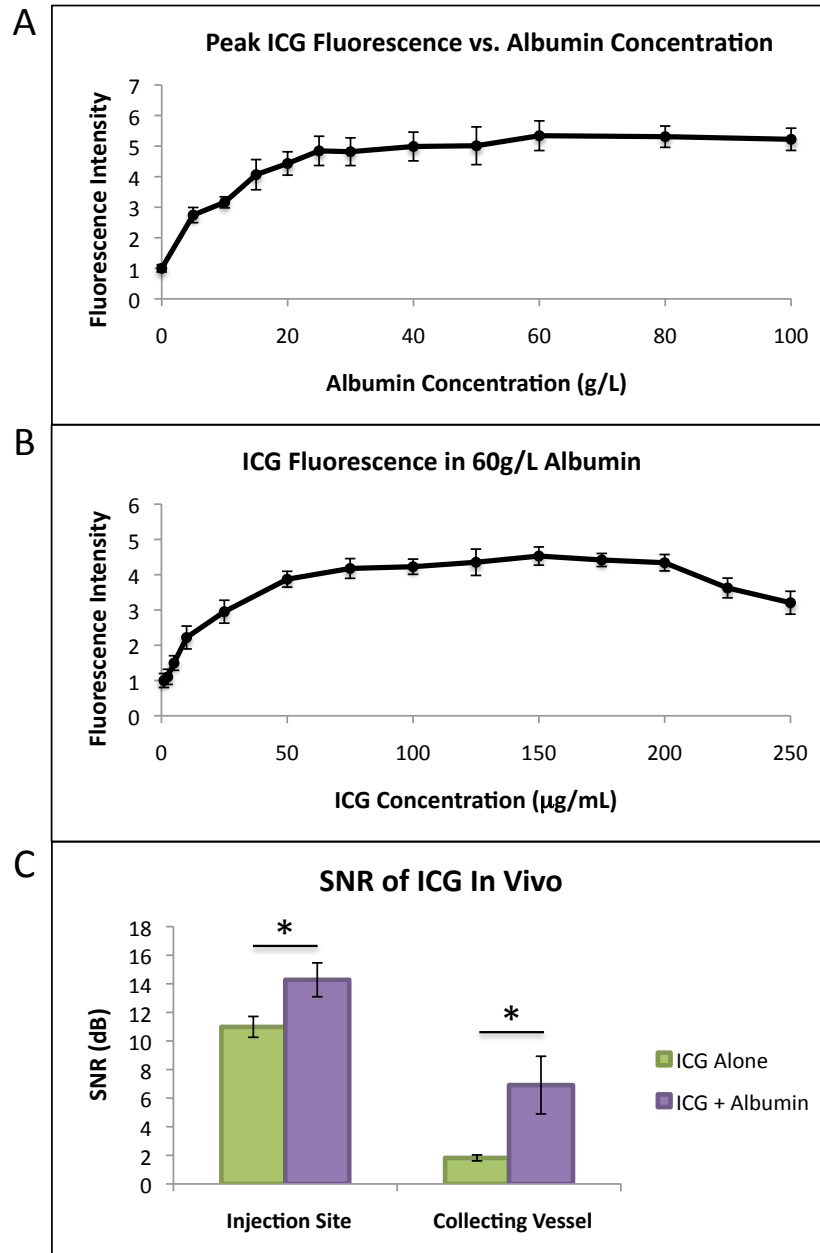
Figure 10: Pre-binding ICG with albumin enhances fluorescence and the resulting SNR upon in vivo intradermal injection. Fluorescence intensity through the phantom at a depth of 2 mm was measured for various concentrations of ICG and albumin to optimize the two concentrations to produce maximum fluorescence intensity of the ICG solution. (A) Peak ICG fluorescence intensity was measured as a function of albumin concentration in APSS ranging from 0 g/L albumin to 100 g/L albumin. Peak ICG fluorescence was produced at 60 g/L albumin. (B) Fluorescence intensity of ICG dissolved in 60 g/L was measured as a function of ICG concentration to determine the final concentrations of the optimal ICG solution for producing maximum fluorescence intensity. Maximum fluorescence intensity was measured at an ICG concentration of 150 µg/mL. (C) 150

μg/mL ICG solution and 150 μg/mL ICG premixed with 60g/L albumin were injected into rat tails and the signal to noise ratio (SNR) was calculated for each sample at the injection site and 10 cm downstream in the collecting lymphatic vessel. ICG premixed with albumin produced greater than a four-fold increase in SNR compared to ICG alone from 1.8dB to 7.8dB in the collecting vessels and an increase from 10.9dB to 14.2dB at the injection site. Error bars represent standard deviation. *=p<0.05.
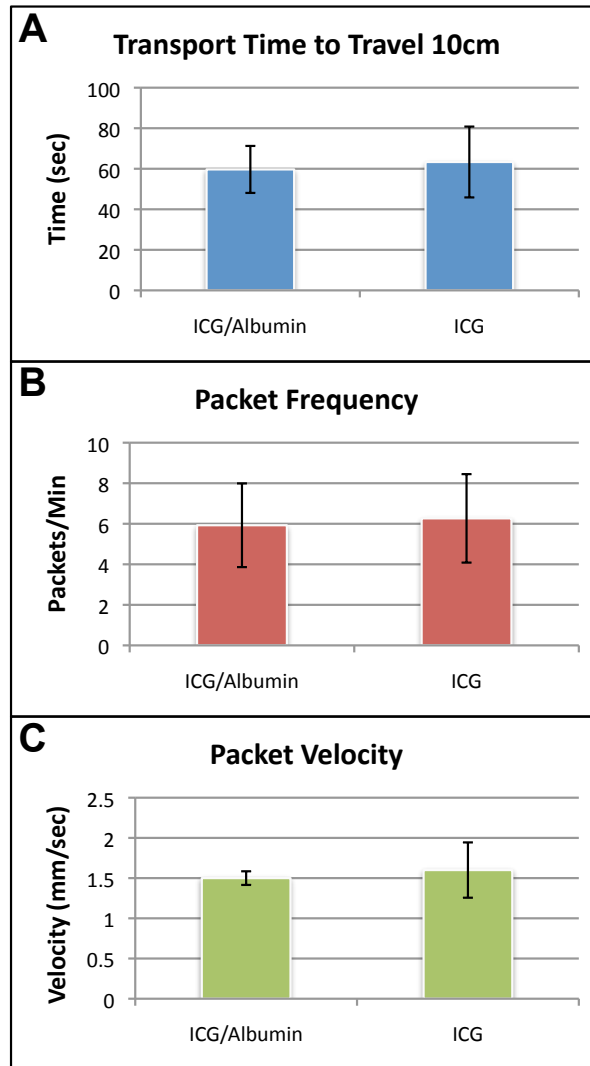
Figure 11: Pre-mixing ICG with albumin does not alter lymphatic function compared to ICG alone. Results of functional lymphatic testing reveal no significant differences between injection of ICG alone and ICG + albumin in the tails of rats (n=3). (A) No significant difference in transport time to travel 10 cm. (B) No significant difference in packet frequency. (C) No significant difference in packet velocity.

Tissue Phantom Sensitivity Analysis

The minimum detectable concentration of ICG at 2mm depth was 0.1 μg/mL, and ICG emission was detectable as deep as 6 mm with the signal at depths below 7 mm being indistinguishable from background (Figure 12). Quantifying excitation light leakage showed a 4-fold increase of signal over the thermal noise background. However, even low ICG concentrations produced a signal much larger than that due to leakage and values of fluorescence typically seen in the vessel in vivo have fluorescence intensity values 14 fold greater than the excitation light source (Figure 13). Vessel diameter calculations were very accurate at a depth of 1mm with a 0.74% error, but error increased with depth to 1095.06% error at 5mm and was incalculable beyond 5mm due to excessive scattering. The results also show that the calculated velocities were within 1% of the true velocities over a range from 0.15 – 1.5mm/s (Figure 14).
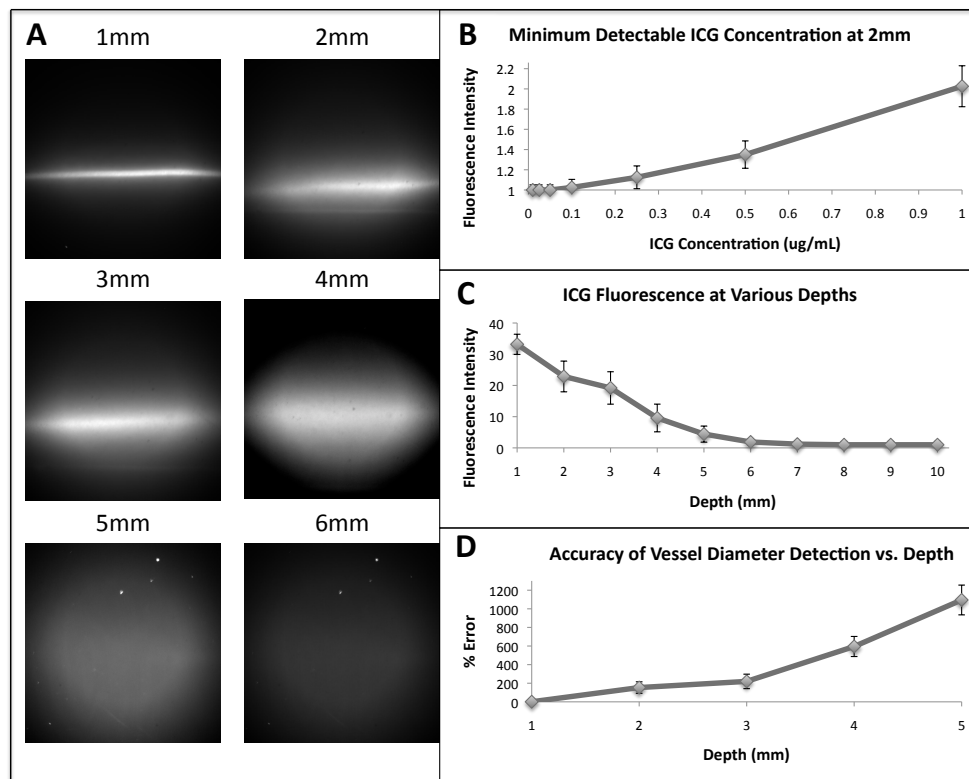
Figure 12: ICG can be detected up to a depth of 6 mm with minimal loss of spatial resolution at a depth of up to 3 mm. The optimal concentration of ICG solution (150 μg/mL ICG, 60 g/L albumin) was flowed through the tissue phantom at depths between 1 mm and 10 mm in 1 mm increments to determine how signal sensitivity changes with depth. (A) Example images of ICG flowing through

the tissue phantom from 1 mm to 6 mm, which was the depth limit of detection. (B) Plot of minimum detectable ICG concentration at 2 mm depth in the tissue phantom. Minimum detectable ICG concentration was 0.1 μg/mL. (C) Plot of ICG fluorescence intensity as a function of depth showing fluorescence intensity decreased successively with depth until 7 mm, which was indistinguishable from background. The depth limit of signal detection was 6 mm. (D) The apparent diameter of the channels at each depth was measured and compared to the true diameter of the channel to determine the accuracy of vessel diameter detection as a function of depth. At 1 mm there was a 0.74% error between the true diameter and the measured diameter. Percent error increased with depth to a maximum of 1095.06% error at 5 mm.
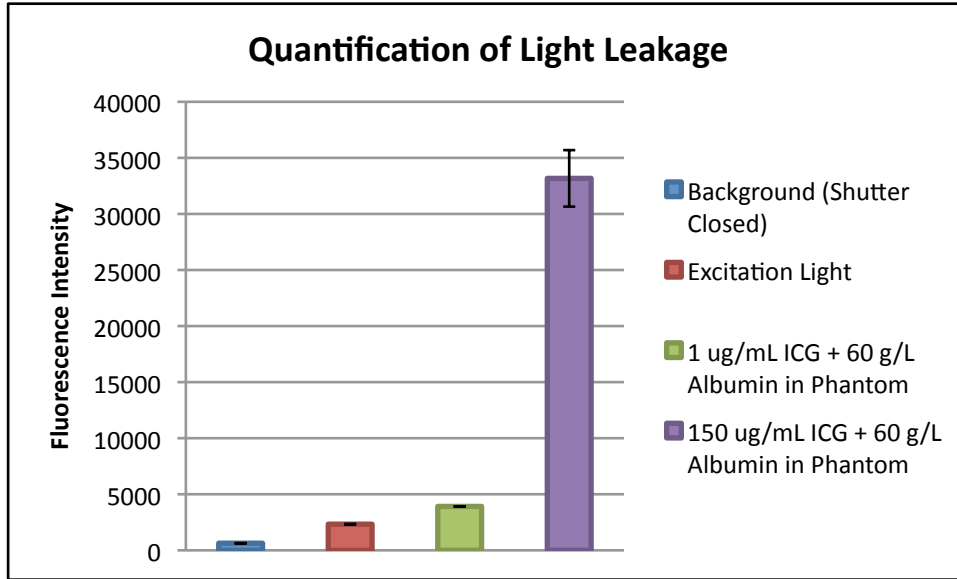
Figure 13: Characterization of excitation light leakage. Intensity values were quantified for 4 conditions: (1) CCD shutter closed (background), (2) excitation light source on and phantom present without ICG, (3) low concentration of ICG in tissue phantom (1 μg/mL + 60 g/L albumin), and (4) ideal concentration of ICG (150 μg/mL + 60 g/L albumin). The results show that the excitation light produces a 4 fold increase in intensity over background, but the ideal concentration of ICG produces a 14 fold increase in intensity over the excitation light source, which corresponds to a SNR of 23.1.
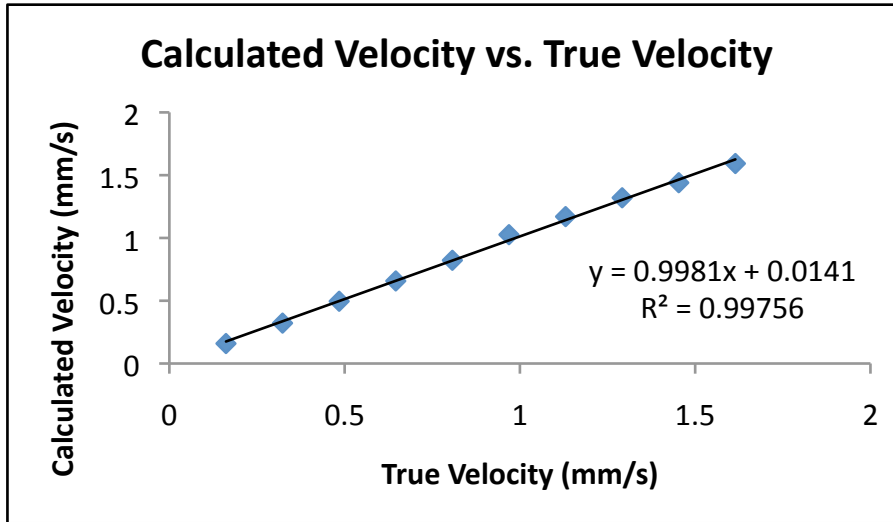
Figure 14: Calculated packet velocity predicts true velocity with less than 1% error. Packets were flowed through the tissue phantom at a depth of 3 mm at velocities ranging from 0.15 – 1.5 mm/s. Velocities were calculated using a custom algorithm and compared to the known true velocities. Calculated velocities were accurate to within less than 1% error.

Quantifying Functional Effects of NO on Lymphatics In Vivo

Application of GTNO significantly reduced lymphatic function (Figure 15). Transport time increased from 60 seconds under normal conditions to 414 seconds after GTNO application ($p < 0.01$). Packet frequency decreased from 5.92 packets per minute and under normal conditions to 3.1 packets per minute after GTNO application ($p < 0.05$). Packet velocity decreased from 1.50 mm/sec under normal conditions to 0.48 mm/sec after GTNO application ($p < 0.05$). GTNO application decreased effective contraction length from 17.6 mm to 5.1 mm ($p < 0.0005$). Contraction duration after GTNO application was significantly increased from 4.1 sec to 5.4 sec ($p < 0.05$) and systolic pumping power per unit mass was drastically reduced after GTNO application from 1.25 mm^2/s^3 to 0.024 mm^2/s^3.
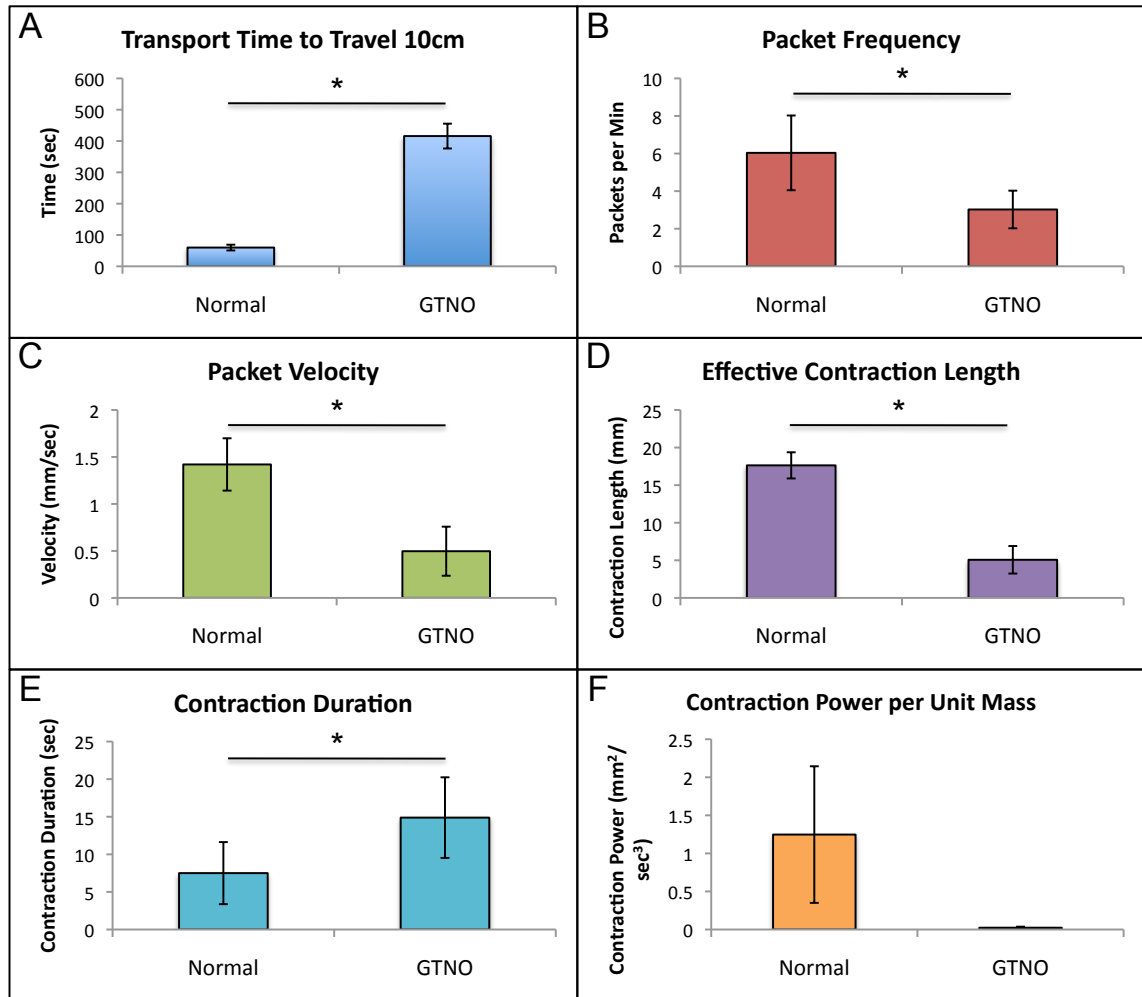
Figure 15: Dermal nitric oxide delivery significantly reduces lymphatic pump function. 10μL of ICG (150μg/mL ICG, 60g/L albumin) was injected intradermally into the tip of the tail hairless rats divided into a treatment group that received a topical application of glyceryl trinitrate ointment (GTNO) prior to ICG injection (n=4) and a control group that did not receive any treatment prior to ICG injection (n=4). The NIR lymphatic imaging system was positioned to view the tail 10 cm downstream (towards the base of the tail) from the injection site. (A) The time required for the initial bolus injection of ICG to travel 10 cm downstream (transport time) significantly increased after GTNO application. (B) Packet frequency was significantly reduced after GTNO application. (C) Packet velocity was significantly reduced after GTNO application. (D) Effective contraction length was significantly decreased after GTNO application. (E) Contraction duration was significantly increased after GTNO application. (F) Contraction power per unit mass was decreased after GTNO treatment. *=p<0.005.

Vessel Contraction Creates Packets

The isolated vessel setup revealed that vessel contraction caused the appearance of packets in NIR imaging (Figure 16). As the vessel constricts below a certain threshold, the amount of fluorophore in the local region is too low to be detected with NIR imaging. Comparing vessel contraction dynamics under brightfield to the appearance of packets in NIR imaging reveals that the two phenomena are perfectly in sync. Furthermore, the in-vivo skin flap experiment revealed that areas of NIR dye stagnation occur immediately downstream (proximal) from the valve regions in the sinus of the lymphangions (Figure 17). The sinuses are almost always visible under NIR, but the remaining segments of the vessel are only visible when it is dilated above a certain threshold.
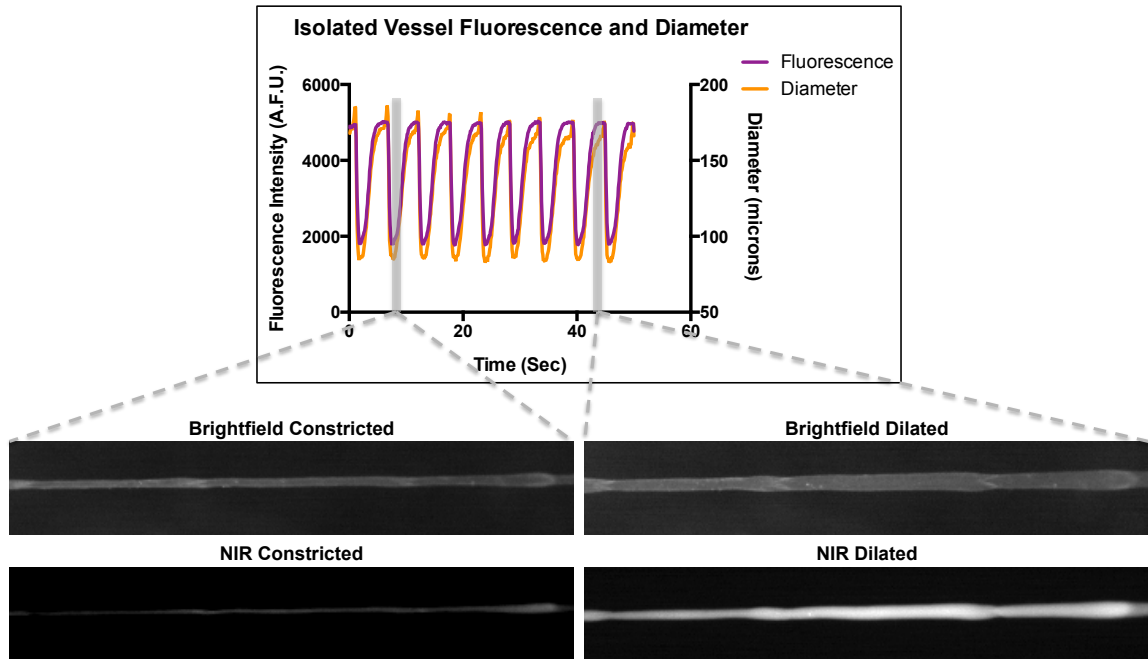
Figure 16: Example plot and representative images of NIR and brightfield imaging of an isolated vessel. Contraction dynamics are in sync with fluorescence intensity indicating that packets are created by the contraction and dilation of the vessels.
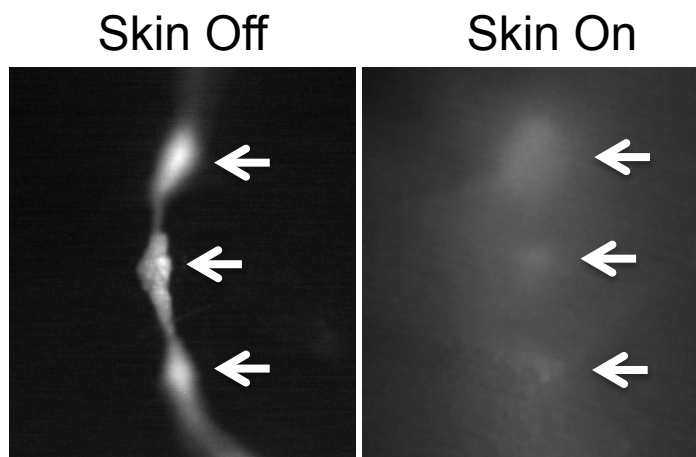
Skin Off   Skin On

Figure 17: Example NIR image with the skin off and the skin on. The image on the left shows NIR dye flowing through the collecting vessel of a rat forelimb with the skin removed. Dye can be seen pooling in the sinus regions of the vessel, but the entire length of vessel is fluorescent. The image on the right shows the same vessel with the skin on. The fluorescent signal is much weaker and more scattered, and fluorescence is only directly visible in the areas corresponding to the sinus regions, where more fluorophore accumulates. White arrows indicate the three sinus regions in each image.

Discussion and Conclusions

Effects of Protein Binding on ICG Fluorescence

The NIR lymphatic imaging system that we developed in this study represents a departure from the setup of many of the NIR lymphatic imaging systems previously reported in that we pre-mixed ICG with albumin, and our system used an excitation wavelength of 808 nm and emission wavelength centered at 840 nm(180, 248). Previous systems have used excitation sources of 785 nm, presumably because of the large availability of diodes at this wavelength. Our results indicate that ICG produces more than a three-fold increase in fluorescence when it binds to albumin, and the peak excitation and emission wavelengths are 805 nm and 840 nm respectively. The same effect is observed when ICG is introduced in APSS, thus suggesting that ICG binds to albumin in the interstitial space. Therefore, ICG-based NIR lymphatic imaging systems that excite at 808nm and capture emission centered at 840 nm will achieve higher SNR.

ICG has previously been shown to rapidly and completely bind to albumin in plasma(39). Given that albumin concentration in the interstitium is approximately half of

its concentration in plasma(67), and the albumin concentration in lymph has been measured to be about 40% of its value in plasma(140), it is reasonable to assume that all of the ICG present in lymph is bound to albumin as well. This assumption is further justified by the fact that the molecular weight of ICG (775 daltons) does not preclude it to lymphatic partitioning. Thus, the preferential uptake of ICG into lymphatics that is observed following dermal injections suggests that it must be bound to something of a much larger size. Since albumin is the most prevalent soluble protein in the interstitium, is preferentially taken up into lymphatics after a dermal injection, and binds readily to ICG, it follows that even after dermal injection of ICG alone, the dye in the lymph is bound to albumin. Pre-mixing ICG with albumin prior to injection thus not only increases the fluorescence of the dye, but it also eliminates interstitial albumin availability as a limiting factor in ICG uptake into lymphatics.

This approach to ICG delivery could be of particular importance when using this imaging technique in pathologies such as lymphedema, as the disease often results in accumulation of macromolecular proteins in the interstitium(187) that could significantly influence the uptake of injected ICG, confounding the interpretation of the experimental data. It is important to note that the injection of 10 μl of 60 mg/ml albumin solution, while a very small volume, will disrupt the local gradients governing plasma filtration, temporarily increasing fluid extravasation from the blood and thus lymph formation. However, these values are well within the range of what the lymphatics would be expected to resolve during a mild inflammatory event as average flow rates in a collecting lymphatic of fasted rats have been reported to range from 40 nl/min to 200 μl/min depending on the vessel size and state of hydration(54, 246).

It should be noted that Ashitate et al. recently reported that ICG alone was a better fluorophore for lymphatic visualization in the thoracic duct than ICG pre-bound to albumin(12), but there are several differences in experimental setup and technique worth exploring. Firstly, the NIR imaging system they employ excites at 760 nm while our system is optimized to excite ICG bound to albumin, which is maximally excited at 805 nm. Their experimental setup also does not require imaging through the dermis, and thus, does not have to account for scattering and absorption effects since most scattering and absorption occurs in the dermis. Interestingly, Ashitate and colleagues report a SNR

for ICG of about 2, which is very similar to our results for ICG in collecting vessels. Given that we also report a SNR of nearly 8 for ICG bound to albumin in collecting vessels, we are confident pre-binding ICG to albumin provides a more fluorescent tracer. Translating this technique into the clinic will produce additional regulatory challenges, but premixing the dye with autologous serum prior to dermal injection could provide one route of protein-bound ICG delivery.

Tissue Phantom Sensitivity Analysis

The tissue phantom was constructed to recapitulate characteristics of lymphatic vessels in vivo that are essential to parameters historically quantified in NIR imaging, such as vessel morphology and propulsion frequency and velocity. Specifically, we constructed channels of similar size to lymphatics and embedded them in a phantom with effective absorption and scattering coefficients of skin at depths characteristic of dermal lymphatics in vivo. According to our tissue phantom sensitivity analysis, the NIR lymphatic imaging system was capable of detecting ICG fluorescence as deep as 6 mm. However, scattering effects resulted in a deterioration of spatial resolution with increasing depth, and geometric vessel features became difficult to accurately identify below a depth of 3 mm. These results suggest that the NIR lymphatic imaging system is best used to detect vessel geometry and architecture above a 3 mm depth, but an assessment of gross ICG accumulation and transport in vivo can be obtained as deep as 6mm (or perhaps deeper if features being resolved are greater than 1 mm, such as lymph nodes). Given that the average human skin layer is between 1 mm and 3 mm thick(239), these imaging characteristics are well-suited for imaging dermal lymphatic function. However, clinically lymphatic diseases often result in a severe remodeling of the dermis, and fibrosis and lipid deposition can increase the thickness of the dermis well beyond this 3 mm limit(187).

In addition to chronic lymphedema resulting in a thickening of the dermis, it is likely that the optical properties of the tissue itself would change as the angiogenesis, adipogenesis, and fibrosis often associated with lymphedema would change the absorption and scattering coefficients of the dermal layer. Therefore, care should be taken in interpreting clinical data from ICG injections in patients with lymphatic disease as the

appearance of "hyperplatic" or "dilated" lymphatics could be due in part to changes in the thickness and the optical properties of the diseased limb, thus increasing the apparent diameter of vessels in these patients. Future studies are warranted to determine how exactly these changes would effect the ability of NIR imaging to assess lymphatic function in diseased patients.

The primary tool in functional ICG imaging is the ability to quantify the kinetics of packet flow in lymphatic vessels in vivo, which we have shown for the first time occur due to the contraction of the vessels in coordination with lymphatic valves creating the appearance of segmented flow of the dye. Sinus regions appear constantly fluorescent while the remainder of the lymphangion only appears fluorescent during dilation periods, and although fluorescent values fluctuate in both segments of the lymphangion as packets travel along the vessel, the greatest changes in fluorescence occur between the sinus regions. While our phantom does not contain these valves or the intrinsic mechanics that promote lymph transport, we have artificially reproduced this packet flow at a physiologically relevant depth in the phantom to quantify our system's accuracy for measuring packet velocity in the presence of a scattering dermal layer and have demonstrated excellent accuracy in measuring velocity. Most NIR lymphatic imaging is performed giving an intradermal ICG injection and monitoring transport through dermal collecting vessels, which we have validated can be achieved with our device with a high degree of accuracy. Future work to enhance the device should focus on the implementation of diffusion theory (e.g. using a Monte Carlo approach to predict light propagation through a tissue of known optical properties) to predict scattering effects and recreate a more accurate image of vessel geometry at various depths(131).

Quantifying Functional Effects of NO on Lymphatics In Vivo

In this study we showed for the first time that immediate changes in lymphatic function resulting from the introduction of NO can be detected using non-invasive NIR lymphatic imaging. Our findings, that GTNO significantly reduces lymphatic transport, corroborates existing knowledge that NO has an inhibitory effect on lymphatic pump function(72, 114, 198). We have shown that NIR lymphatic imaging can provide real-time in vivo measurements of lymphatic pump function in response to NO, which has

never previously been available, and may help to further elucidate the relationship between NO and lymphatic contractile regulatory mechanisms. The ability to measure this response non-invasively would be particularly useful given recent findings that certain immune cells migrate to the lymphatics and release NO as a means of regulating local lymphatic draining(114).

The gold standard for quantifying lymphatic pump function has been to utilize diameter tracking of contracting vessels to calculate parameters such as stroke volume and ejection fraction. These temporal traces of diameter changes have been achieved in isolated vessel preparations(71, 72), invasive in vivo intravital brightfield microscopy(26, 54), and more recently through invasive intravital fluorescence microscopy using vessels filled with FITC labeled dextran(114). All of these approaches require invasive surgery to access and visualize the lymphatics, thus allowing for accurate diameter tracings. While the approach reported here has the advantage of being non-invasive, the scattering effects of the dermal layer and the lower frame rates do not currently provide the necessary spatial and temporal resolution to achieve accurate diameter tracings, which explains why this and other NIR lymphatic imaging systems have been unable to quantify these more traditional metrics of pump function. Thus we sought to define quantitative metrics of pump function similar to these parameters that could be calculated from our system, namely effective contraction length and systolic pumping power.

Effective contraction length describes, on average, how far a packet of fluid would travel down the lymphatic vessels before another contraction event is needed. Stronger contractions would propel fluid further (assuming that the immediate downstream valves are open), when compared to weaker contractions with lower ejection fractions. Systolic pumping power provides an estimation of the average power generated per unit mass by lymphatic pumping. A calculation of the actual power would require knowing the mass of the fluid packet, but this is difficult to estimate since accurate diameter measurements are difficult to achieve given the limitations of NIR imaging discussed above. It is likely that this mass would be different between treatment groups since it is known that NO increases the vessel diameter(72). However any changes that would occur in packet mass due to vessel dilation would be small (~2-fold increase) when compared to the changes seen in the power per unit mass parameter (~50-fold

56

decrease). Both of the new parameters developed here demonstrate the potential to describe remarkable differences in lymphatic pump function that could be difficult to capture when tracking packet frequency or velocity alone.

Our findings also have the potential to establish NIR lymphatic imaging as an early-stage lymphatic disease diagnostic. To date, NIR imaging has been reported in the literature to be capable of identifying differences in lymphatic pump function between healthy states and several late-stage disease states(128, 209, 247). However, given that most lymphatic disorders are characterized by a progressive deterioration of lymphatic pump function prior to the presentation of clinical manifestations, NIR imaging may be capable of detecting changes in lymphatic pump function in the very early stages of the disease before visible symptoms begin to present. Our findings suggest that NIR imaging is very sensitive to detecting differences in lymphatic transport function and could be used as a screening mechanism for patients at a high-risk for developing lymphatic disorders, such as post-mastectomy breast cancer patients. In this way, corrective measures could be taken before irreversible tissue damage would occur, thus improving patient outcomes with lymphatic diseases.

CHAPTER 3: DIFFERENTIAL TRANSPORT FUNCTION OF LYMPHATIC VESSELS IN THE RAT TAIL MODEL AND THE LONG-TERM EFFECTS OF INDOCYANINE GREEN

Near-infrared (NIR) imaging has emerged as a novel imaging modality for assessing lymphatic function in vivo. While the technique has provided quantitative data previously unavailable, questions remain in regards to the spatiotemporal capabilities of the approach. We address three of the more important issues here using the rodent tail, one of the most widely utilized in vivo model systems in the lymphatic literature. Specifically we demonstrate 1) the transient vs. steady state response of lymphatics to tracer injection, 2) the functional characteristics of multiple collecting vessels draining the same tissue space in parallel, and 3) the long-term consequences of fluorescent tracers on lymphatic function to repeated functional measurements.

Rat tails were imaged with NIR and metrics of function were calculated for both collecting vessels that drain the tail. A nitric oxide donor cream (GTNO) was applied to the tail. Additionally, two different NIR dyes, indocyanine green (ICG) and LI-COR IRDye 800CW PEG, were utilized for function imaging at the time of initial injection and at 1, 2, and 4 week follow-up time points after which both draining lymph nodes were harvested.

Significant differences were found between the two collecting vessels such that the vessel first showing fluorescence (dominant) produced enhanced functional metrics compared to the second vessel (non-dominant). GTNO significantly reduced lymphatic function in the non-dominant vessel compared to the dominant. ICG remained visible in the tail for 2 weeks after injection and was accompanied by significant losses in lymphatic function and enlarged draining lymph nodes. The Licor tracer also remained visible for 2 weeks. However, the dye produced significantly lower effects on lymphatic

function than ICG, and lymph nodes were not enlarged at any time point, suggesting that this may be a more appropriate contrast agent for longitudinal lymphatic imaging.

Introduction

The lymphatic vasculature is present in nearly every tissue of the body to serve essential functions in fluid homeostasis (57, 156), immune cell trafficking (230, 265), and lipid transport (56), and it has been implicated in the progression of several diseases (189, 240). Despite the critical roles that this system performs, very little is known about the lymphatic vasculature in comparison to the blood vasculature, which can be attributed, in part, to the historic difficulty associated with imaging lymphatic vessels(212). With the growing interest in studying lymphatics, near-infrared (NIR) imaging has emerged as a novel lymphatic imaging modality to simultaneously improve spatial resolution to visualize small initial lymphatics and increase temporal resolution to capture the dynamic lymphatic pump function responsible for fluid propulsion.

To date, NIR lymphatic imaging has produced exciting results quantifying lymphatic transport (181), illustrating differences in lymphatic architecture between normal and severe disease cases (247), showing differences in function and architecture due to genetic mutation (34), and assessing changes in lymphatic function in response to various manipulations (29, 268). However, the technique remains immature, and the field is still learning to understand and interpret the wealth of data NIR functional lymphatic imaging can uniquely provide compared to other modalities. In particular, recent work has suggested functional differences between two collecting vessels in a rodent hind limb (171), but no studies have specifically examined the differential transport abilities of multiple collecting vessels draining a single tissue space. Such an analysis is a necessary advancement of NIR functional lymphatic imaging, which has historically focused on quantification of only a single vessel, to better understand the physiology of draining lymphatic networks at the tissue level.

Therefore, we have chosen to simultaneously characterize the two collecting vessels in the rat tail model using NIR lymphatic imaging. The rat tail provides the simplest model of lymphatic network drainage for NIR imaging purposes due to the

59

simple geometry and the consistent position of the two collecting vessels. Using the rodent tail also allows comparisons to many previous studies as it has been one of the most widely used models in lymphatic research, providing insight into basic lymphatic physiology and lymph flow (111, 268), lymphangiogenesis (30, 42, 78, 276), and lymphedema pathology (195, 237, 279). The results of this characterization will establish a framework by which future lymphatic research can be performed using NIR imaging in the tail model and will enhance our understanding of differential vessel function.

Additional controversy also remains regarding the most appropriate fluorophore for NIR lymphatic imaging. Some studies are beginning to explore novel probes with higher quantum yields that specifically target lymphatic vessels (47, 171, 173), but the most commonly used probe to date has been indocyanine green (ICG). Despite the low quantum yield of the molecule, ICG remains the hallmark of NIR lymphatic imaging because it is FDA approved for use in humans and represents the most likely probe for the development of a point-of-care diagnostic. However, the literature is mixed regarding the effects of ICG on lymphatic function.

It has been shown in isolated lymphatic vessels that ICG inhibits vessel contraction in a dose-dependent manner and continues to alter function even beyond complete washout from the vessel (73). Given that near-infrared fluorophores have been shown to accumulate in the intracellular space (69), and ICG, in particular, has been shown to exhibit extremely cumulative cellular uptake (1, 62), we hypothesize that ICG is retained in the tissue space and contributes to a decrease in lymphatic function for an extended period of time following initial injection. A follow-up study using NIR imaging was unable to detect changes in lymphatic function after ICG injections of various concentrations (5), but the study only examined this phenomenon at one time point. Therefore, in this study we will first examine the retention of ICG in the tissue space of the rat tail and measure lymphatic function with NIR imaging beyond the duration of retention to analyze the time course changes in lymphatic function following initial ICG injection. For comparison purposes, we will also perform this analysis with a competing NIR fluorophore, the LI-COR IRDye 800CW PEG. The results of this study will contribute to a further characterization of the rat tail model for NIR lymphatic imaging

and will inform future studies involving multiple, repeat injections of NIR probes in this model.

Hypotheses

<u>Aim 2 Hyopotheses</u>

H2.1: When multiple collecting vessels drain the same tissue space, they will have heterogeneous transport capacities, and may exhibit a differential response to stimuli.
H2.2: Lymphatic transport as measured through NIR imaging will vary as a function of time after initial injection due to the transient alteration in interstitial fluid pressure resulting from the bolus injection.
H2.3: ICG has a time-delayed effect on lymphatic function such that it will decrease lymphatic transport capacity in the context of time-course experiments with repeat fluorophore injections. Specifically:

> H2.3.1: ICG remains present in the tissue space for an extended period of time following a bolus injection for NIR lymphatic imaging.
> H2.3.2: ICG will cause a reduction in lymphatic function in a time-delayed manner such that repeat measurements at later time-points will exhibit significant reductions in NIR lymphatic measurements. This time-course of reduced lymphatic function may correlate with the retention of ICG in the tissue space.
> H2.3.3: ICG will demonstrate evidence of inflammation that will correlate with retention of the dye in the tissue space.

Methods

Hardware Configuration

NIR imaging hardware (Figure 18-A) consisted of a 150mW 808nm laser diode (Thorlabs part no. M9-808-0150) powered by accompanying diode driver and temperature control boxes to provide excitation light. A 20° beam diffuser (Thorlabs part no. ED1-C20) was mounted in front of the diode to achieve a uniform excitation field. Fluorescence emission centered at 840 nm was captured using a PIXIS 1024B back-

illuminated CCD camera (Princeton Instruments) with an attached Infinity K2/SC video microscope lens (Edmund Optics) and a bandpass filter (CW:840 nm, FWHM:15 nm, Omega Optical). NIR images were recorded via a custom LabVIEW (National Instruments) image acquisition code.

NIR Imaging Procedure

Lymphatic function was quantified in vivo in the tail of six-week-old female Sprague Dawley rats (Charles River Laboratories, Wilmington, MA) according to procedures approved by the Georgia Institute of Technology IACUC Review Board and performed in our laboratory previously (268). All animals were first anesthetized using an intramuscular injection of Fentanyl (0.12 mg/kg), Droperidol (6 mg/kg), and Diazepam (2.5 mg/kg given 10 minutes after Fentanyl/Droperidol). A 10 μL fluorophore solution of either ICG (Across Organics) pre-mixed with bovine serum albumin (BSA) (MP Biomedicals, New Zealand) at a concentration of 150 μg/mL ICG and 60 mg/mL BSA or LI-COR IRDye 800CW PEG was then injected intradermally into the tip of the tail for fluorescence imaging (Figure 18-B). An injection volume of 10 μL was chosen based upon past success in rodent models, so as to not overload the lymphatics with unnecessary fluid volume while at the same time providing enough tracer for sufficient detection (108, 268). The injection was given at an entry angle of approximately 10 degrees to an approximate depth of 1 mm to specifically target the lymphatic vasculature. Care was taken to position the injection as close to the midline of the tail as possible to avoid favoring one collecting vessel over the other. The excitation source and the field of view of the CCD emission detector were centered on the rats' tail 10cm downstream (towards the base of the tail) from the injection site at the tip of tail (Figure 18-C). This location ensured that only the downstream collecting lymphatics would be visualized so as to avoid any potential complications from fluorescence uptake by initial lymphatics. The small volume of fluid injection and the use of NIR to enhance tissue penetration

ensures that only fluorescence in the deeper collecting lymphatics is visible downstream of the injection site. The animals were imaged continuously from the time of injection until 20 minutes post-injection with a 50ms exposure time.
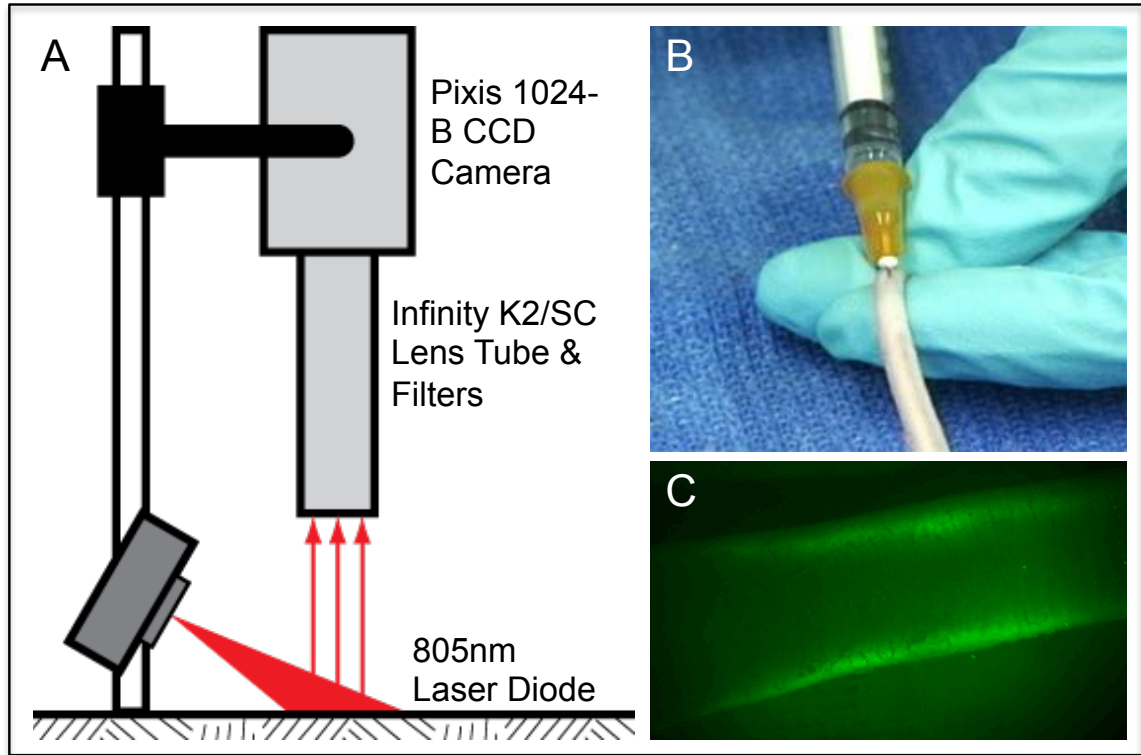
Figure 18: Near-infrared lymphatic imaging setup. (A) Schematic of near-infrared imaging hardware. (B) Intradermal tail injection of near-infrared fluorophore. (C) Example of imaging window 10 cm proximal to injection site showing fluorescence uptake in the two collecting lymphatic vessels.

Quantifying Lymphatic Function

To evaluate lymphatic function, three parameters were measured: the time necessary for the bolus injection of ICG to travel the 10 cm distance from injection site to emission recording site (transport time), the average velocity of the packets traveling through the field of view of the recording site, and the average frequency of packets passing through the field of view according to previously published methods (268). In order to characterize the individual function of the two collecting lymphatic vessels of the rat tail and to quantify the relationship between them, the three lymphatic function

metrics were separately calculated for the two vessels of the tail. For the purposes of this analysis, the vessel in which fluorescence first arrived (marked by a 20% increase in intensity) was defined as the dominant vessel and the other vessel was defined as non-dominant. An example of intensity plots in the two vessels can be seen in Figure 2A. To evaluate differences in the transient response to fluid injection from the steady state response, lymphatic function metrics were calculated in two separate 100-second segments after injection: the arrival segment beginning 60 seconds after fluorescence arrival in each vessel and the steady state segment beginning 10 minutes after injection. A representative example of the functional metrics calculated for both segments in a healthy animal is shown in Figure 2B-E. A paired, two-tail t-test with a Bonferonni correction for multiple comparisons was used to test for significance with $\alpha = 0.05$.

Lymphatic Imaging in Response to Nitric Oxide Treatment

A nitric oxide (NO) donor cream (glyceryl trinitrate ointment, GTNO) was applied to the tail as a second experimental condition to observe the effects of NO on the lymphatic function metrics of the two vessels (n=3). GTNO was applied to the whole tail one-minute prior to injection. Lymphatic function was calculated for both collecting vessels in the same manner described above. Comparisons between normal and GTNO-treated animals were checked for significance using an unpaired, two-tail t-test with a Bonferroni correction and $\alpha = 0.05$. Significance within the GTNO treatment group was analyzed using a paired, two-tail t-test with a Bonferroni correction and $\alpha = 0.05$.

Time-course analysis of ICG

To characterize the long-term effects of ICG on lymphatic function, a time course study was performed. Initially, a single 10 μL intradermal ICG injection (150 μg/mL ICG and 60 mg/mL BSA) was given in the tip of the tail (n=4) and fluorescence measurements were taken every two days to track ICG retention.

Based upon the results of the retention study, a second study was performed to monitor changes in lymphatic function during the ICG retention period, which is depicted graphically in Table 1. All animals in this group were given an initial 10 μL intradermal ICG injection (150 μg/mL ICG and 600 mg/mL BSA) in the tip of the tail at week 0 and baseline lymphatic function measurements were recorded for both collecting vessels.

The animals were divided into three treatment groups with follow-up 10 μL intradermal ICG injections and functional measurements at 1, 2, and 4-week time points (n=4). Follow-up injections were given as close to the original injection site as possible with particular care to keep the injection at the midline of the tail. Definitions of dominant and non-dominant vessels were made based upon week 0 measurements and remained consistently defined throughout follow-up screenings regardless of follow-up transport times (although the dominant vessel continued to produce the fastest transport times in nearly 90% of cases). Control animals were given a 10 μL intradermal BSA injection in the tip of the tail at week 0 with follow-up 10 μL intradermal ICG injections and functional measurements at the same three time points (n=4). Comparisons of function between time points was checked for significance using a paired, one-tail t-test with $\alpha = 0.05$.

A third set of animals was used to observe the effects ICG on lymph node size. All animals were again given a single 10 μL intradermal ICG injection in the tip of the tail. The sciatic lymph node (nearest draining node) was harvested for both collecting vessels without any additional follow-up injections at the week 0, 1, 2, and 4 time points (n=3). Control animals were given a 10 μL intradermal BSA injection in the tip of the tail and lymph nodes were harvested at each time point (n=3) without any follow-up injections. Lymph node size was calculated using projected two-dimensional area from microscopy images. We attempted to take fluorescence images to observe ICG retention in the nodes, but fluorescence was only detectable at the week 0 time point. Comparisons of lymph node size were checked for significance using an unpaired, two-tail t-test with a Bonferroni correction and $\alpha = 0.05$.

In order to compare the results of ICG to another popular NIR fluorophore, the same procedure outlined above was also performed using the LI-COR IRDye 800CW

PEG including retention (n=4), time course functional measurements (n=4), and lymph node harvesting (n=3).

Table 1: ICG Time-Course Experimental Setup. Animals were divided into three groups for follow-up imaging at 1, 2, and 4 weeks. All animals were given a 10 μL intradermal injection of either ICG, IR Dye, or BSA at week 0, and function metrics were recorded as a baseline for treatment animals. During the follow-up session for each group, the animals were given a 10 μL fluorophore injection for lymphatic function measurements and lymph nodes were harvested.

		Week 0	Week 1	Week 2	Week 4
Group 1	Treatment	ICG/IR Dye Injection	ICG/IR Dye Injection LN Harvest		
	Control	BSA Injection	ICG/IR Dye Injection LN Harvest		
Group 2	Treatment	ICG/IR Dye Injection		ICG/IR Dye Injection LN Harvest	
	Control	BSA Injection		ICG/IR Dye Injection LN Harvest	
Group 3	Treatment	ICG/IR Dye Injection			ICG/IR Dye Injection LN Harvest
	Control	BSA Injection			ICG/IR Dye Injection LN Harvest

Results

Spatial and Temporal Characterization of Lymphatic Function in the Tail

Figure 19 shows a representative example of fluorescence intensity measurements over time and packet frequency and velocity measured during the arrival and steady-state

segments. We have denoted the first arrival vessel as dominant and the other as non-dominant. All imaging sessions showed at least a 2 second difference in fluorescence arrival times between the two vessels with greater than 70% of cases showing a difference of 20 seconds or more. The dominant vessel nearly always produced higher intensity values than the non-dominant vessel throughout the imaging session (Figure 19-A) and remained consistent across multiple injections in the majority of animals.
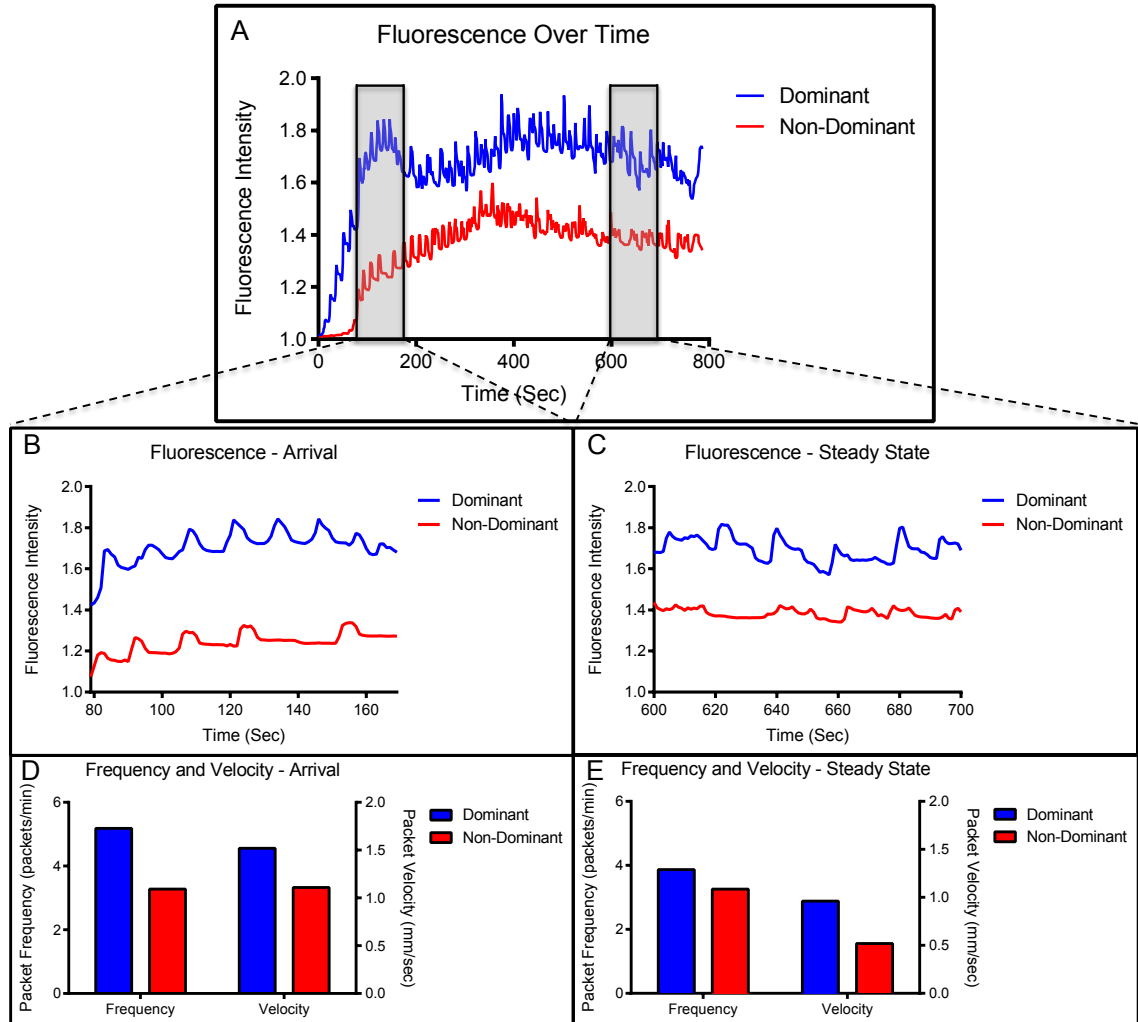
Figure 19: Representative vessel transport characteristics. (A) Representative data set showing fluorescence over time for dominant and non-dominant vessel. Arrival and steady-state segments are highlighted in the gray boxes. (B) Close-up view of intensity signal during arrival segment. (C) Close-up view of intensity signal during steady-state segment. (D) Packet frequency and packet velocity during arrival segment. (E) Packet frequency and packet velocity during steady-state segment.

During the arrival period the dominant vessel exhibited a rapid increase in fluorescence while the non-dominant vessel usually produced a more gradual rise in fluorescence. Packet frequency and velocity in both vessels peaked during or shortly after the arrival stage. The values then tapered off towards a lower, constant value during the steady-state period with the dominant vessel constantly producing larger or equal frequencies and velocities than the non-dominant vessel (Figure 19 D-E and Figure 20). The dominant vessel produced significantly reduced transport times, and significantly increased packet frequencies and packet velocities compared to the non-dominant vessel in the arrival segment, but there were no significant differences in the three functional metrics between the two vessels in the steady-state pumping period (Figure 21). Packet frequencies and packet velocities were significantly higher during the arrival stage than the steady-state period in the dominant vessel, but not in the non-dominant vessel.
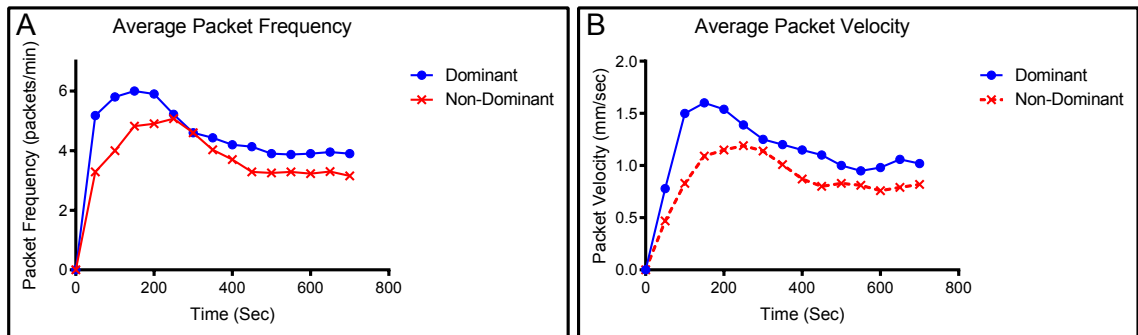
Figure 20: Representative packet frequency and velocity tracings. Representative data set showing (A) average packet frequency and (B) average packet velocity for the dominant and non-dominant vessel over time.

Differential Effects of Nitric Oxide on Lymphatic Function

The application of GTNO significantly increased transport times in both vessels compared to healthy animals as we have reported previously (268), but a much larger increase was seen in the non-dominant vessel in which transport times increased nearly 6-fold (Figure 21). NO-mediated vessels also showed significantly decreased packet frequency and packet velocity in both vessels during the arrival period and in the non-dominant vessel during the steady state period.
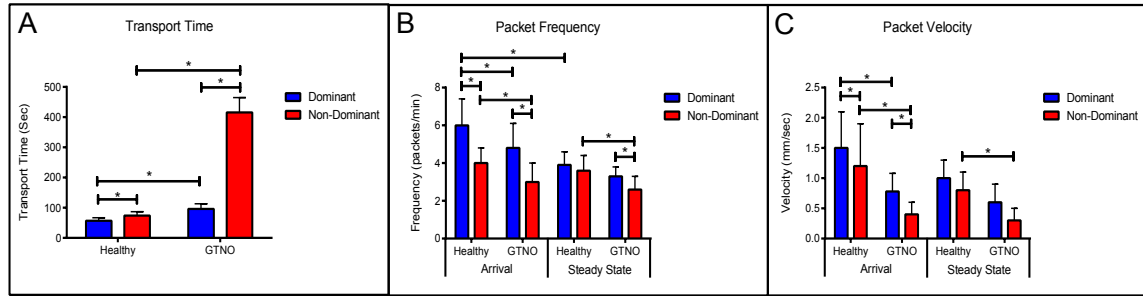
Figure 21: Lymphatic function metrics in healthy and GTNO-treated cases. Compiled data for (A) transport time, (B) packet frequency, and (C) packet velocity for the dominant and non-dominant vessel during arrival and steady-state segments in healthy and GTNO-treated animals (n=3). Error bars represent standard deviation. * = p<0.01.

Consequences of ICG Retention on Lymphatic Function

ICG remained visible (as defined by a signal to noise ratio greater than 3 dB) in the tissue space for more than two weeks after initial injection (Figure 22). NIR lymphatic function measurements after follow-up ICG injections of 1 week showed significant reductions in all three lymphatic function metrics in both vessels during the arrival and steady state segments (Figure 23). Transport time remained significantly elevated in the non-dominant vessel at the week 2 time point. Packet frequency and velocity likewise remained elevated in the non-dominant vessel at week 2, but only during the arrival period. No significant differences in function were observed at week 4. Control animals did not produce significant differences in lymphatic function at any time point.
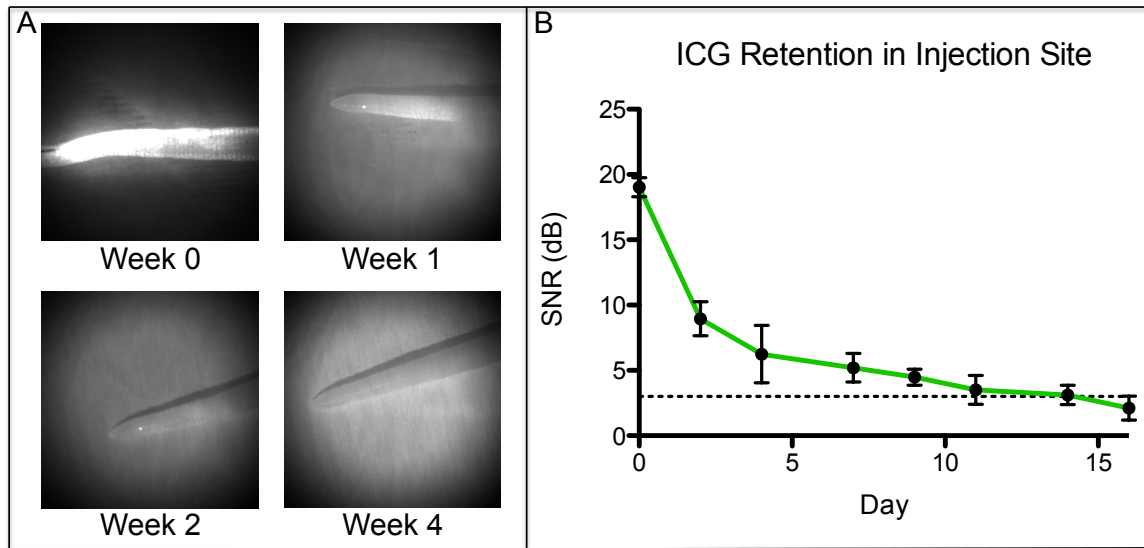
Figure 22: ICG is retained in tissue space for 2 weeks. (A) Representative images of the tip of a rat tail at four time points: immediately following ICG injection (week 0) and 1, 2, and 4 weeks after injection. (B) Average signal-to-noise ratio (SNR) of ICG in the tip of the rat tail (n=4). Dotted line represents limit of detection at 3 dB. Error bars represent standard deviation.

Lymph nodes were also significantly enlarged in both vessels at the 1 and 2 week time points with more than a 350% increase in projected two-dimensional area at week 1 and almost a 200% increase at week 2 (Figure 24). Lymph nodes harvested at week 4 were not significantly enlarged from their baseline values. Control animals did not produce significant differences in lymph node size at any time point.
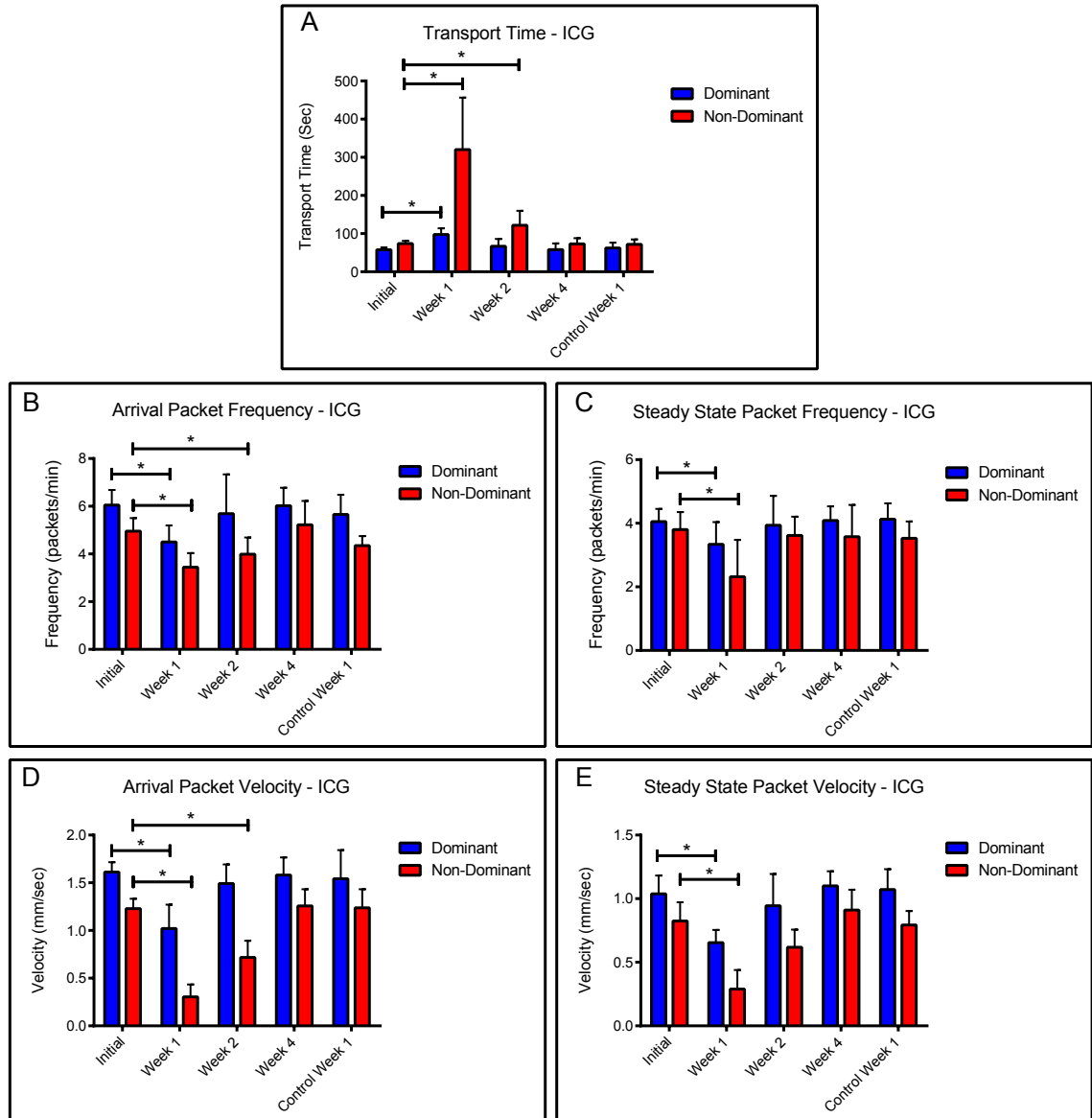
Figure 23: ICG reduces lymphatic function 1 and 2 weeks after initial injection. Compiled (A) transport time, packet frequency during (B) arrival and steady-state (C), and packet velocity during (D) arrival and (E) steady-state periods for dominant and non-dominant vessels during the four time points and for the control animals at week 1. Error bars represent standard deviation. * = p<0.05.

The LI-COR IRDye 800CW PEG likewise remained visible in the rat collecting lymphatics for approximately 2 weeks. However, the only function metric observed to be significantly different during the follow-up sessions was an increased transport time in the non-dominant vessel at week 1. When compared with ICG, the LI-COR dye produced much less severe effects on lymphatic function at the week 1 and 2 follow-up time points (Figure 25). The LI-COR dye produced a significantly lower percent change

in transport time in both vessels at week 1 and in the non-dominant vessel in week 2 as compared to ICG. Similarly for packet frequency, the LI-COR dye produced a significantly reduced change at the week 1 time point in both vessels and at the 2 week time point in the non-dominant vessel as compared to ICG. Additionally, for packet velocity, the LI-COR dye produced a significantly reduced effect compared to ICG at the week 1 and 2 time points only in the non-dominant vessel. Finally, the LI-COR dye did not produce any significant changes in lymph node size at any time point.
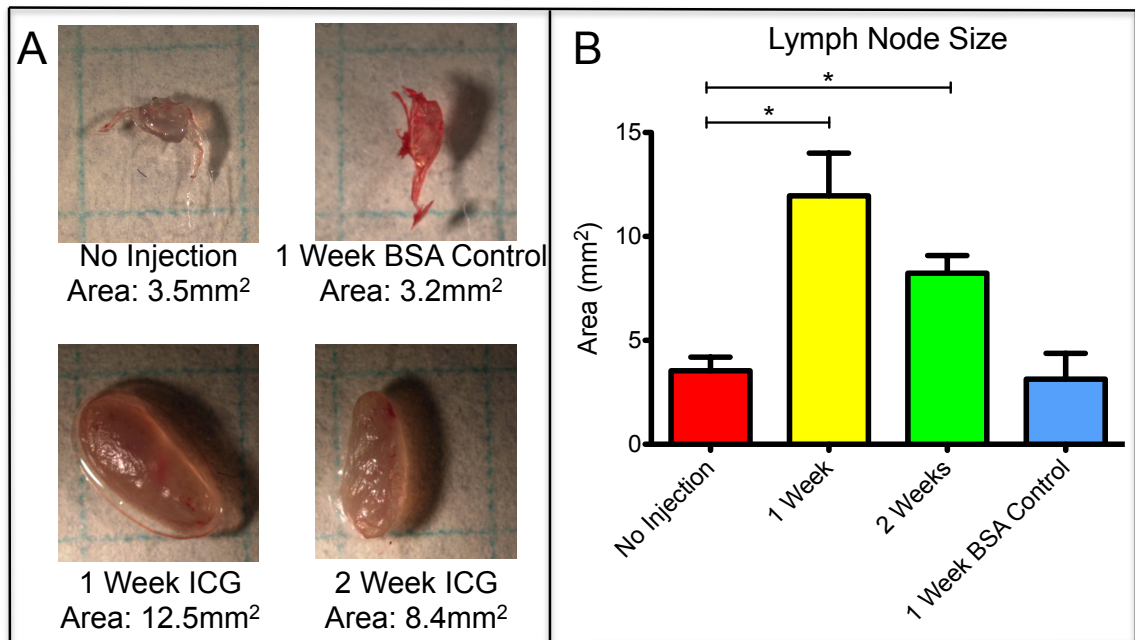
Figure 24: Draining lymph nodes enlarge 1 and 2 weeks after ICG injection. (A) Representative microscopy images of sciatic lymph nodes without injection, 1 week after BSA control injection, and 1 and 2 weeks after ICG injection. Grid squares = 25 mm^2. (B) Projected two-dimensional area of lymph nodes prior to injection, 1 and 2 weeks after ICG injection, and 1 week after control BSA injection. Data is compiled for both sciatic lymph nodes at each time point. Error bars represent standard deviation. * = p<0.001.

Discussion

Vessel Transport Characteristics

The lymphatic vasculature is a complex network of interconnected vessels and nodes whose fluid transport capabilities are still not well understood at the tissue level. This study represents a new effort towards quantifying the differential effects of multiple

collecting lymphatic vessels draining a single tissue space, which will help to explain how the organ system functions as a whole in the context of fluid transport. We have provided a new framework for analyzing lymphatic function across multiple vessels to better assess cumulative lymphatic drainage of the interstitium. This framework will make NIR imaging more sensitive to lymphatic function, which may prove useful in distinguishing subtle changes between health and disease in the context of lymphatic research and the development of a point-of-care diagnostic.
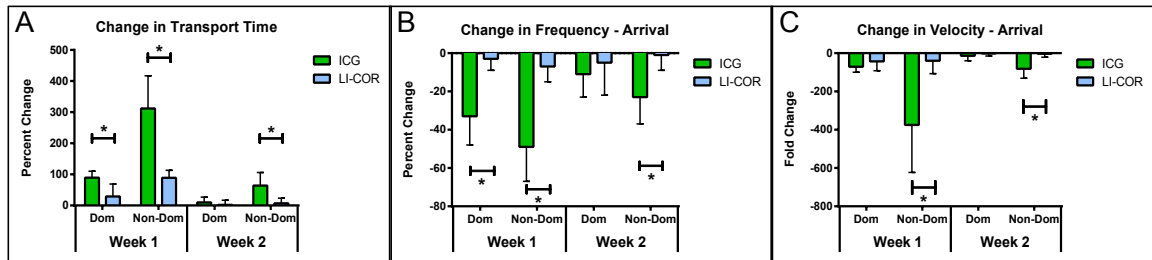
Figure 25: LI-COR IRDye 800CW PEG reduces lymphatic function less than ICG. Percent change in (A) transport time, (B) packet frequency, and (C) packet velocity between initial measurement and 1 and 2 week follow-up time points for ICG and LI-COR IRDye 800CW PEG. Error bars represent standard deviation. * = p<0.01.

Our results revealed that one vessel always produced fluorescence before the other with the difference in 10 cm transport time between the two vessels usually exceeding 20 seconds. In nearly every case, the first arrival vessel exhibited higher fluorescence intensity values, packet frequencies and packet velocities than the second arrival vessel, although both vessels consistently produced values in a range consistent with previously reported mesenteric lymph velocities (54, 98) and packet frequencies and velocities in rat tail lymphatics (268). We defined the first arrival vessel as dominant and the second arrival vessel as non-dominant in an effort to describe the observed difference in function between the two vessels. Importantly, the dominant vessel remained consistent across multiple injections in the same animal in the vast majority of cases, suggesting this phenomenon is repeatable and inherent to the function of that particular vessel network. Similar differential transport characteristics were also observed by Proulx et al. in two afferent collecting vessels of the mouse hind limb (171), which indicates that our results may not be restricted to simply the rodent tail model and may be representative of general systemic lymphatic function. Future work will need to be done to address the relevance of these observations in rodents to human lymphatic physiology.

There are several potential explanations for the observation of differential transport function between the two collecting vessels. Firstly, it is possible that preferential lymphatic drainage patterns exist such that for a given tissue space, fluid drainage is the primary responsibility of one single vessel, while any additional vessels in the area serve as overflow or reserve transport routes for large fluid loads. Preferential drainage patterns could be the result of regional variability in the location and distribution of different lymphatic vessel networks in the tissue space or the composition and organization of the interstitium at the injection site such that drainage into one collector over is favored over the other. Since our repeat injections in the same animal were performed as close to the original injection site as possible, either of these two potential explanations could account for the consistency of the dominant vessel across multiple injections. Although the utmost care was taken to ensure all injections were consistently given at the same angle, depth, and location, there is a substantial degree of inherent variability in the intradermal injection procedure, which could also be contributing to the observed differences in vessel function by differentially or inconsistently favoring drainage into one vessel over another. Furthermore, there were no detectable differences in vessel size within the spatial resolution limits of our imaging system, but fluorescence scattering makes accurate measurements of vessel diameter very difficult in vivo. Thus, it remains unclear whether subtle differences in vessel depth or vessel diameter may be a contributing factor favoring transport through one vessel over the other. Finally, the degree to which nodal resistance may contribute to the observed results is unknown and could be significant. Future work should specifically focus on the differences in function between multiple lymphatic vessels in several anatomic regions and under various experimental conditions to better characterize systemic lymphatic transport.

Our results also revealed a transient period during early fluorescence arrival in which lymphatic function was generally enhanced as compared to the subsequent steady-state period. This observation is not surprising when considering the bolus delivery and high albumin concentration of our injection. The duration of the transient arrival period was typically between 2 - 5 minutes, which is consistent with the small 10 μL volume of our injections and the time kinetics associated with responses to changes in Starling's forces observed in the microvasculature (113). After the initial response of the

lymphatics to this change in the local interstitial fluid parameters that govern filtration, steady-state values of lymphatic transport were reached. Interestingly, more significant differences in function were observed between the dominant and non-dominant vessel during the transient arrival period than the steady-state period. This is consistent with the method we have utilized to categorize these two vessels (i.e. the vessel with a shorter arrival time is the dominant), as the arrival time is a metric that is reflective of vessel function during the initial transient response. Thus the larger packet velocities and frequencies in the dominant vessel immediately after injection explain in part why transport time is shorter than in the non-dominant vessel.

These observations generally illustrate the importance of using a consistent framework to quantify lymphatic vessel function using NIR imaging. That is, we have shown that significant differences in transport characteristics are obtained by taking measurements during different periods following fluorophore injection or by quantifying different vessels draining the same tissue space. An optimal strategy for NIR quantification of vessel function remains undefined at this point, but future studies should be performed with careful consideration of the measurement framework, especially given that the selection of methodology for analysis can drastically affect results.

Effects of Nitric Oxide

The effects of NO on vessel function further exemplify the importance of choosing an appropriate framework for transport quantification using NIR imaging. Our previous work showed that GTNO significantly reduced lymphatic drainage as evaluated by several function metrics (268), but that analysis was limited to a single vessel and response time. Analyzing the effects of GTNO in the context of this more robust two-vessel, two-time-period framework may begin to provide a more broad understanding of the effects of NO on cumulative lymphatic drainage. Specifically, the results indicated that GTNO generally reduced function in both vessels, but more severely affected the non-dominant vessel.

The transport time metric, in particular, was very different between the two vessels after GTNO application. This metric incorporates extrinsic factors affecting uptake such as interstitial fluid pressure and matrix resistance as well as intrinsic factors

affecting transport such as vessel contraction. Given that previous work has shown NO acts on lymphatics by strongly inhibiting vessel contractility (72, 114), these results could suggest a difference between the two vessels in the balance of intrinsic contractions versus extrinsic factors in fluid transport following a large fluid load. That is, if preferential drainage patterns exist as we suspect, the increased interstitial fluid pressure after bolus injection would drive flow more favorably into the dominant vessel, while the non-dominant vessel would be forced to rely more exclusively on intrinsic contractions to transport fluid. The resultant vessel dilation following GTNO application would severely impair transport in the non-dominant vessel by inhibiting contractility. However, the effects would be much less severe in the dominant vessel because dilation would decrease vessel resistance, thus enhancing the effects of elevated interstitial fluid pressure driving flow into the vessel. This could help to explain why NO more significantly affected the non-dominant vessel, especially in the transport time metric.

Alternatively, these observations could be the result of secondary effects of NO on lymph formation, which could differentially affect uptake and subsequent transport in the two vessels. The lymphatic community has recently become very interested in the modulating effects of NO on lymphatic function in health and disease (32, 114, 201), and future work devoted to a more thorough characterization of NO on lymphatic network drainage would be well-warranted.

Effects of NIR Fluorophores

In this study, we have shown for the first time with NIR imaging that injection of ICG contributed to long-term decreases in lymphatic function. The results of the long-term follow-up screenings revealed that ICG was retained in the local tissue space for approximately two weeks after injection, and lymphatic transport was reduced during this period. There was a fairly dramatic decrease in function at the 1 week time point in which all metrics were reduced in both vessels, but week 2 produced a less severe reduction in function and was limited exclusively to the non-dominant vessel. Lymph nodes were also enlarged at 1 and 2 weeks after injection, but interestingly, there was not a significant difference in size between lymph nodes of the dominant and non-dominant vessel. Very importantly, control animals in which the initial injection contained albumin

but lacked ICG did not produce any significant change in function or lymph node size at any time point. Since the control injections were the same volume and given in the same manner as the ICG injections, this data suggests that the observed decreases in lymphatic function following initial injection of ICG were due to the fluorophore itself rather than the injection procedure or any other constituent of the injection solution.

Fortunately, the effects of ICG appear to be reversible since all of the functional metrics returned to baseline levels in both vessels and lymph nodes returned to normal size at the week 4 time point. Despite the data showing a functional decrease in lymphatic transport after ICG injection, it is difficult to determine whether the observed effect sizes are substantial enough to warrant physiological concern. Although lymph nodes showed signs of enlargement after ICG injection, the level of hypertrophy was not nearly as large as the 20- to 30-fold increase in nodal weight seen in models of chronic inflammation (20, 61). No detectable edema was observed in the tail of any of the animals at any point during the time course, which suggests that ICG does not decrease lymphatic drainage to the point of causing significant fluid stagnation or inflammation. It does not appear that ICG needs to be treated as a health concern at least at frequencies that don't exceed once per month, but care should be taken in interpreting NIR functional data with this fluorophore, especially in the context of repeat injections. Repeat injections with ICG may need to be spaced as far apart as 4 weeks in order to avoid erroneous measurements in function, although a similar investigation of time-course effects of ICG in humans would be valuable for the continued development of a point-of-care diagnostic.

The observed decreases in lymphatic function are consistent with the investigation of ICG in isolated lymphatic vessels by Gashev et al. (73). Our result, that reduced function appeared to coincide with ICG retention, is similar to their observation that vessel contraction was inhibited even beyond the period of ICG washout. Gashev et al. was able to show ICG binds to the endothelial cell layer in the isolated vessel setup, but in our study, ICG was most visibly retained at the injection site. A small amount of fluorescence was visible in the collecting vessels for 1-2 days immediately after the injection, but the intensity quickly dropped below the limit of detection due to scattering effects and a low concentration of dye. With our imaging system the limit of detection of

ICG in tail collecting vessels is in the micromolar range, which is consistent with concentrations used by Gashev et al. It is difficult, therefore, to make strong conclusions from our data regarding the mechanism by which ICG affected lymphatic function. At the very least, however, the injection site would have been constantly releasing small amounts of ICG into the lymphatic vessels over the course of the retention period, which could have contributed to the long duration of decreased function. Given the evidence of ICG toxicity with prolonged exposure in the retina (90), it is possible that the decrease in lymphatic function could also be a result of ICG reported mild toxicity.

One limitation of our study is that we only used one concentration of ICG for injection. Although the volume of the injection is very small, the concentration is optimized for fluorescence visualization rather than consideration of vessel function. It is possible that a more dilute solution, while negatively influencing fluorescence intensity, may contribute to shorter retention periods and have less of a long-term impact on function.

An additional investigation by Aldrich et al. did not detect a change in lymphatic function in response to ICG injections (5), but these results do not necessarily conflict with ours and there are several explanations for these results. Firstly, it should also be noted that our initial baseline readings for ICG and the LI-COR IRDye 800CW are similar to those reported by the authors. The principal difference between the two studies is the time-point of interest after injection. Aldrich et al. examined lymphatic function effects immediately after injection while we used this value as a baseline and instead focused on time course differences 1, 2, and 4 weeks later. Given that ICG has been shown accumulate in the intracellular space for a period beyond 24 hours (1, 62), time may be a necessary component for the cumulative dose to affect vessel function. Another difference between our study and that of Aldrich et al. is the above-mentioned framework used for analysis of NIR imaging. This framework was critical to generating our results, especially since more profound effects were seen in the non-dominant vessel and during the arrival period initially after injection. Finally, our study was performed in the rat tail, while Aldrich et al. used the mouse inguinal-to-axillary model, and it remains unclear if and how lymphatic function may vary between the two regions and the two species.

The functional results of the LI-COR IRDye 800CW PEG provide an interesting comparison to ICG. The dye produced a mild decrease in lymphatic function at week 1, but it did not contribute to a deterioration of function nearly as severe as ICG and did not affect lymph node size. These results are not meant to indicate that the LI-COR IRDye is an optimal solution for NIR lymphatic imaging, although it appears to have less of a long-term effect on lymphatics than ICG, but rather to illustrate that the choice of fluorophore impacts NIR lymphatic functional measurements. Thus, optimizing the tracer of choice to minimize its biological impact is warranted, particularly in the context of longitudinal lymphatic imaging. The difference in functional response between ICG and the IRDye may suggest that the chemical composition and three-dimensional structure of the fluorophore either directly modulates lymphatic transport or indirectly affects lymphatic function through eliciting an immune response (114), especially given the observed differential effects on lymph node size between the two dyes in this study. The NIR lymphatic imaging community has been directing research towards the development and optimization of fluorophores specifically for the purpose of lymphatic imaging (47, 171, 172). While these efforts have concentrated primarily on using dyes with higher quantum yields than ICG or altering the size of the carrier molecule to optimize lymphatic uptake, future work in the development of new probes should also focus on the long-term effects of the dyes on local lymphatic and immune function. Repeat injections, either in the context of research or a point-of-care diagnostic will need to have no effect on lymphatic function in order to obtain meaningful and consistent results.

CHAPTER 4: NEAR-INFRARED IMAGING ANALYSIS OF LYMPHATIC FUNCTION IN LYMPHEDEMA

Introduction

More than 130 million individuals worldwide suffer from lymphedema, a chronic disease that presents with the accumulation of fluid, proteins, and adipocytes in the interstitium, resulting in in a drastic enlargement of the affected limb(186, 187). The most common form is secondary (acquired) lymphedema, which results from the disruption of previously normal lymphatic networks, usually through injury or surgical procedure(233). In developed countries, the two main contributors to secondary lymphedema are surgical and radiotherapeutic cancer interventions, with breast-cancer related lymphedema being the most encountered and studied form(188). Surprisingly, most secondary lymphedema cases present 1-3 years or more after the insulting event, rather than immediately following the trauma(187). It is this latency period that makes lymphedema so difficult to diagnose early and treat effectively. Despite the prevalence of the disease, there is very little known about the exact mechanisms of disease progression, especially as it relates to lymphatic transport function and the progressive loss thereof.

It remains unclear how the response of the lymphatic system during the post-trauma period contributes to the onset of lymphedema, which has severely limited our ability to understand the disease mechanism and cascade. It is well documented that the injury or surgical wound space forms into scar tissue, which subsequently limits new lymphatic vessel growth in the space and hampers interstitial fluid flows(13, 164, 221, 253, 263). There is also evidence that an inability of the lymphatic system to adequately regenerate during normal wound repair may predispose the tissue to swell during secondary lymphedema(164, 253). However, one study found that the resolution of acute lymphedema through the recovery of functional fluid drainage was not inhibited by VEGF-R3 neutralization, which suggests that lymphangiogenesis did not contribute to the lymphedema recovery(135). It has been shown that accumulating lymph may experience compensatory drainage through a reduced number of surviving local

lymphatics, rerouted lymphatics that bypass the obstructive tissue, or lymphovenous communications(144, 219). Additionally, inflammation has been shown to contribute to the degree of swelling in lymphedema(150, 279, 281) and may influence the appearance and perpetuation of the swelling(136).

Since lymphatic flow is driven primarily through the contractility of collecting lymphatic vessels, the ability to quantify lymphatic pump function through the imaging of functional lymphatic transport in the context of early lymphedema onset would greatly enhance our understanding of the disease progression. We hypothesize that lymphedema is associated with a progressive loss of lymphatic function, which can be visualized and subsequently quantified with NIR imaging, thus affording novel insights into the disease cascade. The latency period commonly associated with lymphedema, in particular, motivates a hypothesis of remodeling-induced lymphatic failure, which has begun to gather support in the literature(136). Importantly, however, all of the animal models reported in the literature to date have severed all of the collecting vessels draining the tissue space of interest, and the analysis has focused exclusively on morphological changes occurring in the dermal layer and functional changes occurring in the initial lymphatics. No study to date has investigated the changes in collecting vessel function associated with lymphedema, and no model currently exists that allows preservation of collecting vessel trunks.

Therefore, we will develop a new rodent tail model of lymphedema allowing for selective preservation of certain lymphatic collectors in order to track changes in the collecting vessel transport metrics over time using NIR lymphatic imaging. We will take baseline NIR functional measurements before surgery, immediately after surgery, and in regular follow-up intervals to record changes in collecting vessel transport function. The goal is to develop a model that exhibits similar pathological progression as the classic rodent tail model of lymphedema while preserving a single intact collecting vessel trunk. Doing so will provide the first opportunity to study the link between lymphedema progression and lymphatic transport as well as help to generate new insights into the potential mechanisms of lymphatic failure during disease progression.

Critical to tracking the progression of lymphatic function through the disease cascade in this study will be the use of the effective lymphatic pumping pressure metric,

which was first developed by Unno et al. and recently adapted for high precision measurement in rodent tails by our laboratory(152, 248). The technique measures the pressure required to occlude the vessel and is indicative of the pumping capacity of the vasculature. This will be the first study to apply such a robust set of metrics towards the assessment of lymphatic transport function in the context of lymphedema, which will begin to provide a wealth of new knowledge regarding the specifics of lymphatic pumping capacity associated with the disease.

Hypotheses

H3.1: Ligating the mouse tail such that one lymphatic collector remains intact will create a pathological model of lymphedema while simultaneously allowing NIR functional metrics to be obtained from the intact vessel. The tails may exhibit slightly less swelling than the standard full ligation tail model.

H3.2: Ligating the dominant vessel will produce significantly increased swelling as compared to ligation of the dominant vessel.

H3.3: Swelling will correlate with reductions in lymphatic function as quantified through NIR lymphatic imaging.

H3.4: The disease cascade will contribute to remodeling of the intact collecting vessel such that the pumping capacity is reduced.

Methods

Surgical Model and Time Course Measurements

The rodent tail model of lymphedema has been used extensively in previous studies(13, 40, 195, 253, 279). Generally, a dermal-layer incision is made spanning the entire circumference of the tail such that all collecting and capillary lymphatics are severed. This technique produces a well-documented swelling cascade that closely resembles the progression of lymphedema, at least in the dermal layer.

In an attempt to study the role of collecting lymphatic vessel function in lymphedema onset and progression, we modified the conventional tail lymphedema model. Specifically, we altered the dermal incision such that it spanned nearly the entire

circumference of the tail with the exception of allowing one collector to remain intact (Figure 26).
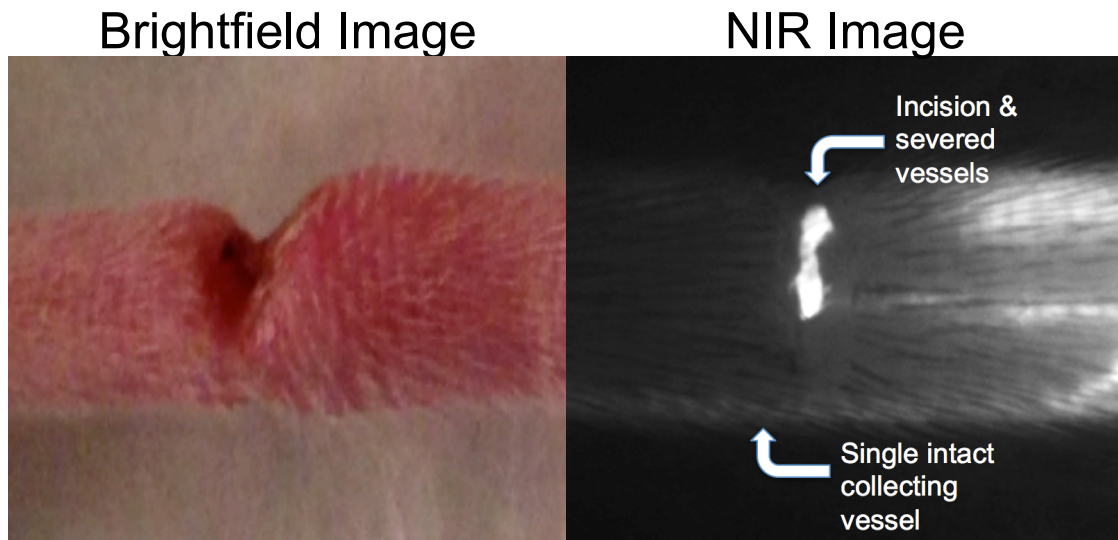
Figure 26: Example NIR Image of Tail Ligation Technique. This NIR image shows the collecting vessel intact on the bottom and the severed vessels on the top. The severed vessels force lymph to travel laterally across the tail through the interstitial space and capillary network to reach the intact collector for transport.

Previously, our group has characterized the lymphatic physiology of the tail as having a dominant and a nondominant collecting trunk(267). The present study included three experimental groups: (1) a vessel ligation group in which the dominant vessel was ligated (n=4), (2) a vessel ligation group in which the nondominant vessel was ligated (n=4), and (3) a sham control group in which both collecting vessels were left intact (n=4). Eight-week-old female balb-c mice (Charles River Laboratories, Wilmington, MA) were used for this study according to procedures approved by the Georgia Institute of Technology IACUC Review Board. All animals were first anesthetized using inhaled isofluorane (5% induction, 2% maintenance). All three groups received incisions 1 cm from the base of the animal spanning 80-90% of the circumference of the tail with particular care to standardize the incisions as much as possible. In the vessel ligation groups, the incision severed one collecting vessel and left one intact, while in the sham control group the incision severed a substantial percentage of the lymphatic capillary network, but none of the collectors were severed. All incisions were cauterized to prevent bleeding and fluid leakage. After the surgical procedures, both collecting vessels were

checked with NIR imaging to ensure they were either severed or remained intact as appropriate. Animals in which vessels were improperly ligated or in which blood vessels were ligated were excluded from the study.

Baseline metrics were collected in all groups prior to surgery. NIR functional metrics were again measured after surgery at 2 day, 4 day, 1 week, 2 week, 3 week, and 3 month time points (Figure 27). Tail measurements were taken every two days via two-dimensional projected area to track swelling progression. Lymphatic pumping pressure measurements were taken before surgery and at 2 day, 4 day, 1 week, and 3 month time points. All animals were euthanized after 3 months, and tissue samples were harvested including cross-sectional tail samples, draining lymph nodes, and excised collecting vessels.
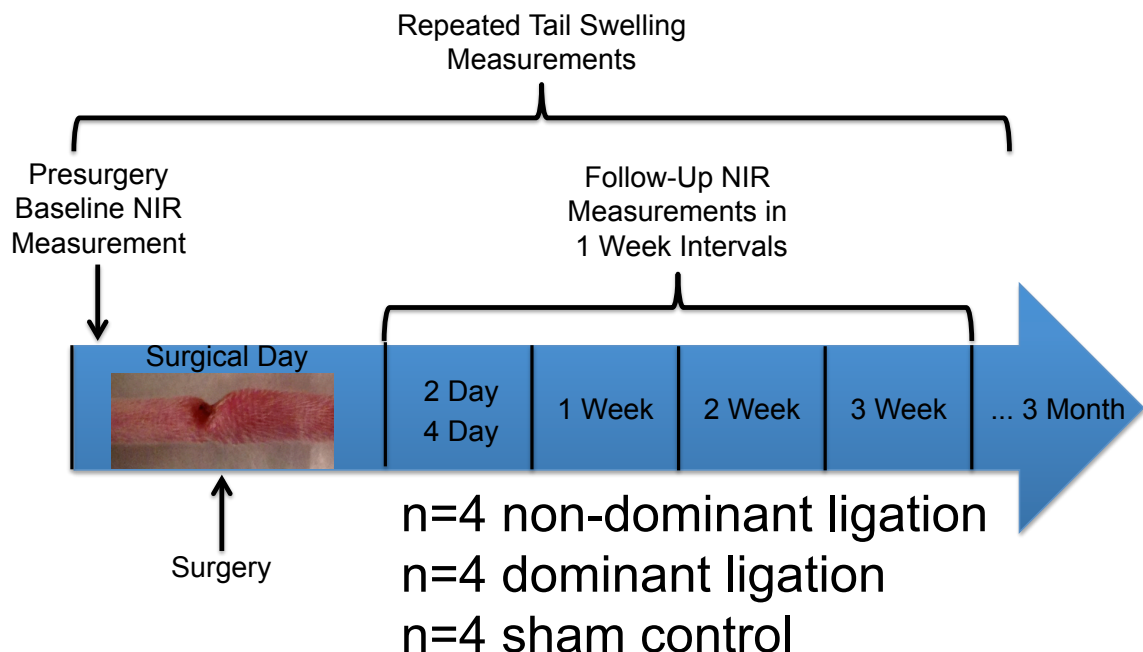
Figure 27: Experimental time-course. Baseline measurements were performed before surgery and routinely after surgery for three weeks, and then a final measurement was made at 3 months. Tails were measured every two days for four weeks.

NIR Functional Imaging

NIR lymphatic imaging was performed according to previously published methods(152, 267, 268). Briefly, lymphatic function was quantified in vivo in the tail of eight-week-old female balb-c mice (Charles River Laboratories, Wilmington, MA)

according to procedures approved by the Georgia Institute of Technology IACUC Review Board and performed in our laboratory previously (268). All animals were first anesthetized using inhaled isoflurane (5% induction, 2% maintenance). 10 µL of LI-COR IRDye 800CW PEG (LI-COR Biosciences, Nebraska, USA) was then injected intradermally into the tip of the tail for fluorescence imaging (the fluorophore was reconstituted according to manufacturer instructions for lymphatic imaging). An injection volume of 10 µL was chosen based upon past success in rodent models, so as to not overload the lymphatics with unnecessary fluid volume while at the same time providing enough tracer for sufficient detection (108, 268). The injection was given at an entry angle of approximately 10 degrees to an approximate depth of 1 mm to specifically target the lymphatic vasculature. Care was taken to position the injection as close to the midline of the tail as possible to avoid favoring one collecting vessel over the other. The excitation source and the field of view of the CCD emission detector were centered on the mouse's tail 7cm downstream (towards the base of the tail) from the injection site at the tip of tail . This location ensured that only the downstream collecting lymphatics would be visualized so as to avoid any potential complications from fluorescence uptake by initial lymphatics. The small volume of fluid injection and the use of NIR to enhance tissue penetration ensures that only fluorescence in the deeper collecting lymphatics is visible downstream of the injection site. The animals were imaged continuously from the time of injection until 20 minutes post-injection with a 50ms exposure time. Analysis of NIR functional metrics was performed during the steady-state period ranging from 5-20 minutes after injection, as defined previously(267).

NIR functional measurements included a combination of previously reported metrics and newly developed metrics for this model. Packet frequency, emptying rate, pumping pressure and fluorescent tail area were measured and recorded as previously published(152, 268). Transport time was used to determine the identity of the dominant and nondominant collector, but was not used during time-course analysis of lymphatic function. Packet velocity was also not used for functional analysis because the dynamics of mouse contractile function, especially in the diseased cases, prevented reliable velocity measurements.

A new NIR functional metric was developed called Lymphatic Flourescence Transport. Packets were detected by first identifying peaks in the fluorescence signal and then identifying the time points at which troughs on either side of the peak occurred (Figure 28). The fluorescence signal was then integrated across each packet and summed over the length of the data set. Lymphatic fluorescence transport was then calculated as the time-normalized sum of the packet integrals such that:

$$Lymphatic\ Fluorescence\ Transport = \frac{\sum_{i=1}^{n} \int_{t\,min\,i}^{t\,max\,i} f(t)dt}{time},$$ where *n* is the number of

packets in the data set and *f(t)* is the fluorescence signal within each packet region (between the minimum and maximum time points corresponding to each packet). This metric represents the cumulative transport of fluorescence through the vessel normalized by time and was used to assess overall lymphatic transport capacity. Average packet amplitude was also measured and recorded to assess contractile function of the vessels.
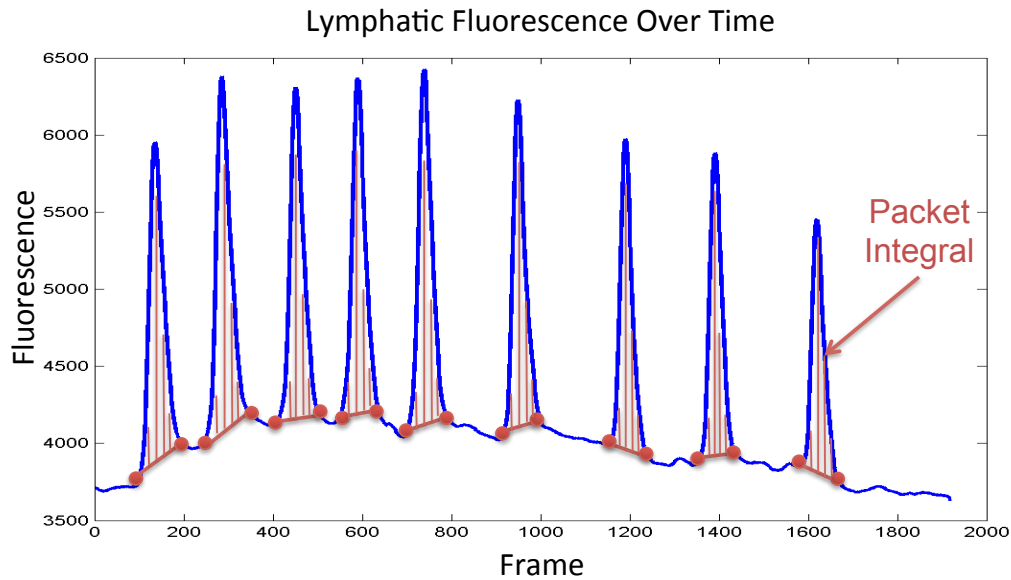
Figure 28: NIR lymphatic transport. This is an example plot of fluorescence over time in a region of interest in a collecting vessel. The packet integral was calculated by first defining the spikes in intensity corresponding to packets and then integrating the signal in these regions. Lymphatic fluorescence transport was calculated by summing the packet integrals and normalizing by time.

Oxazolone Application

In order to introduce an immune challenge, oxazolone (Sigma, catalog number E0753) was applied to the tails of dominant ligation and sham animals according to previously published methods(136). Briefly, at three months post-surgery, at which time no edema was present in either experimental group, the animals were sensitized by applying 300 μL of 2% oxazolone in ethanol to a shaved 1 inch by 1 inch area on the abdomen. Seven days after the initial sensitization, 300 μL of 1.6% oxazolone in a solution of acetone and olive oil (4:1) was applied evenly to the entire tail using a micropipette, and this procedure was repeated three more times every three days for a total of four applications spanning 12 days post-sensitization. Tail circumference and NIR functional measurements were taken before and after oxazolone application.

Statistical Analysis

Tail swelling and lymphatic function metrics were compared between the two ligation groups and between each ligation group and the sham group via an unpaired two-tail t-test with Bonferroni's multiple comparison correction as appropriate. The correlation between tail swelling and lymphatic transport was calculated using Pearson r correlation, and correlation coefficients were tested for significant differences using the Fisher r-to-z transformation. Alpha was equal to 0.05 for all statistical analysis.

Results

Single Vessel Ligation Lymphedema Model Produces Differential Swelling Response

Tail swelling significantly increased as a result of collecting lymphatic vessel ligation compared to the sham group, and ligating the dominant vessel produced significantly more swelling than ligation of the non-dominant vessel (Figure 29). Dominant ligation swelling peaked at 45% on day 4, while non-dominant ligation swelling reached a maximum of 28% swelling on day 14. Both ligation groups returned to normal circumference values on or soon after day 28. The sham control group experienced a mild swelling response with peak swelling of 16% on day 4 and full resolution by day 14.
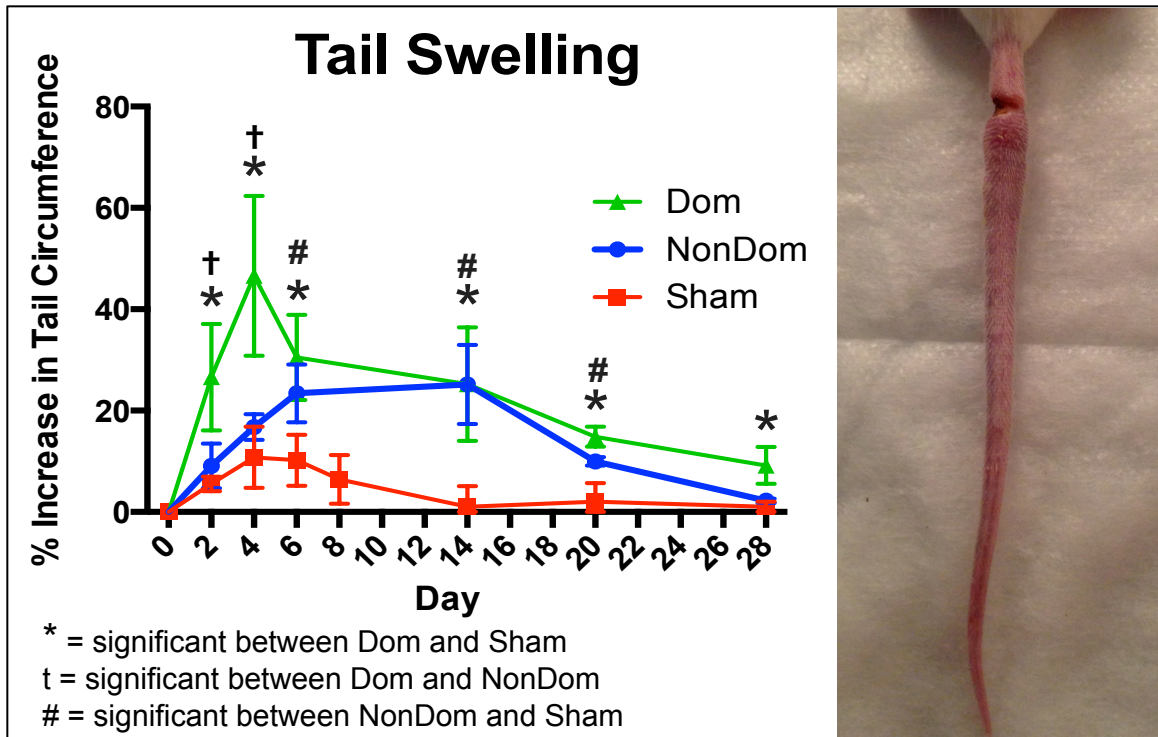
Figure 29: Tail Swelling Cascade. Plot of tail swelling of three experimental groups. Both ligation groups produced increased swelling compared to the sham between the 1 week and 3 week time points. The dominant ligation produced significantly increased swelling compared to the nondominant ligation at the 2 day and 4 day time points.

Reductions in Lymphatic Transport Correlate with Disease Progression

Normalized lymphatic fluorescence transport was significantly reduced in both the dominant and non-dominant ligation cases as compared to baseline presurgical values and the sham control group (Figure 30). Specifically, the nondominant group produced significantly reduced transport values as compared to baseline at the 1, 2, and 3 week periods and compared to the sham group at the 1 and 2 week time points. The dominant group produced significantly reduced transport values relative to baseline at all time points and relative to the sham group at the 1, 2, 3 week and 3 month periods. The sham group did not produce significantly altered transport values at any time points. Lymphatic transport decreased to a minimum value at the 1-week time point in the dominant (8% of healthy transport) and non-dominant cases (35% of healthy transport) before beginning to improve at later time points. The dominant ligation also resulted in significantly lower transport than the non-dominant ligation at the 1 and 2 week time

points. At the three-month time point transport in the dominant ligation was still significantly reduced, while transport in the non-dominant ligation was not significantly reduced from baseline healthy values. In both ligation conditions swelling significantly correlated with lymphatic function in the negative direction, producing a Pearson r value of -0.65 ($p<0.0001$) while the sham group produced a Pearson r of 0.34, which was not significant (Figure 31). Using a Fisher r-to-z transformation, the Pearson coefficients between the sham and ligation groups were significantly different ($p<0.0001$).
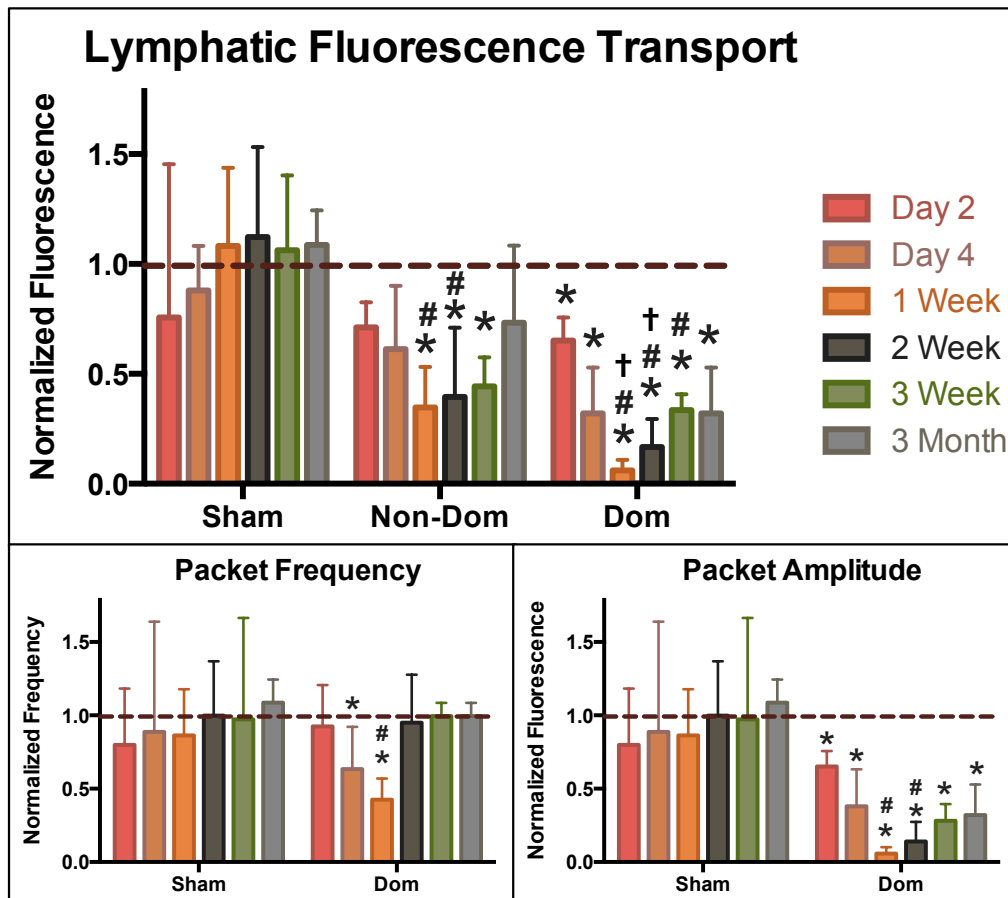
Figure 30: Lymphatic fluorescence transport over time. Plot showing normalized lymphatic fluorescence transport for three experimental conditions. Values are normalized to presurgery baseline. Both ligation groups produced significantly reduced transport compared to the sham at the 1, 2, and 3 week time points. The dominant ligation produced significantly reduced transport compared to the nondominant ligation at the 1 and 2 week time points. * = significant compared to baseline, # = significant compared to sham, t = significant compared to NonDom.

89
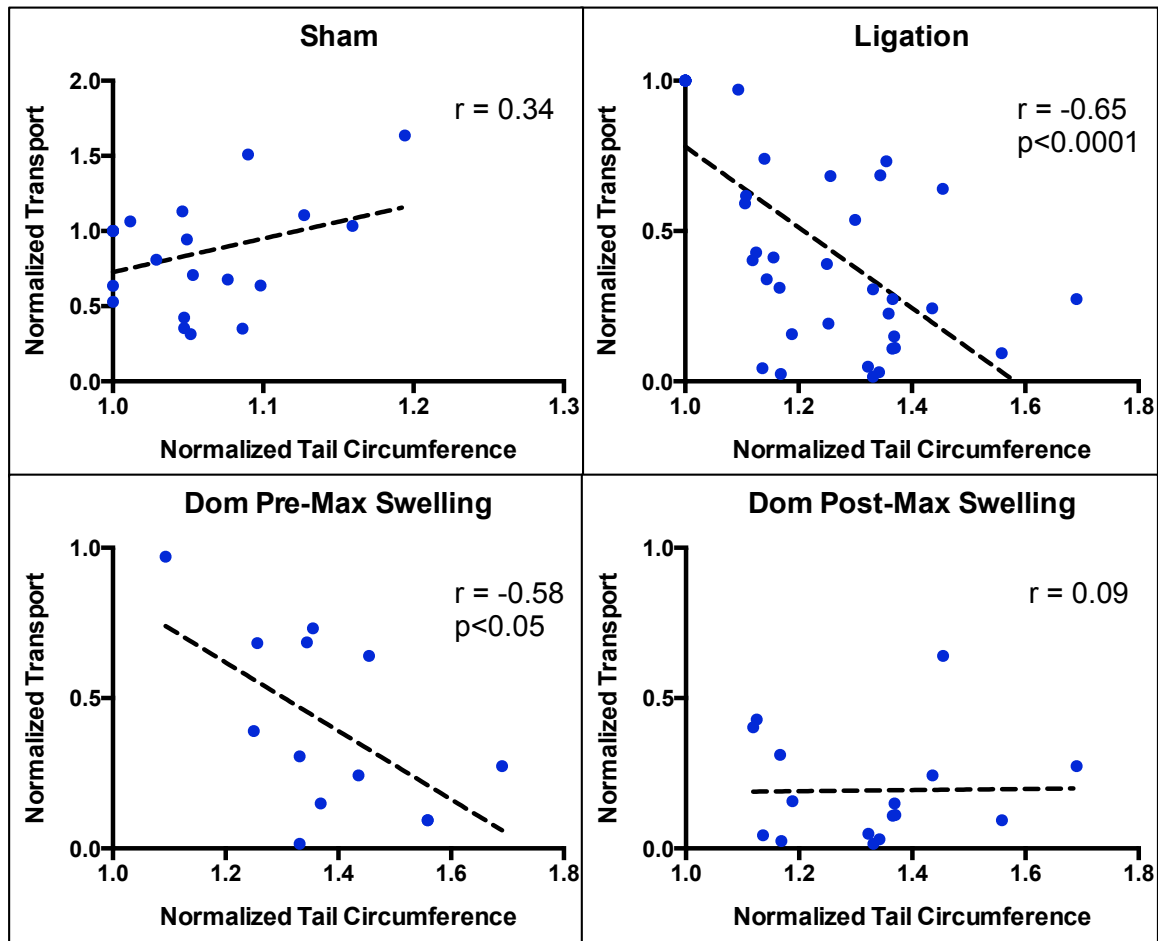
Figure 31: Correlation between tail circumference and lymphatic transport. Plots of normalized lymphatic transport versus normalized tail circumference for the sham group (top left), the two ligation groups combined (top right), the dominant ligation group prior to the point of max swelling (bottom left), and the dominant ligation group after the point of max swelling (bottom right). The sham group produced a Pearson r of 0.34 while the ligation group produced a Pearson r of -0.65. Using a Fisher r-to-z transformation, this difference in correlation coefficients is significant (p<0.0001).

Lymphatic Vasculature Remodels After Lymphedema

At the three-month time point swelling in all conditions completely subsided, but several factors suggest that the dominant ligation resulted in substantial remodeling in lymphatic function compared to the sham control. Percent positive fluorescent tail area, a measure of the relative distribution of lymphatic transport between the collecting vessels and the initial capillary network, was significantly increased in the dominant ligation (Figure 32). Emptying rate was not significantly different between the dominant ligation

90

and the sham at the three-month time point. Effective lymphatic pumping pressure, a measure of the pumping capacity of the collecting vessels, was not significantly different from the baseline measurement through the day 4 time point but became significantly reduced at the three month time point, while the sham group did not produce any significant differences in effective pumping pressure at any time point (Figure 32). Additionally, in the sham, the dominant lymph node was significantly larger and retained significantly more fluorescence than the non-dominant node, but this result was reversed in the dominant ligation (Figure 33).
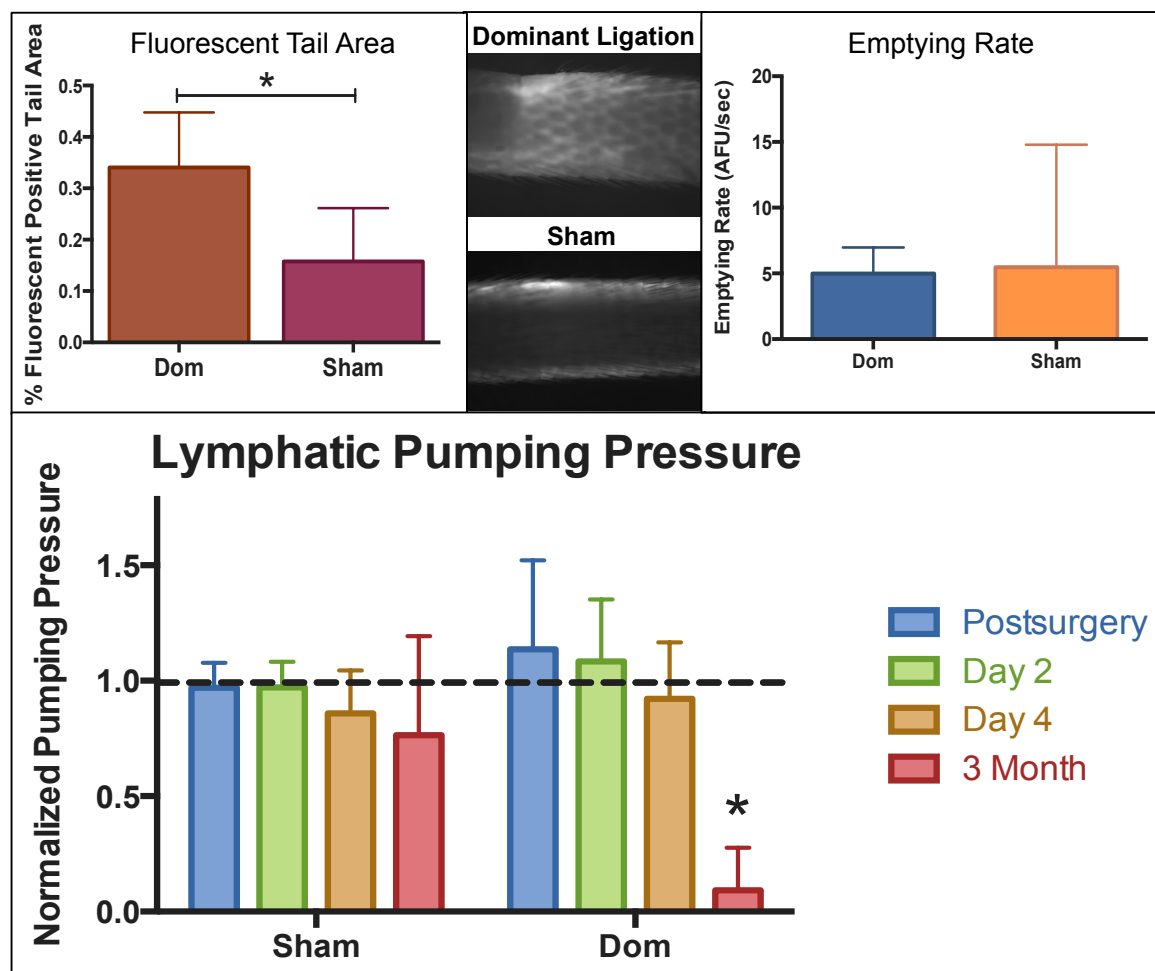
Figure 32: Vessel remodeling at the 3 month time point. Fluorescent tail area was significantly larger in the dominant ligation compared to the sham. Images in the center are representative of transport of NIR dye through the tail after injection in the dominant ligation group (top) and the sham group (bottom). Emptying rate was not significantly different between the dominant ligation and the sham.

Pumping pressure was reduced in the dominant ligation group at the 3 month time point compared to baseline and the sham.
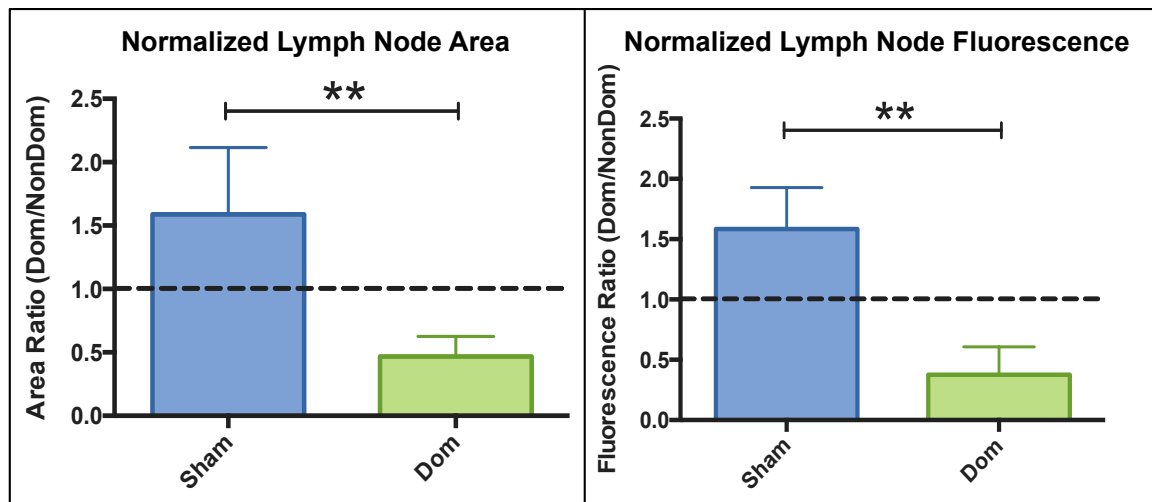
Figure 33: Ligation alters node size and retained fluorescence. Left: Plot showing normalized lymph node area ratios between the dominant and nondominant node for the dominant ligation and sham groups. Right: Plot showing normalized lymph node fluorescence between dominant and nondominant node for the dominant ligation and sham groups.

Discussion

Single Vessel Ligation Model

This is the first model known to the authors that allows preservation of an intact collecting lymphatic vessel in a lymphedema model and the first model to enable functional analysis lymphatic transport during the course of lymphedema. The timeline for tail swelling and eventual recovery followed similar trends reported in the literature for full tail ligation models, but the magnitude of swelling in our model was on average less than half that reported for the full ligation model(195, 279). Given that we keep one collector fully intact, the magnitude difference in swelling in our model is not surprising and may actually serve to test the sensitivity of NIR functional metrics in more mild cases of the disease.

The tail swelling results also confirmed our hypothesis that ligation of the dominant vessel would produce significantly more swelling than ligation of the nondominant vessel, which we presume is due to the dominant vessel having a larger

lymphatic reserve(22, 267). That is, when the dominant vessel is left intact it is better able to handle the elevated fluid loads forced upon it after surgery than the nondominant vessel. It is interesting to note that the difference in swelling produced by the dominant and nondominant ligation only occurs prior to the 1 week time point, which could suggest that remodeling in the matrix and interstitium begins to occur at and beyond this point to help alleviate fluid loads, as has been shown to occur in lymphedema models previously(164, 253). It is possible with our experimental setup to track and quantify transport through the interstitium and the capillary level lymphatics, and future versions of this study with particular emphasis on quantifying transport in this regard could provide additional insight to the remodeling cascade.

In the spectrum of lymphedema-related swelling, our effect size between the dominant and nondominant ligation is relatively small, and it remains unclear what implication, if any, these results may have on human lymphedema. However, these are the first results that show a significant difference in outcomes based upon selective lymphatic ligation, which could have future implications for surgical planning or targeted therapy if the phenomenon is found to be widespread. Future studies utilizing selective vessel ligation in other models would be well warranted, especially models incorporating a gravitational load (such as in the limb of a large animal), which may be particularly useful in exacerbating the swelling response and highlighting the effects of preferential drainage patterns.

Reductions in Lymphatic Transport and Remodeling

In this study we have demonstrated the first direct link between swelling and the progressive loss of lymphatic transport function during the lymphedema disease cascade in vivo. The results show that lymphatic transport is significantly reduced after surgery in both ligation groups, and the reduction in transport strongly correlates with the level of swelling in the ligation groups. This is consistent with the vast number of studies reporting the link between inflammation and the progression of lymphedema; recent data from numerous animal and human studies of lymphedema have made it abundantly clear that inflammation is perhaps the most important factor in driving lymphedema progression, (7, 15, 16, 115, 136, 199, 237, 279) particularly as it relates to the changes

that occur in the interstitium. Given that inflammatory cytokines have also been demonstrated to adversely affect collecting lymphatic pump function (37, 38, 114, 283), it is likely that the consequences of inflammatory driven lymphedema progression not only alter the interstitium, but severely compromise pump function and drainage by the collectors. Future work devoted to the application of anti-inflammatories in this model may provide valuable insights regarding therapeutic strategies to preserve collecting vessel function.

It is interesting to note that when the data is divided between the time period prior to maximum swelling and after maximum swelling, the correlation only exists in the time period prior to maximum swelling. This presents a potential inconsistency in that increased swelling is correlated with reduced lymphatic transport, but decreased swelling is not correlated with improved lymphatic transport. This suggests that the two variables are linked only until the swelling reaches its peak, but after that point, residual damage and remodeling has occurred such that the relationship is altered, which is supported by the observed remodeling and phenotypic changes of excised vessels from human lymphedema patients(139). Such a remodeling event would also be very consistent with the observed lymphatic pumping pressure and fluorescent tail area results from this study. Lymphatic pumping pressure was not significantly different within the first week, but by 3 months it was reduced down to less than 10% of the baseline value in the dominant ligation group. The observed increase in fluorescent tail area in the dominant ligation group suggests that the interstitium and the initial capillary network were recruited to transport a larger percentage of fluid than normal in order to compensate for the chronic reduction in lymphatic transport through the collecting vessels, which is a phenomenon observed recently in human lymphedema(117).

The significant reduction in transport of the dominant group compared to the nondominant group further supports the theory of preferential lymphatic drainage pathways, at least in the rodent tail. It is unclear whether the increased swelling associated with the dominant group contributed to the reductions in transport or vice versa, but it appears obvious that functional differences between the two vessels exist. Unfortunately, no data was acquired in this study that can help to establish a mechanism or explanation for this relative difference in function between the two collectors, but

94

future studies in this regard would be extremely useful. For instance, the ability to excise collecting vessels from the tail to perform mechanical testing and whole-mount staining, while very challenging and approaching the lower limits of the size scale for the technique, could help to provide insight as to whether the observed differences are potentially due to geometrical and/or structural/compositional variances.

Analyzing the packet frequency and packet amplitude results provides additional insight into the observed decrease in fluorescence transport of the dominant group. The average packet frequency was reduced only at the 4 day and 1 week time points, while the average packet amplitude was reduced at all time points. This means that the majority of the observed reduction in transport was due to reductions in packet amplitude. From isolated vessel studies in our lab (not shown), packet amplitude correlates very highly with the ejection fraction of the vessel such that larger packet amplitudes occur when the ejection fraction is larger. Since we perform our fluorescence analysis in regions of the vessel that are typically dark (vessel constricted), we can further infer that observed reductions in packet amplitude are primarily caused by reductions in end diastolic diameter, which would be consistent with reports of thickening of the vessel wall and decreases in the diameter of the lumen as the remodeling cascade occurs(139).

The chronic reduction in lymphatic transport in the dominant ligation group through the three-month time point was an unexpected result. By this time period the tissue did not exhibit any signs of swelling, and the ligation scar was no longer visible. Based upon visual inspection and volume measurements, the animals did not have lymphedema at this point. However, it is obvious from looking at the transport and pumping pressure data that the underlying lymphatic function remained severely compromised. This result is in line with those of Mendez et al. and helps to explain the latent lymphatic insufficiency they observed after axillary lymph node dissection in the forelimb(136). It is clear from our data that the lymphatic system sufficiently recovered to maintain fluid balance levels, which is why the tissue volume returned to normal. The fact that no significant difference was observed in emptying rate further supports the lymphatics accommodate normal fluid loads in the post-lymphedema phase. The reductions in transport and pumping pressure reveal that despite the appearance of normal tissue, the vessels have remodeled such that they've lost a significant ability to pump,

which would explain the inability to handle the elevated fluid loads associated with the immune challenge introduced by Mendez and colleagues. It should be noted that we attempted to recreate the results of Mendez by applying oxazolone to the tails after lymphedema, but we were unable to achieve a response.

Ogata et al. also recently reported substantial phenotypic modulation of smooth muscle cells in collecting vessels excised from lymphedema patients such that smooth muscle myosin heavy chain isoforms SM1 and SM2 were significantly reduced(161), which could explain the observed decline in pumping pressure in our study. Smooth muscle cell content and composition was not investigated in this study, but future work in this regard could provide the most meaningful new insights. Alternatively, the reductions in transport and pumping pressure could have been caused by changes in valve function in response to altered mechanical loading resulting in an inability to maintain unidirectional flow and decreasing pumping capacity (49). Under modest mechanical loading, the valves of isolated lymphatic vessel chains have been demonstrated to "lock" resulting in an inability to pump flow against an adverse pressure gradient (49). Given that the behavior of lymphatic valves are highly sensitive to pressure (50) and mutations affecting the proper formation of lymphatic valves is one of the most common causes of primary lymphedema (132, 143, 167), it is reasonable to suspect non-optimal valve function may be contributing to the observed decreases in pumping capacity. Conducting these experiments in a transgenic mouse model without valves or with valve deformations, such as the transgenic ephrinB2$^{\Delta V/\, \Delta V}$ model(125), may help to specifically elucidate the role of valvular function in lymphedema progression.

Analysis of the draining lymph nodes from the dominant ligation and sham groups revealed interesting trends regarding lymph transport routes. In the sham group the node draining the dominant vessel was larger and retained more fluorescence than the nondominant node, which again supports the theory of differential drainage patterns between the two vessels. Not surprisingly, the lymphatic drainage patterns were altered after the dominant ligation to favor the non-dominant node, which drained the fully intact vessel. Interestingly, in the dominant group, the nondominant node was approximately as large and retained approximately as much fluorescence as the dominant node of the sham group, perhaps suggesting some type of ideal physiological set point. It is unclear what

the ramifications of this change in drainage patterns might be, but it could have implications for immune response. Future investigation regarding the transport of immune cells, both through the local tissue environment and to the draining lymph nodes may help to provide insight on the link between lymphatic function and immune surveillance, especially in the context of reduced lymphatic function.

As an additional note, we should also mention that in our study we had two mice that had abnormally low baseline lymphatic transport values, and both of these mice experienced tail swelling well above the group average. Unfortunately, both of these mice suffered unrelated complications and had to be euthanized early in the time course, but it may suggest that research into predisposition of lymphedema would be a worthwhile study in this model. Studies have been reported in the literature citing factors potentially leading to a predisposition to lymphedema(17, 18, 218), but this phenomenon has not yet been investigated under the control of an animal model. Given the results of our study, we might hypothesize that baseline transport values below a certain threshold result in significantly worse disease outcomes or potentially that the baseline difference in function between the dominant and nondominant vessels is a predictor of disease severity. Performing this model in aged animals, as has been done in several other lymphatic studies(38, 74, 149, 250), may provide a population better suited to study the link between the loss of lymphatic function and lymphedema onset and progression.

Limitations and Future Work

Every effort was made to make the ligation and cauterization procedure as consistent as possible between animals and between groups, especially attempting to ensure that the sham surgeries were as similar in size to those of the vessel ligation groups as possible. We believe we maintained an excellent level of consistency, which was aided by only using one person to perform all the surgeries. However, the ligation and cauterization process was not quantified in any way in terms of circumferential distance or depth. It is unclear exactly how the ligation itself affects the subsequent outcomes, but this process almost certainly has an affect. Future efforts to standardize this part of the procedure would greatly improve the reproducibility of the results.

The rodent tail model is obviously not a perfect model of human lymphedema for a few reasons, perhaps the most glaring of which is the fact that the condition resolves itself in the rodent. This may not be surprising given that the system only needs to overcome a gravitational pressure gradient of about 1 cmH$_2$O. In this model fluid can rely upon interstitial flow to a larger degree than may be expected in animals with larger gravitational loads, which may limit our ability to isolate the true effects of lymphatic failure. Additionally, this model, by design, is specifically for fatigue-induced lymphedema. While we believe the model provides insights that can be generalized to many types of lymphedema and lymphatic failure, it does not specifically address potential nuances that may be specific to other causes of lymphedema.

Conclusion

In this study we reported a new lymphedema model that for the first time allows assessment of collecting lymphatic function during the lymphedema cascade. Using the model we were able to show the first definitive correlation between swelling and the loss of lymphatic function as well as evidence that the vessel remodels in response to the swelling such that it loses its pumping capacity. This model will provide a platform to investigate more detailed mechanisms of lymphatic dysfunction associated with lymphedema.

CHAPTER 5: CONCLUSION AND FUTURE IMPLICATIONS

Summary

We strongly believe that NIR lymphatic imaging will prove to be an extremely useful tool to study the lymphatic vasculature in new and exciting ways and will generate insights unobtainable with conventional research techniques. With that said, the methodology remains in an immature state, and we have taken specific steps to advance the technique in the physical and physiological aspects. We performed the first engineering analysis of NIR lymphatic imaging, focusing specifically on characterizing the limitations of the system with regard to depth penetration and spatial resolution. We demonstrated that fluorophore uptake is dependent on protein concentration and offered

an optimal delivery solution of ICG premixed with albumin to maximize SNR in the collecting vessels. Our modulation of the lymphatic system with a dermal nitric oxide donor was the first effort to demonstrate that NIR lymphatic function metrics are, indeed, sensitive to changes in collecting vessel pumping. We also provided the first proof that packets are directly linked to contractile events in the vessel. Cumulatively, the first aim of this work provided a much-needed assessment of the physical aspects of the technique as they relate specifically to imaging and quantifying lymphatic collecting vessel function. The results of this aim have helped to enhance the physiological relevance of the metrics and have provided a guide for utilizing the technique specifically in rodent research models.

The second aim of this work was focused on the physiology of collecting lymphatic vessels operating as an organ system. Specifically, we attempted to address the question of how multiple collecting vessels drain a single tissue space. We were able to show that the two collecting trunks draining the rodent tail consistently display differential transport function, and we created a new framework for classifying these vessels for subsequent analysis by creating the terms "dominant" and "nondominant" vessels. This classification system has proven to be extremely useful in much of our subsequent work and has specifically aided our analysis of disease models. We also focused extensive efforts to understanding the limitations of NIR imaging in the context of time-course experiments with repeat injections. Our results helped to clarify a conflict in the literature by showing ICG reduces lymphatic function in a time-delayed fashion such that repeat imaging sessions produce lower lymphatic function than normal if the ICG is not allowed to clear out of the system. Importantly, we were able to show that a commercially available fluorophore limits these time-course effects, which enabled the repeat injection procedures necessary for studying lymphedema progression.

The final aim of this work represents the crux of the research and provides arguably the most impactful results for the field. We developed the first model of lymphedema that allows the assessment of lymphatic collecting vessel function during the progression of the disease. This model has the potential for extensive use by a wide-range of researchers to probe mechanisms of lymphatic remodeling and pump failure. We specifically used the model to provide the first direct correlation increases in swelling

and decreases in lymphatic function. Furthermore, we provided significant evidence that fatigue-induced remodeling events occurred in the vessels during the disease cascade such that the pumping capacity of the vessels was drastically reduced. Future work with this model will allow the study of specific mechanisms of lymphatic remodeling that lead to pump failure, and perhaps more importantly, will allow the investigation of therapeutic and prevention strategies to minimize the loss of pump function.

Limitations

There are several limitations to this work that inform the need for future work in this area. Arguably, the largest limitation of our model, and NIR lymphatic imaging in general, is the injection of a fluorophore. The bolus injection increases interstitial fluid pressures, the fluorophore itself has effects on the vasculature, and the consistency of the injection itself affects uptake. These are all inherent limitations of the technique that cannot be eliminated, but can be managed. While we've attempted to minimize the effects of this process on lymphatic function as much as possible by optimizing the choice of fluorophore and minimizing the volume of injection, there is no doubt that this procedure alters lymphatic function, at least to a small degree. We attempted to make every effort to standardize our injection procedure because differences in injection depth and angle can dramatically affect fluorophore uptake and resultant NIR functional metrics. We spent considerable time perfecting the technique before performing our studies, and we only used one person for injections in a given study to minimize variations in technique. Despite these efforts, variability in the injection was unavoidable and contributes to variance in our data. Future work devoted to the development of microneedles specifically optimized for intradermal injection of fluorophores for lymphatic imaging would be a monumental improvement to enhance the consistency and reproducibility of the technique. Continued work towards the development of new fluorophores specific for lymphatic imaging would also help to eliminate unwanted side-effects of fluorophore introduction, especially in time-course studies with repeat procedures.

The second significant limitation of this work centers around the NIR metrics and measurement process. Despite the significant work we devoted to expanding the breadth

and utility of existing NIR lymphatic functional metrics, we are still only using a fraction of the available data from these procedures. Perhaps the largest inconsistency in the measurement process results from the choice of regions of interest for post-processing packet analysis. We have standardized this procedure internally within our own lab by always choosing "dark" regions of the vessel for packet analysis, which provides a similar fluorescence profile of packet spikes over time, but much more work could be directed towards standardizing and automating this process. By selecting one or two regions of interest along the vessel, we ignore the data from the remaining 80% of the collector in the field of view. Ideally, NIR functional metrics should be calculated using as much of the vessel as can fit in the field of view in order to obtain spatially averaged transport characteristics along the length of the vessel. Advanced image processing and other computational methods devoted to this effort would almost certainly reveal additional insight currently lost in the data sets. There is also undoubtedly room to develop novel metrics beyond those based on packet identification that can more robustly assess lymphatic transport and function.

An additional limitation is the use of the rodent tail as the anatomic region for our model. The tail provides distinct benefits such as a simple geometry and the ability to visualize two collecting vessels simultaneously. However, it is difficult to translate these results directly to other anatomic regions and to other species. The packet dynamics seen in the tail appear to be relatively similar to those reported in rodent and human limbs, although a quantitative comparison has not yet been done. Similarly, the differential transport phenomenon between collecting vessels has been reported in rodent limbs, which suggests the results of our study can be generalized to other models to at least a certain degree. It seems most likely that research developments in the tail model will be used mainly address specific questions regarding lymphatic vessel function, which can then be tested and validated in other models.

Additional Hypotheses and Future Work

The development of our new single vessel ligation model of lymphedema provides a tremendous platform for future work investigating the link between lymphatic

function and lymphedema progression. I have outlined a few targets for future research and have provided some potential hypotheses to guide the investigations.

Therapeutic and Prevention Strategies

Given our results showing the correlation between swelling and reduced lymphatic function, the extensive research showing the detrimental effects of inflammation(7, 15, 16, 115, 136, 199, 237, 279), and literature reports of anti-inflammatories improving lymphedema outcomes(150), a study investigating the effects of anti-inflammatories on collecting vessel function in a lymphedema model would be an impactful next step. Since our results showed that lower levels of peak swelling resulted in better long-term collecting vessel transport, I would generally hypothesize that the addition of anti-inflammatories to reduce swelling after surgery would help to preserve collecting vessel pumping capacity by minimizing remodeling activity within the vessel. Of course, to help address these questions, we would first need to better characterize the remodeling activity that has occurred in our model with a thorough histological analysis, which is a top priority for future work.

Other potential therapeutic strategies could potentially include cellular regeneration strategies to repair dysfunctional collectors. Since collecting lymphatic vessels are extremely sensitive to their mechanical environment, rebuilding lymphatic networks at the cellular may provide a novel regenerative strategy for lymphedema treatment. Recently, Lee et al. have developed a culture system to direct bone marrow derived pluripotent stem cells into lymphatic precursor cells. These precursor cells, termed Lymphatic Endothelial Progenitor Cells (LEPCs), are capable of melding into new lymphatic vasculature (through lymphatic neovascularization) and spurring new lymphatic growth (lymphangiogensis)(110). To date, it is unclear exactly what effect these cells may have on collecting vessel function, but it has been shown that LEPC-treated mouse tails exhibit increased fluorescence transport through collecting vessels (unpublished). Therefore, I would hypothesize that injection of LEPCs in the lymphedema tail model would have either a protective or regenerative effect on collecting vessel pump function. Given the literature regarding the change in coverage and composition of smooth muscle cells along vessels from lymphedema patients(161), a

similar approach could potentially be taken with the injection of smooth muscle cells to potentially restore pumping capacity.

Vessel Function

A phenomenon seen but not explored or quantified in our studies was the presence of backflow in our NIR images. With additional enhancements to our processing algorithms, it should be possible to generate a reliable metric of backflow within the vessels. This new data may provide valuable insight regarding the propagation of flow, which could potentially be used to assess the functionality of valve segments. Initially, I would hypothesize that elevated levels of backflow in baseline measurements would be a predictor of worse disease outcomes because it may indicate the vasculature is predisposed to fail.

Another factor that could be explored as a potential predisposing factor is the relative difference in baseline transport between the dominant and nondominant collectors. There are several scenarios that could play out in this regard, but based on our results to date, I would hypothesize that normal lymphatic function is characterized by a modest increase in transport in the dominant vessel compared to the nondominant vessel, and significant deviations in baseline function from this optimal ratio, may indicate a predisposition to lymphedema.

Finally, one additional factor that could be investigated in our model is the presence and quantity of shunting vessels from the ligated vessel to the intact vessel. This is a phenomenon that was occasionally observed, but not specifically assessed or quantified. Investigation into the number and functional capacity of these shunt vessels could provide interesting data regarding new vessel growth and resultant tissue remodeling. I would hypothesize that larger numbers of functional shunting vessels would correlate with reduced levels of swelling because fluid can more effectively be transported through the tissue.

Overall, we believe the impact of NIR imaging on lymphatic research has only just begun and that the technique will provide new opportunities to gain insight about this understudied vasculature, both in health and disease.

REFERENCES

1.   **Abels C**, **Fickweiler S**, **Weiderer P**, **Baumler W**, **Hofstädter F**, **Landthaler M**, **Szeimies RM**. Indocyanine green (ICG) and laser irradiation induce photooxidation. *Arch. Dermatol. Res.* 292: 404–411, 2000.

2.   **Adams K**, **Rasmussen J**, **Darne C**, **Tan I**. Direct evidence of lymphatic function improvement after advanced pneumatic compression device treatment of lymphedema. *Biomedical Optics Express* 1: 114–125, 2010.

3.   **Adriaenssens N**, **Belsack D**, **Buyl R**, **Ruggiero L**, **Breucq C**, **De Mey J**, **Lievens P**, **Lamote J**. Ultrasound elastography as an objective diagnostic measurement tool for lymphoedema of the treated breast in breast cancer patients following breast conserving surgery and radiotherapy. *Radiology and Oncology* 46, [no date].

4.   **Ahmed RL**, **Schmitz KH**, **Prizment AE**, **Folsom AR**. Risk factors for lymphedema in breast cancer survivors, the Iowa Women's Health Study. *Breast Cancer Res Treat* 130: 981–991, 2011.

5.   **Aldrich MB**, **Davies-Venn C**, **Angermiller B**, **Robinson H**, **Chan W**, **Kwon S**, **Sevick-Muraca EM**. Concentration of indocyanine green does not significantly influence lymphatic function as assessed by near-infrared imaging. *Lymphat Res Biol* 10: 20–24, 2012.

6.   **Alitalo K**, **Tammela T**, **Petrova T**. Lymphangiogenesis in development and human disease. *Nature* 438: 946–953, 2005.

7.   **Anuradha R**, **George PJ**, **Hanna LE**, **Chandrasekaran V**, **Kumaran P**, **Nutman TB**, **Babu S**. IL-4-, TGF-β-, and IL-1-Dependent Expansion of Parasite Antigen-Specific Th9 Cells Is Associated with Clinical Pathology in Human Lymphatic Filariasis. *J Immunol* 191: 2466–2473, 2013.

8.   **Armer JM**, **Hulett JM**, **Bernas M**, **Ostby P**, **Stewart BR**, **Cormier JN**. Best-Practice Guidelines in Assessment, Risk Reduction, Management, and Surveillance for Post-Breast Cancer Lymphedema. *Curr Breast Cancer Rep* 5: 134–144, 2013.

9.   **Armer JM**, **Radina ME**, **Porock D**, **Culbertson SD**. Predicting Breast Cancer-Related Lymphedema Using Self-Reported Symptoms. *Nursing Research* 52: 370, 2003.

10.   **Armer JM**, **Stewart BR**, **Wanchai A**. Rehabilitation concepts among aging survivors living with and at risk for lymphedema: a framework for assessment, enhancing strengths, and minimizing vulnerability. *Topics in Geriatric ….*

11. **Aschen S**, **Aschen S**, **Zampell JC**, **Zampell JC**, **Elhadad S**, **Elhadad S**, **Weitman E**, **Weitman E**, **De Brot M**, **De Brot M**, **Mehrara BJ**, **Mehrara BJ**. Regulation of Adipogenesis by Lymphatic Fluid Stasis: Part II. Expression of Adipose Differentiation Genes. *Plast Reconstr Surg* 129: 838–847, 2012.

12. **Ashitate Y**, **Tanaka E**, **Stockdale A**, **Choi HS**, **Frangioni JV**. Near-infrared fluorescence imaging of thoracic duct anatomy and function in open surgery and video-assisted thoracic surgery. *J. Thorac. Cardiovasc. Surg.* 142: 31–38.e2, 2011.

13. **Avraham T**, **Clavin NW**, **Daluvoy SV**, **Fernandez J**, **Soares MA**, **Cordeiro AP**, **Mehrara BJ**. Fibrosis is a key inhibitor of lymphatic regeneration. *Plast Reconstr Surg* 124: 438–450, 2009.

14. **Avraham T**, **Yan A**, **Zampell JC**, **Daluvoy SV**, **Haimovitz-Friedman A**, **Cordeiro AP**, **Mehrara BJ**. Radiation therapy causes loss of dermal lymphatic vessels and interferes with lymphatic function by TGF-beta1-mediated tissue fibrosis. *AJP: Cell Physiology* 299: C589–605, 2010.

15. **Avraham T**, **Zampell JC**, **Yan A**, **Elhadad S**, **Weitman ES**, **Rockson SG**, **Bromberg J**, **Mehrara BJ**. Th2 differentiation is necessary for soft tissue fibrosis and lymphatic dysfunction resulting from lymphedema. *FASEB J* 27: 1114–1126, 2013.

16. **Babu S**, **Bhat SQ**, **Pavan Kumar N**, **Lipira AB**, **Kumar S**, **Karthik C**, **Kumaraswami V**, **Nutman TB**. Filarial lymphedema is characterized by antigen-specific Th1 and th17 proinflammatory responses and a lack of regulatory T cells. *PLoS Negl Trop Dis* 3: e420, 2009.

17. **Bains SK**, **Peters AM**, **Zammit C**, **Ryan N**, **Ballinger J**, **Glass DM**, **Allen S**, **Stanton AWB**, **Mortimer PS**, **Purushotham AD**. Global abnormalities in lymphatic function following systemic therapy in patients with breast cancer. *Br J Surg* 102: 534–540, 2015.

18. **Bains SK**, **Stanton AWB**, **Cintolesi V**, **Ballinger J**, **Allen S**, **Zammit C**, **Levick JR**, **Mortimer PS**, **Peters AM**, **Purushotham AD**. A constitutional predisposition to breast cancer-related lymphoedema and effect of axillary lymph node surgery on forearm muscle lymph flow. *The Breast* (January 5, 2015). doi: 10.1016/j.breast.2014.11.010.

19. **Baker A**, **Semple JL**, **Moore S**, **Johnston M**. Lymphatic Function Is Impaired Following Irradiation of a Single Lymph Node. *Lymphat Res Biol* (May 16, 2014). doi: 10.1089/lrb.2013.0036.

20. **Baluk P**. Pathogenesis of persistent lymphatic vessel hyperplasia in chronic airway inflammation. *J Clin Invest* 115: 247–257, 2005.

21. **Barrett T**, **Choyke PL**, **Kobayashi H**. Imaging of the lymphatic system: new

horizons. *Contrast Media Mol Imaging* 1: 230–245, 2006.

22.   **Bates DO**, **Bates D**. An interstitial hypothesis for breast cancer related lymphoedema. *Pathophysiology* 17: 289–294, 2010.

23.   **Bellin MF**, **Beigelman C**, **Precetti-Morel S**. Iron oxide-enhanced MR lymphography: initial experience. *Eur J Radiol* 34: 257–264, 2000.

24.   **Bellin MF**, **Roy C**, **Kinkel K**, **Thoumas D**, **Zaim S**, **Vanel D**, **Tuchmann C**, **Richard F**, **Jacqmin D**, **Delcourt A**, **Challier E**, **Lebret T**, **Cluzel P**. Lymph node metastases: safety and effectiveness of MR imaging with ultrasmall superparamagnetic iron oxide particles--initial clinical experience. *Radiology* 207: 799–808, 1998.

25.   **Bennuru S**, **Nutman TB**. Lymphangiogenesis and lymphatic remodeling induced by filarial parasites: implications for pathogenesis. *PLoS Pathog* 5: e1000688, 2009.

26.   **Benoit J**, **Zawieja DC**, **Goodman A**, **Granger H**. Characterization of intact mesenteric lymphatic pump and its responsiveness to acute edemagenic stress. *Am J Physiol-Heart C* 257: H2059–H2069, 1989.

27.   **Berk D**, **Swartz MA**, **Leu A**, **Jain R**. Transport in lymphatic capillaries 2. Microscopic velocity measurement with fluorescence photobleaching. *Am J Physiol* 39: H330–H337, 1996.

28.   **Bernas MJ**, **Askew RL**, **Armer JM**, **Cormier JN**. Lymphedema: How Do We Diagnose and Reduce the Risk of This Dreaded Complication of Breast Cancer Treatment? *Curr Breast Cancer Rep* 2: 53–58, 2010.

29.   **Blum KS**, **Proulx ST**, **Luciani P**, **Leroux J-C**, **Detmar M**. Dynamics of lymphatic regeneration and flow patterns after lymph node dissection. *Breast Cancer Res Treat* 139: 81–86, 2013.

30.   **Boardman K**, **Swartz MA**. Interstitial flow as a guide for lymphangiogenesis. *Circ Res* 92: 801–808, 2003.

31.   **Boccardo FM**, **Casabona F**, **Friedman D**, **Puglisi M**, **De Cian F**, **Ansaldi F**, **Campisi C**. Surgical prevention of arm lymphedema after breast cancer treatment. *Annals of Surgical Oncology* 18: 2500–2505, 2011.

32.   **Bohlen HG**, **Gasheva OY**, **Zawieja DC**. Nitric oxide formation by lymphatic bulb and valves is a major regulatory component of lymphatic pumping. *Am J Physiol-Heart C* 301: H1897–906, 2011.

33.   **Bohlen HG**, **Wang W**, **Gashev AA**, **Gasheva OY**, **Zawieja DC**. Phasic contractions of rat mesenteric lymphatics increase basal and phasic nitric oxide generation in vivo. *Am J Physiol-Heart C* 297: H1319–28, 2009.

34. **Burrows PE**, **Gonzalez-Garay ML**, **Rasmussen JC**, **Aldrich MB**, **Guilliod R**, **Maus EA**, **Fife CE**, **Kwon S**, **Lapinski PE**, **King PD**, **Sevick-Muraca EM**. Lymphatic abnormalities are associated with RASA1 gene mutations in mouse and man. *Proc Natl Acad Sci USA* 11: 8621–8626, 2013.

35. **Campisi C**, **Bellini C**, **Eretta C**, **Zilli A**, **da Rin E**, **Davini D**, **Bonioli E**, **Boccardo F**. Diagnosis and management of primary chylous ascites. *YMVA* 43: 1244–1248, 2006.

36. **Carter J**, **Raviv L**, **Appollo K**, **Baser RE**, **Iasonos A**, **Barakat RR**. A pilot study using the Gynecologic Cancer Lymphedema Questionnaire (GCLQ) as a clinical care tool to identify lower extremity lymphedema in gynecologic cancer survivors. *Gynecologic Oncology* 117: 317–323, 2010.

37. **Chakraborty S**, **Zawieja S**, **Wang W**, **Zawieja DC**, **Muthuchamy M**. Lymphatic system: a vital link between metabolic syndrome and inflammation. *Ann N Y Acad Sci* 1207 Suppl 1: E94–102, 2010.

38. **Chatterjee V**, **Gashev AA**. Aging-associated shifts in functional status of mast cells located by adult and aged mesenteric lymphatic vessels. *Am J Physiol-Heart C* 303: H693–702, 2012.

39. **CHERRICK GR**, **STEIN SW**, **LEEVY CM**, **DAVIDSON CS**. Indocyanine green: observations on its physical properties, plasma decay, and hepatic extraction. *J Clin Invest* 39: 592–600, 1960.

40. **Cheung L**, **Han J**, **Beilhack A**, **Joshi S**, **Wilburn P**, **Dua A**, **An A**, **Rockson SG**. An experimental model for the study of lymphedema and its response to therapeutic lymphangiogenesis. *BioDrugs* 20: 363–370, 2006.

41. **Choi I**, **Lee YS**, **Chung HK**, **Choi D**, **Ecoiffier T**, **Lee HN**, **Kim KE**, **Lee S**, **Park EK**, **Maeng Y-S**, **Kim NY**, **Ladner RD**, **Petasis NA**, **Koh CJ**, **Chen L**, **Lenz H-J**, **Hong Y-K**. Interleukin-8 reduces post-surgical lymphedema formation by promoting lymphatic vessel regeneration. *Angiogenesis* 16: 29–44, 2013.

42. **Clavin NW**, **Avraham T**, **Fernandez J**, **Daluvoy SV**, **Soares MA**, **Chaudhry A**, **Mehrara BJ**. TGF-beta1 is a negative regulator of lymphatic regeneration during wound repair. *Am J Physiol-Heart C* 295: H2113–27, 2008.

43. **Clément O**, **Luciani A**. Imaging the lymphatic system: possibilities and clinical applications. *Eur Radiol* 14: 1498–1507, 2004.

44. **Corot C**, **Robert P**, **Idée J-M**, **Port M**. Recent advances in iron oxide nanocrystal technology for medical imaging. *Adv Drug Deliver Rev* 58: 1471–1504, 2006.

45. **Cuzzone DA**, **Weitman ES**, **Albano NJ**, **Ghanta S**, **Savetsky IL**, **Gardenier**

JC, **Joseph WJ**, **Torrisi JS**, **Bromberg JF**, **Olszewski WL**, **Rockson SG**, **Mehrara BJ**. IL-6 regulates adipose deposition and homeostasis in lymphedema. *Am J Physiol-Heart C* 306: H1426–H1434, 2014.

46. **Czerniecki BJ**, **Bedrosian I**, **Faries M**, **Alavi A**. Revolutionary impact of lymphoscintigraphy and intraoperative sentinel node mapping in the clinical practice of oncology. *Semin Nucl Med* 31: 158–164, 2001.

47. **Davies-Venn CA**, **Angermiller B**, **Wilganowski N**, **Ghosh P**, **Harvey BR**, **Wu G**, **Kwon S**, **Aldrich MB**, **Sevick-Muraca EM**. Albumin-Binding Domain Conjugate for Near-Infrared Fluorescence Lymphatic Imaging. *Mol Imaging Biol* 14: 301–314, 2011.

48. **Davis MJ**, **Davis AM**, **Lane MM**, **Ku CW**, **Gashev AA**. Rate-sensitive contractile responses of lymphatic vessels to circumferential stretch. *J Physiol (Lond)* 587: 165–182, 2009.

49. **Davis MJ**, **Moore JE**, **Zawieja DC**, **Gashev AA**, **Scallan JP**. Lymphatic valve lock in response to modest gravitational loads: a contributing mechanism to peripheral lymphedema? *FASEB journal : official publication of the Federation of American Societies for Experimental Biology* 26: 677.2, 2012.

50. **Davis MJ**, **Rahbar E**, **Gashev AA**, **Zawieja DC**, **Moore JE**. Determinants of valve gating in collecting lymphatic vessels from rat mesentery. *Am J Physiol-Heart C* 301: H48–H60, 2011.

51. **Dayton PA**, **Rychak JJ**. Molecular ultrasound imaging using microbubble contrast agents. *Front. Biosci.* 12: 5124–5142, 2007.

52. **Delbeke D**. Oncological applications of FDG PET imaging: brain tumors, colorectal cancer, lymphoma and melanoma. *J. Nucl. Med.* 40: 591–603, 1999.

53. **Dixon JB**, **Gashev AA**, **Zawieja DC**, **Moore JE Jr**, **Cote G**. Image correlation algorithm for measuring lymphocyte velocity and diameter changes in contracting microlymphatics. *Ann Biomed Eng* 35: 387–396, 2007.

54. **Dixon JB**, **Moore JE Jr**, **Cote G**, **Gashev AA**, **Zawieja DC**. Lymph flow, shear stress, and lymphocyte velocity in rat mesenteric prenodal lymphatics. *Microcirculation* 13: 597–610, 2006.

55. **Dixon JB**, **Zawieja DC**, **Gashev AA**, **Cote G**. Measuring microlymphatic flow using fast video microscopy. *J Biomed Opt* 10: 064016, 2005.

56. **Dixon JB**. Lymphatic lipid transport: sewer or subway? *Trends in Endocrinology & Metabolism* 21: 480–487, 2010.

57. **Dongaonkar RM**, **Laine GA**, **Stewart RH**, **Quick CM**. Balance point characterization of interstitial fluid volume regulation. *Am J Physiol Regul Integr*

Comp Physiol 297: R6–16, 2009.

58.   **Dreyer G**, **Addiss D**, **Noroes J**, **Amaral F**, **Rocha A**, **Coutinho A**.
        Ultrasonographic assessment of the adulticidal efficacy of repeat high-dose
        ivermectin in bancroftian filariasis. *Trop Med Int Health* 1: 427–432, 1996.

59.   **Dreyer G**, **Addiss D**, **Roberts J**, **Norões J**. Progression of lymphatic vessel
        dilatation in the presence of living adult Wuchereria bancrofti. *Trans R Soc Trop
        Med Hyg* 96: 157–161, 2002.

60.   **Ege GN**. Internal mammary lymphoscintigraphy. The rationale, technique,
        interpretation and clinical application: a review based on 848 cases. *Radiology*
        118: 101–107, 1976.

61.   **Ezaki T**, **Baluk P**, **Thurston G**, **La Barbara A**, **Woo C**, **McDonald DM**. Time
        course of endothelial cell proliferation and microvascular remodeling in chronic
        inflammation. *Am J Pathol* 158: 2043–2055, 2001.

62.   **Fickweiler S**, **Szeimies RM**, **Baumler W**, **Steinbach P**, **Karrer S**, **Goetz AE**,
        Abels C, **Hofstädter F**, **Landthaler M**. Indocyanine green: intracellular uptake
        and phototherapeutic effects in vitro. *J. Photochem. Photobiol. B, Biol.* 38: 178–
        183, 1997.

63.   **Finegold DN**, **Baty CJ**, **Knickelbein KZ**, **Perschke S**, **Noon SE**, **Campbell D**,
        Karlsson JM, **Huang D**, **Kimak MA**, **Lawrence EC**, **Feingold E**, **Meriney SD**,
        Brufsky AM, **Ferrell RE**. Connexin 47 mutations increase risk for secondary
        lymphedema following breast cancer treatment. *Clin Cancer Res* 18: 2382–2390,
        2012.

64.   **Finegold DN**, **Schacht V**, **Kimak MA**, **Lawrence EC**, **Foeldi E**, **Karlsson JM**,
        Baty CJ, **Ferrell RE**. HGF and MET mutations in primary and secondary
        lymphedema. *Lymphat Res Biol* 6: 65–68, 2008.

65.   **Fischer M**, **Costanzo U**, **Hoffmann U**. Flow velocity of cutaneous lymphatic
        capillaries in patients with primary lymphedema. *Journal of Vascular ….*

66.   **Flister MJ**, **Wilber A**, **Hall KL**, **Iwata C**, **Miyazono K**, **Nisato RE**, **Pepper
        MS**, **Zawieja DC**, **Ran S**. Inflammation induces lymphangiogenesis through up-
        regulation of VEGFR-3 mediated by NF-kappaB and Prox1. *Blood* 115: 418–
        429, 2010.

67.   **Fogh-Andersen N**, **Altura BM**, **Altura BT**, **Siggaard-Andersen O**.
        Composition of interstitial fluid. *Clinical Chemistry* 41: 1522–1525, 1995.

68.   **Foldi M**. Foldi's Textbook of Lymphology: For Physicians and Lymphedema
        Therapists.

69.   **Frangioni J**. In vivo near-infrared fluorescence imaging. *Current Opinion in*

Chemical Biology 7: 626–634, 2003.

70. **Gardner GC**, **Nickerson JP**, **Watts R**, **Nelson L**, **Dittus KL**, **O'Brien PJ**. Quantitative and Morphologic Change Associated with Breast Cancer-Related Lymphedema. Comparison of 3.0T MRI to External Measures. *Lymphat Res Biol* (March 21, 2014). doi: 10.1089/lrb.2013.0026.

71. **Gashev AA**, **Davis MJ**, **Delp M**, **Zawieja DC**. Regional variations of contractile activity in isolated rat lymphatics. *Microcirculation* 11: 477–492, 2004.

72. **Gashev AA**, **Davis MJ**, **Zawieja DC**. Inhibition of the active lymph pump by flow in rat mesenteric lymphatics and thoracic duct. *Journal of Physiology* 540: 1023–1037, 2002.

73. **Gashev AA**, **Nagai T**, **Bridenbaugh EA**. Indocyanine green and lymphatic imaging: current problems. *Lymphat Res Biol* 8: 127–130, 2010.

74. **Gashev AA**, **Zawieja DC**. Hydrodynamic regulation of lymphatic transport and the impact of aging. *Pathophysiology* (March 10, 2010). doi: 10.1016/j.pathophys.2009.09.002.

75. **Gaw R**, **Box R**, **Cornish B**. Bioimpedance in the assessment of unilateral lymphedema of a limb: the optimal frequency. *Lymphat Res Biol* 9: 93–99, 2011.

76. **Giuliano AE**, **Kirgan DM**, **Guenther JM**, **Morton DL**. Lymphatic mapping and sentinel lymphadenectomy for breast cancer. *Annals of Surgery* 220: 391–8; discussion 398–401, 1994.

77. **Goldberg BB**, **Merton DA**, **Liu J-B**, **Thakur M**, **Murphy GF**, **Needleman L**, **Tornes A**, **Forsberg F**. Sentinel lymph nodes in a swine model with melanoma: contrast-enhanced lymphatic US. *Radiology* 230: 727–734, 2004.

78. **Goldman J**, **Conley K**, **Raehl A**, **Bondy D**, **Pytowski B**, **Swartz MA**, **Rutkowski JM**, **Jaroch D**, **Ongstad E**. Regulation of lymphatic capillary regeneration by interstitial flow in skin. *Am J Physiol-Heart C* 292: H2176–H2183, 2007.

79. **Gramiak R**, **Shah PM**, **Kramer DH**. Ultrasound cardiography: contrast studies in anatomy and function. *Radiology* 92: 939–948, 1969.

80. **Harisinghani M**, **Barentsz J**, **Hahn P**. Noninvasive detection of clinically occult lymph-node metastases in prostate cancer. *... England Journal of ....*

81. **Harvey AJ**, **Kaestner SA**, **Sutter DE**, **Harvey NG**, **Mikszta JA**, **Pettis RJ**. Microneedle-Based Intradermal Delivery Enables Rapid Lymphatic Uptake and Distribution of Protein Drugs. *Pharm Res* 28: 107–116, 2011.

82. **Harvey N**, **Srinivasan R**, **Dillard M**, **Johnson N**, **Witte M**, **Boyd K**, **Sleeman**

M, **Oliver G**. Lymphatic vascular defects promoted by Prox1 haploinsufficiency cause adult-onset obesity. *Nat Genet* 37: 1072–1081, 2005.

83. **Hasebroock KM**, **Serkova NJ**. Toxicity of MRI and CT contrast agents. *Expert Opin Drug Metab Toxicol* 5: 403–416, 2009.

84. **Hauff P**, **Reinhardt M**, **Briel A**, **Debus N**, **Schirner M**. Molecular targeting of lymph nodes with L-selectin ligand-specific US contrast agent: a feasibility study in mice and dogs. *Radiology* 231: 667–673, 2004.

85. **Helm C**, **Fleury M**, **Zisch A**, **Boschetti F**, **Swartz MA**. Synergy between interstitial flow and VEGF directs capillary morphogenesis in vitro through a gradient amplification mechanism. *Proc Natl Acad Sci USA* 102: 15779–15784, 2005.

86. **Helyer LK**, **Varnic M**, **Le LW**, **Leong W**, **McCready D**. Obesity is a Risk Factor for Developing Postoperative Lymphedema in Breast Cancer Patients. *Breast J* 16: 48–54, 2010.

87. **Herborn CU**, **Lauenstein TC**, **Vogt FM**, **Lauffer RB**, **Debatin JF**, **Ruehm SG**. Interstitial MR lymphography with MS-325: characterization of normal and tumor-invaded lymph nodes in a rabbit model. *AJR Am J Roentgenol* 179: 1567–1572, 2002.

88. **Hoffman JM**, **Gambhir SS**. Molecular imaging: the vision and opportunity for radiology in the future. *Radiology* 244: 39–47, 2007.

89. **Hutteman M**, **Choi HS**, **Mieog JSD**, **Vorst JR**, **Ashitate Y**, **Kuppen PJK**, **Groningen MC**, **Löwik CWGM**, **Smit VTHBM**, **Velde CJH**, **Frangioni JV**, **Vahrmeijer AL**. Clinical Translation of Ex Vivo Sentinel Lymph Node Mapping for Colorectal Cancer Using Invisible Near-Infrared Fluorescence Light. *Annals of Surgical Oncology* 18: 1006–1014, 2010.

90. **Ikagawa H**. Chemical Toxicity of Indocyanine Green Damages Retinal Pigment Epithelium. *Investigative Ophthalmology & Visual Science* 46: 2531–2539, 2005.

91. **Jane M Armer BRSRPS**. 30-MONTH POST-BREAST CANCER TREATMENT LYMPHOEDEMA. *Journal of lymphoedema* 4: 14, 2009.

92. **Ji RC**. Characteristics of lymphatic endothelial cells in physiological and pathological conditions. *Histol. Histopathol.* 20: 155–175, 2005.

93. **Jurisic G**, **Detmar M**. Lymphatic endothelium in health and disease. *Cell Tissue Res* 335: 97–108, 2009.

94. **Kafejian-Haddad AP**, **Perez JMC**, **Castiglioni MLV**, **Miranda Júnior F**, **de Figueiredo LFP**. Lymphscintigraphic evaluation of manual lymphatic drainage

for lower extremity lymphedema. *Lymphology* 39: 41–48, 2006.

95. **Kaminskas LM**, **Porter CJH**. Targeting the lymphatics using dendritic polymers (dendrimers). *Adv Drug Deliver Rev* 63: 890–900, 2011.

96. **Karlsen TV**, **McCormack E**, **Mujic M**, **Tenstad O**, **Wiig H**. Minimally invasive quantification of lymph flow in mice and rats by imaging depot clearance of near-infrared albumin. *Am J Physiol-Heart C* 302: H391–H401, 2012.

97. **Karpanen T**, **Alitalo K**. Molecular biology and pathology of lymphangiogenesis. *Annu Rev Pathol* 3: 367–397, 2008.

98. **Kassis T**, **Kohan AB**, **Weiler MJ**, **Nipper ME**, **Cornelius R**, **Tso P**, **Dixon JB**. Dual-channel in-situ optical imaging system for quantifying lipid uptake and lymphatic pump function. *J Biomed Opt* 17: 086005, 2012.

99. **Kesler CT**, **Kuo AH**, **Wong H-K**, **Masuck DJ**, **Shah JL**, **Kozak KR**, **Held KD**, **Padera TP**. Vascular endothelial growth factor-C enhances radiosensitivity of lymphatic endothelial cells. *Angiogenesis* 17: 419–427, 2013.

100. **Kilbreath SL**, **Refshauge KM**, **Ward LC**, **Kastanias K**, **Yee J**, **Koelmeyer LA**, **Beith JM**, **French JR**, **Ung OA**, **Black D**. Factors affecting the preoperative and postoperative extracellular fluid in the arm on the side of breast cancer: a cohort study. *Lymphat Res Biol* 11: 66–71, 2013.

101. **Kim H**, **Kataru RP**, **Koh GY**. Inflammation-associated lymphangiogenesis: a double-edged sword? *J Clin Invest* 124: 936–942, 2014.

102. **Kimura K**, **Tanigawa N**, **Matsuki M**, **Nohara T**, **Iwamoto M**, **Sumiyoshi K**, **Tanaka S**, **Takahashi Y**, **Narumi Y**. High-resolution MR lymphography using ultrasmall superparamagnetic iron oxide (USPIO) in the evaluation of axillary lymph nodes in patients with early stage breast cancer: preliminary results. *Breast Cancer* 17: 241–246, 2010.

103. **Kobayashi H**, **Kawamoto S**, **Brechbiel MW**, **Bernardo M**, **Sato N**, **Waldmann TA**, **Tagaya Y**, **Choyke PL**. Detection of lymph node involvement in hematologic malignancies using micromagnetic resonance lymphangiography with a gadolinum-labeled dendrimer nanoparticle. *Neoplasia* 7: 984–991, 2005.

104. **Kornuta JA**, **Brandon Dixon J**. Ex vivo lymphatic perfusion system for independently controlling pressure gradient and transmural pressure in isolated vessels. *Ann Biomed Eng* 42: 1691–1704, 2014.

105. **Kos S**, **Haueisen H**, **Lachmund U**, **Roeren T**. Lymphangiography: forgotten tool or rising star in the diagnosis and therapy of postoperative lymphatic vessel leakage. *Cardiovasc Intervent Radiol* 30: 968–973, 2007.

106. **Krag D**, **Weaver D**, **Ashikaga T**, **Moffat F**, **Klimberg VS**, **Shriver C**, **Feldman S**, **Kusminsky R**, **Gadd M**, **Kuhn J**, **Harlow S**, **Beitsch P**. The sentinel node in breast cancer--a multicenter validation study. *N Engl J Med* 339: 941–946, 1998.

107. **Kwon S**, **Sevick-Muraca EM**. Noninvasive quantitative imaging of lymph function in mice. *Lymphat Res Biol* 5: 219–232, 2007.

108. **Kwon S**, **Sevick-Muraca EM**. Functional lymphatic imaging in tumor-bearing mice. *Journal of Immunological Methods* 360: 167–172, 2010.

109. **Lee JH**, **Shin BW**, **Jeong HJ**, **Kim GC**, **Kim DK**, **Sim Y-J**. Ultrasonographic Evaluation of Therapeutic Effects of Complex Decongestive Therapy in Breast Cancer-Related Lymphedema. *Ann Rehabil Med* 37: 683, 2013.

110. **Lee JY**, **Park C**, **Cho YP**, **Lee E**, **Kim H**, **Kim P**, **Yun SH**, **Yoon Y-S**. Podoplanin-expressing cells derived from bone marrow play a crucial role in postnatal lymphatic neovascularization. *Circulation* 122: 1413–1425, 2010.

111. **Leu A**, **Berk D**, **Yuan F**, **Jain R**. Flow Velocity in the Superficial Lymphatic Network of the Mouse Tail. *Am J Physiol-Heart C* 36: H1507–H1513, 1994.

112. **Leung G**, **Baggott C**, **West C**, **Elboim C**, **Paul SM**, **Cooper BA**, **Abrams G**, **Dhruva A**, **Schmidt BL**, **Kober K**, **Merriman JD**, **Leutwyler H**, **Neuhaus J**, **Langford D**, **Smoot BJ**, **Aouizerat BE**, **Miaskowski C**. Cytokine candidate genes predict the development of secondary lymphedema following breast cancer surgery. *Lymphat Res Biol* 12: 10–22, 2014.

113. **Levick JR**, **Michel CC**. Microvascular fluid exchange and the revised Starling principle. *Cardiovascular research* 87: 198–210, 2010.

114. **Liao S**, **Cheng G**, **Conner DA**, **Huang Y**, **Kucherlapati RS**, **Munn LL**, **Ruddle NH**, **Jain RK**, **Fukumura D**, **Padera TP**. Impaired lymphatic contraction associated with immunosuppression. *Proc Natl Acad Sci USA* 108: 18784–18789, 2011.

115. **Lin S**, **Kim J**, **Lee M-J**, **Roche L**, **Yang NL**, **Tsao PS**, **Rockson SG**. Prospective Transcriptomic Pathway Analysis of Human Lymphatic Vascular Insufficiency: Identification and Validation of a Circulating Biomarker Panel. *PLoS One* 7: e52021, 2012.

116. **Liu N-F**, **Lu Q**, **Jiang Z-H**, **Wang C-G**, **Zhou J-G**. Anatomic and functional evaluation of the lymphatics and lymph nodes in diagnosis of lymphatic circulation disorders with contrast magnetic resonance lymphangiography. *J Vasc Surg* 49: 980–987, 2009.

117. **Liu N-F**, **Wang B-S**. Functional Lymphatic Collectors in Breast Cancer-Related Lymphedema Arm. *Lymphat Res Biol* 12: 232–237, 2014.

118. **Lohrmann C**, **Foeldi E**, **Bartholomae J-P**, **Langer M**. Gadoteridol for MR imaging of lymphatic vessels in lymphoedematous patients: initial experience after intracutaneous injection. *Br J Radiol* 80: 569–573, 2007.

119. **Lohrmann C**, **Foeldi E**, **Langer M**. Indirect magnetic resonance lymphangiography in patients with lymphedema preliminary results in humans. *Eur J Radiol* 59: 401–406, 2006.

120. **Lohrmann C**, **Foeldi E**, **Speck O**, **Langer M**. High-resolution MR lymphangiography in patients with primary and secondary lymphedema. *AJR Am J Roentgenol* 187: 556–561, 2006.

121. **Lu Q**, **Bui D**, **Liu NF**, **Xu JR**, **Zhao XH**, **Zhang XF**. Magnetic resonance lymphography at 3T: a promising noninvasive approach to characterise inguinal lymphatic vessel leakage. *Eur J Vasc Endovasc Surg* 43: 106–111, 2012.

122. **Lu Q**, **Xu J**, **Liu N**. Chronic lower extremity lymphedema: A comparative study of high-resolution interstitial MR lymphangiography and heavily T2-weighted MRI. *Eur J Radiol* 73: 365–373, 2010.

123. **Lualdi M**, **Colombo A**, **Farina B**, **Tomatis S**, **Marchesini R**. A phantom with tissue-like optical properties in the visible and near infrared for use in photomedicine. *Lasers Surg Med* 28: 237–243, 2001.

124. **Luo S**, **Zhang E**, **Su Y**, **Cheng T**, **Shi C**. A review of NIR dyes in cancer targeting and imaging. *Biomaterials* 32: 7127–7138, 2011.

125. **Makinen T**, **Adams RH**, **Bailey J**, **Lu Q**, **Ziemiecki A**, **Alitalo K**, **Klein R**, **Wilkinson GA**. PDZ interaction site in ephrinB2 is required for the remodeling of lymphatic vasculature. *Genes & development* 19: 397–410, 2005.

126. **Markhus CE**, **Karlsen TV**, **Wagner M**, **Svendsen ØS**, **Tenstad O**, **Alitalo K**, **Wiig H**. Increased interstitial protein because of impaired lymph drainage does not induce fibrosis and inflammation in lymphedema. *Arterioscler Thromb Vasc Biol* 33: 266–274, 2013.

127. **Matsushima S**, **Ichiba N**, **Hayashi D**, **Fukuda K**. Nonenhanced magnetic resonance lymphoductography: visualization of lymphatic system of the trunk on 3-dimensional heavily T2-weighted image with 2-dimensional prospective acquisition and correction. *J Comput Assist Tomogr* 31: 299–302, 2007.

128. **Maus EA**, **Tan I-C**, **Rasmussen JC**, **Marshall MV**, **Fife CE**, **Smith LA**, **Guilliod R**, **Sevick-Muraca EM**. Near-infrared fluorescence imaging of lymphatics in head and neck lymphedema. *Head & Neck* 34: 448–453, 2010.

129. **McGreevy JM**, **Cannon MJ**, **Grissom CB**. Minimally invasive lymphatic mapping using fluorescently labeled vitamin B12. *J Surg Res* 111: 38–44, 2003.

130. **McLaughlin SA**, **Wright MJ**, **Morris KT**, **Giron GL**, **Sampson MR**, **Brockway JP**, **Hurley KE**, **Riedel ER**, **Van Zee KJ**. Prevalence of lymphedema in women with breast cancer 5 years after sentinel lymph node biopsy or axillary dissection: objective measurements. *Journal of Clinical Oncology* 26: 5213–5219, 2008.

131. **McShane MJ**, **Rastegar S**, **Pishko M**, **Coté GL**. Monte Carlo modeling for implantable fluorescent analyte sensors. *IEEE Trans Biomed Eng* 47: 624–632, 2000.

132. **Meens MJ**, **Sabine A**, **Petrova TV**, **Kwak BR**. Connexins in lymphatic vessel physiology and disease. *FEBS Letters* 588: 1271–1277, 2014.

133. **Meeske KA**, **Sullivan-Halley J**, **Smith AW**, **McTiernan A**, **Baumgartner KB**, **Harlan LC**, **Bernstein L**. Risk factors for arm lymphedema following breast cancer diagnosis in Black women and White women. *Breast Cancer Res Treat* 113: 383–391, 2009.

134. **Mellor R**, **Stanton A**, **Azarbod P**, **Sherman M**, **Levick J**, **Mortimer P**. Enhanced cutaneous lymphatic network in the forearms of women with postmastectomy oedema. *J Vasc Res* 37: 501–512, 2000.

135. **Mendez U**, **Brown EM**, **Ongstad EL**, **Slis JR**, **Goldman J**. Functional recovery of fluid drainage precedes lymphangiogenesis in acute murine foreleg lymphedema. *Am J Physiol-Heart C* 302: H2250–H2256, 2012.

136. **Mendez U**, **Stroup EM**, **Lynch LL**, **Waller AB**, **Goldman J**. A Chronic and Latent Lymphatic Insufficiency Follows Recovery from Acute Lymphedema in the Rat Foreleg. *Am J Physiol-Heart C* 303: H1107–H1113, 2012.

137. **Miaskowski C**, **Miaskowski C**, **Dodd M**, **Dodd M**, **Paul SM**, **Paul SM**, **West C**, **West C**, **Hamolsky D**, **Hamolsky D**, **Abrams G**, **Abrams G**, **Cooper BA**, **Cooper BA**, **Elboim C**, **Elboim C**, **Neuhaus J**, **Neuhaus J**, **Schmidt BL**, **Schmidt BL**, **Smoot B**, **Smoot B**, **Aouizerat BE**, **Aouizerat BE**. Lymphatic and Angiogenic Candidate Genes Predict the Development of Secondary Lymphedema following Breast Cancer Surgery. *PLoS One* 8: e60164, 2013.

138. **Mihara M**, **hara H**, **Araki J**, **Kikuchi K**, **Narushima M**, **Yamamoto T**, **Iida T**, **Yoshimatsu H**, **Murai N**, **Mitsui K**, **Okitsu T**, **Koshima I**. Indocyanine Green (ICG) Lymphography Is Superior to Lymphoscintigraphy for Diagnostic Imaging of Early Lymphedema of the Upper Limbs. *PLoS One* 7: e38182, 2012.

139. **Mihara M**, **hara H**, **Hayashi Y**, **Narushima M**, **Yamamoto T**, **Todokoro T**, **Iida T**, **Sawamoto N**, **Araki J**, **Kikuchi K**, **Murai N**, **Okitsu T**, **Kisu I**, **Koshima I**. Pathological Steps of Cancer-Related Lymphedema: Histological Changes in the Collecting Lymphatic Vessels after Lymphadenectomy. *PLoS One* 7: e41126, 2012.

140. **Miller NE**, **Michel CC**, **Nanjee MN**, **Olszewski WL**, **Miller IP**, **Hazell M**, **Olivecrona G**, **Sutton P**, **Humphreys SM**, **Frayn KN**. Secretion of adipokines by human adipose tissue in vivo: partitioning between capillary and lymphatic transport. *Am J Physiol Endocrinol Metab* 301: E659–67, 2011.

141. **Misselwitz B**. MR contrast agents in lymph node imaging. *Eur J Radiol* 58: 375–382, 2006.

142. **Modi S**, **Stanton AWB**, **Svensson WE**, **Peters AM**, **Mortimer PS**, **Levick JR**. Human lymphatic pumping measured in healthy and lymphoedematous arms by lymphatic congestion lymphoscintigraphy. *J Physiol (Lond)* 583: 271–285, 2007.

143. **Mortimer PS**, **Rockson SG**. New developments in clinical aspects of lymphatic disease. *J Clin Invest* 124: 915–921, 2014.

144. **Mortimer PS**. The pathophysiology of lymphedema. *Cancer* 83: 2798–2802, 1998.

145. **Morton DL**, **Wen DR**, **Wong JH**, **Economou JS**, **Cagle LA**, **Storm FK**, **Foshag LJ**, **Cochran AJ**. Technical details of intraoperative lymphatic mapping for early stage melanoma. *Archives of surgery (Chicago, Ill : 1960)* 127: 392–399, 1992.

146. **Moseley A**, **Piller N**. Reliability of bioimpedance spectroscopy and tonometry after breast conserving cancer treatment. *Lymphat Res Biol* 6: 85–87, 2008.

147. **Mouli SK**, **Zhao LC**, **Omary RA**, **Thaxton CS**. Lymphotropic nanoparticle enhanced MRI for the staging of genitourinary tumors. *Nat Rev Urol* 7: 84–93, 2010.

148. **Muthuchamy M**, **Gashev AA**, **Boswell N**, **Dawson N**, **Zawieja DC**. Molecular and functional analyses of the contractile apparatus in lymphatic muscle. *The FASEB Journal* 17: 920–922, 2003.

149. **Nagai T**, **Bridenbaugh EA**, **Gashev AA**. Aging-Associated Alterations in Contractility of Rat Mesenteric Lymphatic Vessels. *Microcirculation* 18: 463–473, 2011.

150. **Nakamura K**, **Radhakrishnan K**, **Wong YM**, **Rockson SG**. Anti-inflammatory pharmacotherapy with ketoprofen ameliorates experimental lymphatic vascular insufficiency in mice. 4: e8380, 2009.

151. **Nakashima K**, **Kurebayashi J**, **Sonoo H**, **Tanaka K**, **Ikeda M**, **Shiiki S**, **Yamamoto Y**, **Nomura T**, **Sohda M**, **Seki M**, **Miyake A**, **Moriya T**, **Sadahira Y**, **Mimura H**, **Fukunaga M**. Preoperative dynamic lymphoscintigraphy predicts sentinel lymph node metastasis in patients with early breast cancer. *Breast Cancer* 17: 17–21, 2010.

152. **Nelson TS**, **AKin RE**, **Weiler MJ**, **Kassis T**, **Kornuta JA**, **Dixon B**. Minimally invasive method for determining the effective lymphatic pumping pressure in rats using near-infrared imaging. *Am J Physiol Regul Integr Comp Physiol* 306: R281–R290, 2014.

153. **Newman AL**, **Rosenthall L**, **Towers A**, **Hodgson P**, **Shay CA**, **Tidhar D**, **Vigano A**, **Kilgour RD**. Determining the precision of dual energy x-ray absorptiometry and bioelectric impedance spectroscopy in the assessment of breast cancer-related lymphedema. *Lymphat Res Biol* 11: 104–109, 2013.

154. **Newman B**, **Lose F**, **Kedda M-A**, **François M**, **Ferguson K**, **Janda M**, **Yates P**, **Spurdle AB**, **Hayes SC**. Possible Genetic Predisposition to Lymphedema after Breast Cancer. *Lymphat Res Biol* 10: 120309115653005, 2012.

155. **Nielsen KR**, **Klyver H**, **Chakera AH**, **Nedergaard L**, **Hesse B**, **Nielsen MB**. Sentinel Node Detection in Melanomas Using Contrast-Enhanced Ultrasound. *Acta Radiologica*.

156. **Nipper ME**, **Dixon JB**. Engineering the Lymphatic System. *Cardiovasc Eng Technol* 2: 296–308, 2011.

157. **Noroes J**, **Addiss D**, **Santos A**, **Mereidos Z**. Ultrasonigraphic Evidence of Abnormal Lymphatic Vessels in Young Men with Adult Wuchereria Bancrofti Infection in the Scrotal Area. *The Journal of …*.

158. **Noroes J**, **Dreyer G**, **Santos A**, **Mendes VG**, **Medeiros Z**, **Addiss D**. Assessment of the efficacy of diethylcarbamazine on adult Wuchereria bancrofti in vivo. *Trans R Soc Trop Med Hyg* 91: 78–81, 1997.

159. **Nune SK**, **Gunda P**, **Majeti BK**, **Thallapally PK**, **Forrest ML**. Advances in lymphatic imaging and drug delivery. *Adv Drug Deliver Rev* 63: 876–885, 2011.

160. **O'Mahony S**, **Solanki CK**, **Barber RW**, **Mortimer PS**, **Purushotham AD**, **Peters AM**. Imaging of Lymphatic Vessels in Breast Cancer–Related Lymphedema: Intradermal Versus Subcutaneous Injection of 99mTc-Immunoglobulin. *AJR Am J Roentgenol* 178: 405–412, 2002.

161. **Ogata F**, **Fujiu K**, **Koshim I**, **Nagai R**, **Manabe I**. Phenotypic modulation of smooth muscle cells in lymphedema. *Br J Dermatol* (October 15, 2014). doi: 10.1111/bjd.13482.

162. **Ohhashi T**, **Azuma T**, **Sakaguchi M**. Active and passive mechanical characteristics of bovine mesenteric lymphatics. *Am J Physiol* 239: H88–95, 1980.

163. **Ohnishi S**, **Lomnes SJ**, **Laurence RG**, **Gogbashian A**, **Mariani G**, **Frangioni JV**. Organic alternatives to quantum dots for intraoperative near-infrared fluorescent sentinel lymph node mapping. *Mol Imaging* 4: 172–181, 2005.

164. **Ongstad EL**, **Bouta EM**, **Roberts JE**, **Uzarski JS**, **Gibbs SE**, **Sabel MS**, **Cimmino VM**, **Roberts MA**, **Goldman J**. Lymphangiogenesis-independent resolution of experimental edema. *Am J Physiol-Heart C* 299: H46–H54, 2010.

165. **Paskett ED**, **Paskett ED**, **Dean JA**, **Dean JA**, **Oliveri JM**, **Oliveri JM**, **Harrop JP**, **Harrop JP**. Cancer-related lymphedema risk factors, diagnosis, treatment, and impact: a review. *J Clin Oncol* 30: 3726–3733, 2012.

166. **Pepper MS**, **Tille J-C**, **Nisato R**, **Skobe M**. Lymphangiogenesis and tumor metastasis. *Cell Tissue Res* 314: 167–177, 2003.

167. **Petrova TV**, **Karpanen T**, **Norrmén C**, **Mellor R**, **Tamakoshi T**, **Finegold D**, **Ferrell R**, **Kerjaschki D**, **Mortimer P**, **Ylä-Herttuala S**, **Miura N**, **Alitalo K**. Defective valves and abnormal mural cell recruitment underlie lymphatic vascular failure in lymphedema distichiasis. *Nat Med* 10: 974–981, 2004.

168. **PhD DTD**, **MAppSc SR**, **PhD PBN**, **PhD SH**. Incidence of unilateral arm lymphoedema after breast cancer: a systematic review and meta-analysis. *Lancet Oncol.* 14: 500–515, 2014.

169. **Philip R**, **Penzkofer A**, **Baumler W**, **Szeimies RM**, **Abels C**. Absorption and fluorescence spectroscopic investigation of indocyanine green. *Journal of Photochemistry and Photobiology A: Chemistry* 96: 137–148, 1996.

170. **Planas-Paz L**, **Strilić B**, **Goedecke A**, **Breier G**, **Fässler R**, **Lammert E**. Mechanoinduction of lymph vessel expansion. *EMBO J* 31: 788–804, 2012.

171. **Proulx ST**, **Luciani P**, **Christiansen A**, **Karaman S**, **Blum KS**, **Rinderknecht M**, **Leroux J-C**, **Detmar M**. Use of a PEG-conjugated bright near-infrared dye for functional imaging of rerouting of tumor lymphatic drainage after sentinel lymph node metastasis. *Biomaterials* 34: 1–10, 2013.

172. **Proulx ST**, **Luciani P**, **Derzsi S**, **Rinderknecht M**, **Mumprecht V**, **Leroux J-C**, **Detmar M**. Quantitative Imaging of Lymphatic Function with Liposomal Indocyanine Green. *Cancer Res* 70: 7053–7062, 2010.

173. **Proulx ST**, **Luciani P**, **Derzsi S**, **Rinderknecht M**, **Mumprecht V**, **Leroux J-C**, **Detmar M**. Quantitative imaging of lymphatic function with liposomal indocyanine green. *Cancer Res* 70: 7053–7062, 2010.

174. **Rabin O**, **Perez J**, **Grimm J**, **Wojtkiewicz G**. An X-ray computed tomography imaging agent based on long-circulating bismuth sulphide nanoparticles. *Nature Materials*.

175. **Radhakrishnan K**, **Rockson SG**. The clinical spectrum of lymphatic disease. *Ann N Y Acad Sci* 1131: 155–184, 2008.

176. **Radina ME**, **Armer JM**, **Stewart BR**. Making Self-Care a Priority for Women

At Risk of Breast Cancer–Related Lymphedema. *Journal of family nursing*.

177. **Rao J**, **Dragulescu-Andrasi A**, **Yao H**. Fluorescence imaging in vivo: recent advances. *Current Opinion in Biotechnology* 18: 17–25, 2007.

178. **Rasmussen J**, **Tan I**. Lymphatic imaging in humans with near-infrared fluorescence. *Current Opinion in Biotechnology* 20: 74–82, 2009.

179. **Rasmussen JC**, **Kwon S**, **Sevick-Muraca EM**, **Cormier JN**. The Role of Lymphatics in Cancer as Assessed by Near-Infrared Fluorescence Imaging. *Ann Biomed Eng* (December 3, 2011). doi: 10.1007/s10439-011-0476-1.

180. **Rasmussen JC**, **Tan I-C**, **Marshall MV**, **Adams KE**, **Kwon S**, **Fife CE**, **Maus EA**, **Smith LA**, **Covington KR**, **Sevick-Muraca EM**. Human Lymphatic Architecture and Dynamic Transport Imaged Using Near-infrared Fluorescence. *Translational Oncology* 3: 362–372, 2010.

181. **Rasmussen JC**, **Tan I-C**, **Marshall MV**, **Fife CE**, **Sevick-Muraca EM**. Lymphatic imaging in humans with near-infrared fluorescence. *Current Opinion in Biotechnology* 20: 74–82, 2009.

182. **Réty F**, **Clément O**, **Siauve N**, **Cuénod CA**, **Carnot F**, **Sich M**, **Buisine A**, **Frija G**. MR lymphography using iron oxide nanoparticles in rats: pharmacokinetics in the lymphatic system after intravenous injection. *J Magn Reson Imaging* 12: 734–739, 2000.

183. **Ridner SH**, **Bonner CM**, **Doersam JK**, **Rhoten BA**, **Schultze B**, **Dietrich MS**. Bioelectrical impedance self-measurement protocol development and daily variation between healthy volunteers and breast cancer survivors with lymphedema. *Lymphat Res Biol* 12: 2–9, 2014.

184. **Ridner SH**, **Dietrich MS**, **Stewart BR**, **Armer JM**. Body mass index and breast cancer treatment-related lymphedema. *Support Care Cancer* 19: 853–857, 2011.

185. **Ristimäki A**, **Narko K**, **Enholm B**, **Joukov V**, **Alitalo K**. Proinflammatory cytokines regulate expression of the lymphatic endothelial mitogen vascular endothelial growth factor-C. *J Biol Chem* 273: 8413–8418, 1998.

186. **Rockson SG**, **Rivera KK**. Estimating the population burden of lymphedema. *Ann N Y Acad Sci* 1131: 147–154, 2008.

187. **Rockson SG**. Lymphedema. *American Journal of Medicine* 110: 288–295, 2001.

188. **Rockson SG**. Addressing the unmet needs in lymphedema risk management. *Lymphat Res Biol* 4: 42–46, 2006.

189. **Rockson SG**. Diagnosis and management of lymphatic vascular disease. *J Am Coll Cardiol* 52: 799–806, 2008.

190. **Ross RW**, **Zietman AL**, **Xie W**, **Coen JJ**, **Dahl DM**, **Shipley WU**, **Kaufman DS**, **Islam T**, **Guimaraes AR**, **Weissleder R**, **Harisinghani M**. Lymphotropic nanoparticle-enhanced magnetic resonance imaging (LNMRI) identifies occult lymph node metastases in prostate cancer patients prior to salvage radiation therapy. *Clin Imaging* 33: 301–305, 2009.

191. **Ruddell A**, **Harrell MI**, **Minoshima S**, **Maravilla KR**, **Iritani BM**, **White SW**, **Partridge SC**. Dynamic contrast-enhanced magnetic resonance imaging of tumor-induced lymph flow. *Neoplasia* 10: 706–13, 1 p following 713, 2008.

192. **Ruehm SG**, **Corot C**, **Debatin JF**. Interstitial MR lymphography with a conventional extracellular gadolinium-based agent: assessment in rabbits. *Radiology* 218: 664–669, 2001.

193. **Ruehm SG**, **Schroeder T**, **Debatin JF**. Interstitial MR lymphography with gadoterate meglumine: initial experience in humans. *Radiology* 220: 816–821, 2001.

194. **Rutkowski JM**, **Markhus CE**, **Gyenge CC**, **Alitalo K**, **Wiig H**, **Swartz MA**. Dermal Collagen and Lipid Deposition Correlate with Tissue Swelling and Hydraulic Conductivity in Murine Primary Lymphedema. *Am J Pathol* (January 28, 2010). doi: 10.2353/ajpath.2010.090733.

195. **Rutkowski JM**, **Moya M**, **Johannes J**, **Goldman J**, **Swartz MA**. Secondary lymphedema in the mouse tail: Lymphatic hyperplasia, VEGF-C upregulation, and the protective role of MMP-9. *Microvasc Res* 72: 161–171, 2006.

196. **Saban MR**, **Mémet S**, **Jackson DG**, **Ash J**, **Roig AA**, **Israël A**, **Saban R**. Visualization of lymphatic vessels through NF-kappaB activity. *Blood* 104: 3228–3230, 2004.

197. **Sampath L**, **Wang W**, **Sevick-Muraca E**. Near infrared fluorescent optical imaging for nodal staging. *J Biomed Opt* 13: 041312, 2008.

198. **Saul M**, **Thomas P**, **Dosen P**, **Isbister G**, **O'Leary M**, **Whyte I**, **McFadden S**, **van Helden D**. A pharmacological approach to first aid treatment for snakebite. *Nat Med* 17: 809–811, 2011.

199. **Savetsky IL**, **Torrisi JS**, **Cuzzone DA**, **Ghanta S**, **Albano NJ**, **Gardenier JC**, **Joseph WJ**, **Mehrara BJ**. Obesity increases inflammation and impairs lymphatic function in a mouse model of lymphedema. *Am J Physiol-Heart C* 139: 81–86, 2014.

200. **Saxena V**, **Sadoqi M**, **Shao J**. Degradation kinetics of indocyanine green in aqueous solution. *J Pharm Sci* 92: 2090–2097, 2003.

201. **Scallan JP**, **Davis MJ**. Genetic removal of basal nitric oxide enhances contractile activity in isolated murine collecting lymphatic vessels. *J Physiol*

(Lond) 591: 2139–2156, 2013.

202.   **Scallan JP**, **Wolpers JH**, **Davis MJ**. Constriction of isolated collecting lymphatic vessels in response to acute increases in downstream pressure. *J Physiol (Lond)* 591: 443–459, 2013.

203.   **Scallan JP**, **Wolpers JH**, **Muthuchamy M**, **Zawieja DC**, **Gashev AA**, **Davis MJ**. Independent and interactive effects of preload and afterload on the pump function of the isolated lymphangion. *Am J Physiol-Heart C* 303: H809–24, 2012.

204.   **Schmid-Schonbein G**. Mechanisms Causing Initial Lymphatics to Expand and Compress to Promote Lymph-Flow. *Archives of Histology and Cytology* 53: 107–114, 1990.

205.   **Schöder H**, **Glass EC**, **Pecking AP**, **Harness JK**, **Wallace AM**, **Hirnle P**, **Alberini JL**, **Vilain D**, **Larson SM**, **Hoh CK**, **Vera DR**. Molecular targeting of the lymphovascular system for imaging and therapy. *Cancer Metastasis Rev* 25: 185–201, 2006.

206.   **Sever A**, **Jones S**, **Cox K**, **Weeks J**, **Mills P**, **Jones P**. Preoperative localization of sentinel lymph nodes using intradermal microbubbles and contrast-enhanced ultrasonography in patients with breast cancer. *Br J Surg* 96: 1295–1299, 2009.

207.   **Sever AR**, **Mills P**, **Hyvelin J-M**, **Weeks J**, **Gumus H**, **Fish D**, **Mali W**, **Jones SE**, **Jones PA**, **Devalia H**. Percutaneous removal of sentinel lymph nodes in a swine model using a breast lesion excision system and contrast-enhanced ultrasound. *Eur Radiol* 22: 545–550, 2012.

208.   **Sevick-Muraca E**, **Rasmussen J**. Molecular imaging with optics: primer and case for near-infrared fluorescence techniques in personalized medicine. *J Biomed Opt* 13: 041303, 2008.

209.   **Sevick-Muraca E**, **Sharma R**, **Rasmussen J**, **Marshall M**, **Wendt J**, **Pham H**, **Bonefas E**, **Houston J**, **Sampath L**, **Adams K**. Imaging of Lymph Flow in Breast Cancer Patients after Microdose Administration of a Near-Infrared Fluorophore: Feasibility Study1. *Radiology* 246: 734–741, 2008.

210.   **Shah C**, **Shah C**, **Arthur D**, **Arthur D**, **Riutta J**, **Riutta J**, **Whitworth P**, **Whitworth P**, **Vicini FA**, **Vicini FA**. Breast-Cancer Related Lymphedema: A Review of Procedure-Specific Incidence Rates, Clinical Assessment Aids, Treatment Paradigms, and Risk Reduction. *Breast J* 18: 357–361, 2012.

211.   **Sharma R**, **Wang W**, **Rasmussen JC**, **Joshi A**, **Houston JP**, **Adams KE**, **Cameron A**, **Ke S**, **Kwon S**, **Mawad ME**, **Sevick-Muraca EM**. Quantitative imaging of lymph function. *Am J Physiol-Heart C* 292: H3109–H3118, 2007.

212.   **Sharma R**, **Wendt JA**, **Rasmussen JC**, **Adams KE**, **Marshall MV**, **Sevick-**

Muraca EM. New horizons for imaging lymphatic function. *Ann N Y Acad Sci* 1131: 13–36, 2008.

213. **Shimizu Y**, **Shibata R**, **Ishii M**, **Ohashi K**, **Kambara T**, **Uemura Y**, **Yuasa D**, **Kataoka Y**, **Kihara S**, **Murohara T**, **Ouchi N**. Adiponectin-Mediated Modulation of Lymphatic Vessel Formation and Lymphedema. *Journal of the American Heart Association* 2: e000438–e000438, 2013.

214. **Silvestri RC**, **Huseby JS**, **Rughani I**, **Thorning D**, **Culver BH**. Respiratory distress syndrome from lymphangiography contrast medium. *Am. Rev. Respir. Dis.* 122: 543–549, 1980.

215. **Soltesz EG**, **Kim S**, **Laurence RG**, **DeGrand AM**, **Parungo CP**, **Dor DM**, **Cohn LH**, **Bawendi MG**, **Frangioni JV**, **Mihaljevic T**. Intraoperative sentinel lymph node mapping of the lung using near-infrared fluorescent quantum dots. *The Annals of thoracic surgery* 79: 269–77; discussion 269–77, 2005.

216. **Song I**, **Hyeon T**. Inorganic nanoparticles for MRI contrast agents. *Advanced Materials*.

217. **Stanton AW**, **Northfield JW**, **Holroyd B**, **Mortimer PS**, **Levick JR**. Validation of an optoelectronic limb volumeter (Perometer). *Lymphology* 30: 77–97, 1997.

218. **Stanton AWB**, **Modi S**, **Bennett Britton TM**, **Purushotham AD**, **Peters AM**, **Levick JR**, **Mortimer PS**. Lymphatic drainage in the muscle and subcutis of the arm after breast cancer treatment. *Breast Cancer Res Treat* 117: 549–557, 2008.

219. **Stanton AWB**, **Modi S**, **Mellor RH**, **Levick JR**, **Mortimer PS**. Recent advances in breast cancer-related lymphedema of the arm: lymphatic pump failure and predisposing factors. *Lymphat Res Biol* 7: 29–45, 2009.

220. **Stout Gergich NL**, **Pfalzer LA**, **McGarvey C**, **Springer B**, **Gerber LH**, **Soballe P**. Preoperative assessment enables the early diagnosis and successful treatment of lymphedema. *Cancer* 112: 2809–2819, 2008.

221. **Suami H**, **Pan W-R**, **Taylor GI**. The lymphatics of the skin filled by a dermal backflow: an observation in a scarred cadaver leg. *Lymphology* 40: 122–126, 2007.

222. **Suehiro K**, **Nakamura K**, **Morikage N**, **Murakami M**, **Yamashita O**, **Ueda K**, **Samura M**, **Hamano K**. Real-time tissue elastography assessment of skin and subcutaneous tissue strains in legs with lymphedema. *J Med Ultrasonics* (March 4, 2014). doi: 10.1007/s10396-014-0526-z.

223. **Suga K**, **Ogasawara N**, **Okada M**, **Matsunaga N**. Interstitial CT lymphography-guided localization of breast sentinel lymph node: preliminary results. *Surgery* 133: 170–179, 2003.

224. **Suga K**, **Ogasawara N**, **Yuan Y**, **Okada M**, **Matsunaga N**, **Tangoku A**. Visualization of breast lymphatic pathways with an indirect computed tomography lymphography using a nonionic monometric contrast medium iopamidol: preliminary results. *Invest Radiol* 38: 73–84, 2003.

225. **Suga K**, **Yamamoto S**, **Tangoku A**, **Oka M**, **Kawakami Y**, **Matsunaga N**. Breast sentinel lymph node navigation with three-dimensional interstitial multidetector-row computed tomographic lymphography. *Invest Radiol* 40: 336–342, 2005.

226. **Suga K**, **Yuan Y**, **Okada M**, **Matsunaga N**, **Tangoku A**, **Yamamoto S**, **Oka M**. Breast sentinel lymph node mapping at CT lymphography with iopamidol: preliminary experience. *Radiology* 230: 543–552, 2004.

227. **Suresh S**, **Kumaraswami V**, **Suresh I**, **Rajesh K**, **Suguna G**, **Vijayasekaran V**, **Ruckmani A**, **Rajamanickam MG**. Ultrasonographic diagnosis of subclinical filariasis. *J Ultrasound Med* 16: 45–49, 1997.

228. **Swartz M**, **Berk D**. Transport in lymphatic capillaries. I. Macroscopic measurements using residence time distribution theory. *American Journal of …*.

229. **Swartz MA**, **Fleury ME**. Interstitial flow and its effects in soft tissues. *Annu Rev Biomed Eng* 9: 229–256, 2007.

230. **Swartz MA**, **Hubbell JA**, **Reddy S**. Lymphatic drainage function and its immunological implications: From dendritic cell homing to vaccine design. *Seminars in Immunology* 20: 147–156, 2008.

231. **Swartz MA**, **Kaipainen A**, **Netti P**, **Brekken C**, **Boucher Y**, **Grodzinsky A**, **Jain R**. Mechanics of interstitial-lymphatic fluid transport: theoretical foundation and experimental validation. *Journal of Biomechanics* 32: 1297–1307, 1999.

232. **Swartz MA**. The physiology of the lymphatic system. *Adv Drug Deliv Rev* 50: 3–20, 2001.

233. **Szuba A**, **Rockson SG**. Lymphedema: classification, diagnosis and therapy. *Vasc Med* 3: 145–156, 1998.

234. **Szuba A**, **Shin WS**, **Strauss HW**, **Rockson S**. The third circulation: radionuclide lymphoscintigraphy in the evaluation of lymphedema. *J. Nucl. Med.* 44: 43–57, 2003.

235. **Szuba A**, **Skobe M**, **Karkkainen MJ**, **Shin WS**, **Beynet DP**, **Rockson NB**, **Dakhil N**, **Spilman S**, **Goris ML**, **Strauss HW**, **Quertermous T**, **Alitalo K**, **Rockson SG**. Therapeutic lymphangiogenesis with human recombinant VEGF-C. *FASEB J* 16: 1985–1987, 2002.

236. **Szuba A**, **Strauss W**, **Sirsikar SP**, **Rockson SG**. Quantitative radionuclide

lymphoscintigraphy predicts outcome of manual lymphatic therapy in breast cancer-related lymphedema of the upper extremity. *Nucl Med Commun* 23: 1171–1175, 2002.

237. **Tabibiazar R**, **Cheung L**, **Han J**, **Swanson J**, **Beilhack A**, **An A**, **Dadras SS**, **Rockson N**, **Joshi S**, **Wagner R**, **Rockson SG**. Inflammatory manifestations of experimental lymphatic insufficiency. *PLoS Med* 3: e254, 2006.

238. **Takahashi M**, **Sasa M**, **Hirose C**, **Hisaoka S**, **Taki M**, **Hirose T**, **Bando Y**. Clinical efficacy and problems with CT lymphography in identifying the sentinel node in breast cancer. *World J Surg Oncol* 6: 57, 2008.

239. **Takema Y**, **Yorimoto Y**, **Kawai M**, **Imokawa G**. Age-related changes in the elastic properties and thickness of human facial skin. *Br J Dermatol* 131: 641–648, 1994.

240. **Tammela T**, **Alitalo K**. Lymphangiogenesis: Molecular mechanisms and future promise. *Cell* 140: 460–476, 2010.

241. **Tan I-C**, **Maus EA**, **Rasmussen JC**, **Marshall MV**, **Adams KE**, **Fife CE**, **Smith LA**, **Chan W**, **Sevick-Muraca EM**. Assessment of Lymphatic Contractile Function After Manual Lymphatic Drainage Using Near-Infrared Fluorescence Imaging. *Archives of Physical Medicine and Rehabilitation* 92: 756–764, 2011.

242. **Taylor MJ**, **Makunde WH**, **McGarry HF**, **Turner JD**, **Mand S**, **Hoerauf A**. Macrofilaricidal activity after doxycycline treatment of Wuchereria bancrofti: a double-blind, randomised placebo-controlled trial. *Lancet* 365: 2116–2121, 2005.

243. **Thompson M**, **Korourian S**, **Henry-Tillman R**, **Adkins L**, **Mumford S**, **Westbrook KC**, **Klimberg VS**. Axillary reverse mapping (ARM): a new concept to identify and enhance lymphatic preservation. *Annals of Surgical Oncology* 14: 1890–1895, 2007.

244. **Tiwari A**, **Cheng K**, **Button M**, **Myint F**. Differential diagnosis, investigation, and current treatment of lower limb lymphedema. *Archives of …*.

245. **Tiwari P**, **Coriddi M**, **Salani R**, **Povoski SP**. Breast and gynecologic cancer-related extremity lymphedema: a review of diagnostic modalities and management options. *World J Surg Oncol* 11: 237, 2013.

246. **Tso P**, **Pitts V**, **Granger D**. Role of lymph flow in intestinal chylomicron transport. *Am J Physiol - Gastrointestinal and Liver Physiology* 249: G21–8., 1985.

247. **Unno N**, **Inuzuka K**, **Suzuki M**, **Yamamoto N**, **Sagara D**, **Nishiyama M**, **Konno H**. Preliminary experience with a novel fluorescence lymphography using indocyanine green in patients with secondary lymphedema. *J Vasc Surg*

45: 1016–1021, 2007.

248. **Unno N**, **Nishiyama M**, **Suzuki M**, **Tanaka H**, **Yamamoto N**, **Sagara D**, **Mano Y**, **Konno H**. A novel method of measuring human lymphatic pumping using indocyanine green fluorescence lymphography. *Journal of Vascular Surgery* 52: 946–952, 2010.

249. **Unno N**, **Nishiyama M**, **Suzuki M**, **Yamamoto N**, **Inuzuka K**, **Sagara D**, **Tanaka H**, **Konno H**. Quantitative lymph imaging for assessment of lymph function using indocyanine green fluorescence lymphography. *European Journal of Vascular and Endovascular Surgery* 36: 230–236, 2008.

250. **Unno N**, **Tanaka H**, **Suzuki M**, **Yamamoto N**, **Mano Y**, **Sano M**, **Saito T**, **Konno H**. Influence of age and gender on human lymphatic pumping pressure in the leg. *Lymphology* 44: 113–120, 2011.

251. **Uren RF**, **Howman-Giles R**, **Chung DKV**, **Spillane AJ**, **Noushi F**, **Gillett D**, **Gluch L**, **Mak C**, **West R**, **Briody J**, **Carmalt H**. SPECT/CT scans allow precise anatomical location of sentinel lymph nodes in breast cancer and redefine lymphatic drainage from the breast to the axilla. *Breast* (December 5, 2011). doi: 10.1016/j.breast.2011.11.007.

252. **Uren RF**. SPECT/CT Lymphoscintigraphy to locate the sentinel lymph node in patients with melanoma. *Annals of Surgical Oncology* 16: 1459–1460, 2009.

253. **Uzarski J**, **Drelles MB**, **Gibbs SE**, **Ongstad EL**, **Goral JC**, **McKeown KK**, **Raehl AM**, **Roberts MA**, **Pytowski B**, **Smith MR**, **Goldman J**. The resolution of lymphedema by interstitial flow in the mouse tail skin. *Am J Physiol-Heart C* 294: H1326–H1334, 2007.

254. **van der Ploeg IMC**, **Olmos RAV**, **Kroon BBR**, **Rutgers EJT**, **Nieweg OE**. The hidden sentinel node and SPECT/CT in breast cancer patients. *Eur. J. Nucl. Med. Mol. Imaging* 36: 6–11, 2009.

255. **van der Ploeg IMC**, **Valdés Olmos RA**, **Kroon BBR**, **Nieweg OE**. The Hybrid SPECT/CT as an Additional Lymphatic Mapping Tool in Patients with Breast Cancer. *World J Surg* 32: 1930–1934, 2008.

256. **Veenstra HJ**, **Vermeeren L**, **Olmos RAV**, **Nieweg OE**. The additional value of lymphatic mapping with routine SPECT/CT in unselected patients with clinically localized melanoma. *Annals of Surgical Oncology* 19: 1018–1023, 2012.

257. **Veronesi U**, **Paganelli G**, **Galimberti V**, **Viale G**, **Zurrida S**, **Bedoni M**, **Costa A**, **de Cicco C**, **Geraghty JG**, **Luini A**, **Sacchini V**, **Veronesi P**. Sentinel-node biopsy to avoid axillary dissection in breast cancer with clinically negative lymph-nodes. *Lancet* 349: 1864–1867, 1997.

258. **Vogl TJ**, **Bartjes M**, **Marzec K**. Contrast-enhanced lymphography. CT or MR

imaging? *Acta Radiol Suppl* 412: 47–50, 1997.

259.   **Voigt J-U**. Ultrasound molecular imaging. *Methods* 48: 92–97, 2009.

260.   **Ward LC**, **Dylke E**, **Czerniec S**, **Isenring E**, **Kilbreath SL**. Reference Ranges for Assessment of Unilateral Lymphedema in Legs by Bioelectrical Impedance Spectroscopy. *Lymphat Res Biol* 9: 43–46, 2011.

261.   **Ward LC**, **Dylke E**, **Czerniec S**. Confirmation of the reference impedance ratios used for assessment of breast cancer-related lymphedema by bioelectrical impedance spectroscopy. *Lymphatic Research ….*

262.   **Ward LC**. Bioelectrical impedance analysis: proven utility in lymphedema risk assessment and therapeutic monitoring. *Lymphat Res Biol* 4: 51–56, 2006.

263.   **Warren AG**, **Slavin SA**. Scar lymphedema: fact or fiction? *Ann Plast Surg* 59: 41–45, 2007.

264.   **Waters EA**, **Wickline SA**. Contrast agents for MRI. *Basic Res Cardiol* 103: 114–121, 2008.

265.   **Weber M**, **Hauschild R**, **Schwarz J**, **Moussion C**, **de Vries I**, **Legler DF**, **Luther SA**, **Bollenbach T**, **Sixt M**. Interstitial Dendritic Cell Guidance by Haptotactic Chemokine Gradients. *Science* 339: 328–332, 2013.

266.   **Weid von der P-Y**, **Zawieja DC**. Lymphatic smooth muscle: the motor unit of lymph drainage. *Int J Biochem Cell Biol* 36: 1147–1153, 2004.

267.   **Weiler M**, **Dixon JB**. Differential transport function of lymphatic vessels in the rat tail model and the long-term effects of Indocyanine Green as assessed with near-infrared imaging. *Front. Physiol.* (August 15, 2013). doi: 10.3389/fphys.2013.00215/abstract.

268.   **Weiler M**, **Kassis T**, **Dixon JB**. Sensitivity analysis of near-infrared functional lymphatic imaging. *J Biomed Opt* 17: 066019, 2012.

269.   **Weiss M**, **Baumeister RGH**, **Hahn K**. Post-therapeutic lymphedema: scintigraphy before and after autologous lymph vessel transplantation: 8 years of long-term follow-up. *Clin Nucl Med* 27: 788–792, 2002.

270.   **Weissleder H**, **Weissleder R**. Lymphedema: evaluation of qualitative and quantitative lymphoscintigraphy in 238 patients. *Radiology* 167: 729–735, 1988.

271.   **Weissleder R**, **Elizondo G**, **Wittenberg J**, **Lee AS**, **Josephson L**, **Brady TJ**. Ultrasmall superparamagnetic iron oxide: an intravenous contrast agent for assessing lymph nodes with MR imaging. *Radiology* 175: 494–498, 1990.

272.   **Wilting J**, **Becker J**, **Buttler K**, **Weich HA**. Lymphatics and inflammation.

Curr. Med. Chem. 16: 4581–4592, 2009.

273. **Wisner ER**, **Ferrara KW**, **Short RE**, **Ottoboni TB**, **Gabe JD**, **Patel D**. Sentinel node detection using contrast-enhanced power Doppler ultrasound lymphography. *Invest Radiol* 38: 358–365, 2003.

274. **Wu H**, **Xu X**, **Ying H**, **Hoffman MR**, **Shen N**, **Sha Y**, **Zhou L**. Preliminary study of indirect CT lymphography-guided sentinel lymph node biopsy in a tongue VX2 carcinoma model. *Int J Oral Maxillofac Surg* 38: 1268–1272, 2009.

275. **Yang Y**, **Oliver G**. Development of the mammalian lymphatic vasculature. *J Clin Invest* 124: 888–897, 2014.

276. **Yoon Y-S**, **Murayama T**, **Gravereaux E**, **Tkebuchava T**, **Silver M**, **Curry C**, **Wecker A**, **Kirchmair R**, **Hu CS**, **Kearney M**, **Ashare A**, **Jackson DG**, **Kubo H**, **Isner JM**, **Losordo DW**. VEGF-C gene therapy augments postnatal lymphangiogenesis and ameliorates secondary lymphedema. *J Clin Invest* 111: 717–725, 2003.

277. **Yu SB**, **Watson AD**. Metal-Based X-ray Contrast Media. *Chem. Rev.* 99: 2353–2378, 1999.

278. **Zampell JC**, **Avraham T**, **Yoder N**, **Fort N**, **Yan A**, **Weitman ES**, **Mehrara BJ**. Lymphatic function is regulated by a coordinated expression of lymphangiogenic and anti-lymphangiogenic cytokines. *Am J Physiol-Cell Ph* 302: C392–C404, 2012.

279. **Zampell JC**, **Elhadad S**, **Avraham T**, **Weitman E**, **Aschen S**, **Yan A**, **Mehrara BJ**. Toll-like receptor deficiency worsens inflammation and lymphedema after lymphatic injury. *AJP: Cell Physiology* 302: C709–C719, 2012.

280. **Zampell JC**, **Shimizu Y**, **Aschen S**, **Shibata R**, **Weitman ES**, **Ishii M**, **Yan A**, **Ohashi K**, **Elhadad S**, **Kambara T**, **De Brot M**, **Uemura Y**, **Mehrara BJ**, **Yuasa D**, **Kataoka Y**, **Kihara S**, **Murohara T**, **Ouchi N**. Regulation of adipogenesis by lymphatic fluid stasis: part I. Adipogenesis, fibrosis, and inflammation. *Plast Reconstr Surg* 129: 825–834, 2012.

281. **Zampell JC**, **Yan A**, **Avraham T**, **Daluvoy S**. HIF-1α coordinates lymphangiogenesis during wound healing and in response to inflammation. *The FASEB Journal*.

282. **Zampell JC**, **Yan A**, **Elhadad S**, **Avraham T**, **Weitman E**, **Mehrara BJ**. CD4(+) cells regulate fibrosis and lymphangiogenesis in response to lymphatic fluid stasis. *PLoS One* 7: e49940, 2012.

283. **Zawieja SD**, **Wang W**, **Wu X**, **Nepiyushchikh ZV**, **Zawieja DC**, **Muthuchamy M**. Impairments in the intrinsic contractility of mesenteric

collecting lymphatics in a rat model of metabolic syndrome. *Am J Physiol-Heart C* 302: H643–53, 2012.

284.   **Zhang F**, **Niu G**, **Lu G**, **Chen X**. Preclinical Lymphatic Imaging. *Mol Imaging Biol* 13: 599–612, 2010.